5-2023

Translational Models for Advancement of Regenerative Medicine and Tissue Engineering

Kristin Marie Bowers
University of Tennessee, Knoxville, kbower17@vols.utk.edu

To the Graduate Council:

I am submitting herewith a dissertation written by Kristin Marie Bowers entitled "Translational Models for Advancement of Regenerative Medicine and Tissue Engineering." I have examined the final electronic copy of this dissertation for form and content and recommend that it be accepted in partial fulfillment of the requirements for the degree of Doctor of Philosophy, with a major in Comparative and Experimental Medicine.

David E. Anderson, Major Professor

We have read this dissertation and recommend its acceptance:

Henry Adair III, Dustin Crouch, Silke Hecht, Pierre-Yves Mulon

Accepted for the Council:

Dixie L. Thompson

Vice Provost and Dean of the Graduate School

(Original signatures are on file with official student records.)

Translational Models for Advancement of Regenerative Medicine and Tissue Engineering

A Dissertation Presented for the
Doctor of Philosophy
Degree
The University of Tennessee, Knoxville

Kristin Marie Bowers
May 2023

DEDICATION

This dissertation is dedicated to David and Patricia Bowers,
my patient, loving, and supportive parents.

ACKNOWLEDGEMENTS

First and foremost, I would like to acknowledge and thank my advisor, Dr. David Anderson. His support, mentorship, enthusiasm, and dedication to lifelong learning have shaped who I am today, and words cannot convey the depth of appreciation and gratitude that I feel. I would also like to thank my committee members, Dr. Steve Adair, Dr. Dustin Crouch, Dr. Silke Hecht, and Dr. Pierre-Yves Mulon, for their support and guidance throughout this program. Next, I would like to thank my previous mentors including but not limited to Dr. Samantha Morello, Dr. Sabrina Brounts, Dr. Amelia Munsterman, Dr. Timo Prange, and Dr. Julie Dechant, all of whom played a huge role in the path that led me to today.

Next, I would like to extend a special thank you to the laboratory of Dr. Madhu Dhar, including but not limited to Dr. Lisa Amelse, Dr. Steven Newby, Dr. Amber MacDonald, Dr. Austin Bow, Ms. Meaghan Harley-Troxell, and Mr. Michael Rivera Orsini. In particular, I would like to thank Dr. Dhar for her guidance and enthusiasm for teaching someone completely new to regenerative medicine. It has been a privilege to work with this amazing group of people.

It truly takes a village, and my case is no exception. I would like to thank everyone who helped with our in vivo projects over the years. Thank you to our veterinary and undergraduate student workers including but not limited to Quinn Adams, Sarah Clabo, Natalie De Gruy, Calyn Fulton, Celeste Johnson, Monica Lee, Zach Lembersky, Emily Misischia, Scott Pharr, Nick Ray, Alex Shanks, Colton Short, Daniel Tallent, Taylor Welton, and Madeline Yarber. Thank you to all the devoted staff at the Johnson Research and Teaching Unit including Alex Anderson, Tammy Howard, Amberly Clark, Jared Beeler, Tanner Thornton, and Julianne Carter. Thank you to the members of the UTCVM Anesthesiology Service for their support on surgery days and special thanks to Dr. Katrina Easton and Mr. Caleb Stubbs for their assistance throughout.

I acknowledge and thank my previous lab-mates, Dr. Caroline Billings and Dr. Alisha Pedersen, for their support and friendship. It has been an honor to follow in their footsteps. Finally, I would like to thank my coworkers and friends, Elizabeth Croy and Lori Terrones, without whom none of this would be possible. Their unfailing support, love, and friendship helped me through all the ups and downs of graduate school and for that and so much more, I am grateful.

ABSTRACT

At the root of each regenerative medicine or tissue engineering breakthrough is a simple goal, to improve quality of healing, thus improving a patient's quality of life. Each tissue presents its own complexities and limitations to healing, whether it is the scarring nature of tendon healing or the mechanical complexity driving bone regeneration. Preclinical, translational models aim to reflect these complexities and limitations, allowing for effective development and refinement of tissue engineered therapeutics for human use. The following body of work explores several of these translational models, both utilizing them for tissue regenerative therapy development and evaluating the benefits and complications incurred with each model. This work begins with a discussion of the complexity of bone healing and how dysfunction in the mechanical, surgical, and systemic fracture environment can lead to delayed healing and nonunion. A comprehensive review of the advances in preventative and corrective therapeutics for bone nonunion is included next, with specific focuses on mechanical and tissue-engineered technology. Then, this work presents a tissue-engineered application of mesenchymal stem cells in acute tendon injury, highlighting experimentation in cell fate direction in vitro and intralesional mesenchymal stem cell implantation in vivo. Next, this work presents a series of experiments that evaluated and refined a commonly utilized preclinical model of delayed bone healing, the caprine segmental tibial defect stabilized using single locking plate fixation. First, the biomechanical stability of the model was evaluated in vivo using plantar-pressure analysis of gait. Then, the surgical technique was refined through a retrospective analysis of the effects of plate length and position on fixation stability in vitro and in vivo. Finally, the comorbidities of this preclinical model were explored via an analysis of the effect of long-term tibial locking plate fixation on cortical dimensions and density.

TABLE OF CONTENTS

LIST OF TABLES

LIST OF FIGURES

CHAPTER I:

DELAYED UNION AND NONUNION: CURRENT CONCEPTS, PREVENTION, AND CORRECTION

ABSTRACT

Surgical management of fractures has advanced with the incorporation of advanced technology, surgical techniques, and regenerative therapies, but delayed bone healing remains a clinical challenge and the prevalence of long bone nonunion ranges from 10 to 15% of surgically managed fractures. Delayed bone healing arises from a combination of mechanical, biological, and systemic factors acting on the site of tissue remodeling, and careful consideration of each case's injury-related, patient-dependent, surgical, and mechanical risk factors is key to successful bone union. In this review, we describe the biology and biomechanics of delayed bone healing, outline the known risk factors for nonunion development, and introduce modern preventative and corrective therapies targeting fracture nonunion.

INTRODUCTION

Surgical management of fractures has advanced with the incorporation of advanced technology, surgical techniques, and tissue-engineered, regenerative therapies, but delayed bone healing remains a clinical challenge [1]. The US Federal Drug Administration (FDA) defines fracture nonunion as persistence of a radiologically visible fracture line at 9 months post-injury [2]. In clinical practice, fractures may be treated as a nonunion as early as 6 months post-injury, and delayed healing can be detected between 3-6 months post-injury [2]. Roughly 10-15% of surgically managed fracture cases will result in nonunion. Specific nonunion rates differ depending on fracture location and fixation, but in general, these nonunion rates have remained consistent over the past 40 years despite medical and surgical advances [3-5]. In a retrospective analysis of U.S.-managed medical claims between 2005 and 2008, nonunion of an open tibial fracture was estimated to cost roughly $25,500 USD in direct medical costs and 6-12 months of work loss [6]. Nonunion patients also face risks of opioid overuse, medical-related mental illness, and persistent pain even after fracture union is achieved [7]. Despite the significant direct and indirect impacts of delayed bone healing, our understanding of fracture nonunion remains incomplete, and both preventative and corrective therapies are under development [8]. This targeted review aims to describe the biology of delayed bone healing, outline the risk factors for nonunion development, and introduce advances in prevention and corrective surgical and medical techniques targeting fracture nonunion.

THE BIOLOGY AND MECHANICS OF BONE HEALING

Successful bone healing relies on a balance of mechanical, biological, and environmental conditions. Mechanical factors include stress across the fracture gap, interfragmentary motion, gap size, and interfragmentary strains [9]. Biologic factors include site-specific vascularity, soft tissue damage, availability of osteoprogenitor cells, and hormone and growth factor concentrations at the site of injury [10]. Environmental conditions are determined by patient-dependent factors or comorbidities that can affect bone healing, such as diabetes mellitus, compartment syndrome, chronic disease, or history of smoking [11]. Modern fracture fixation and regenerative therapies target the mechanical and biological factors of bone healing to optimize healthy bone formation via primary or secondary bone healing. Primary bone healing is defined as the reunion of fractured cortices without the formation of a callus [12]. Osteoid is laid down on the

exposed cortices themselves and through intracortical remodeling, cutting cones establish new Haversian systems across the original fracture line [13]. Thus, absolute stability between the fracture fragments and substantial interfragmentary compression is necessary to achieve union, and modern compression plate fixation has optimized both conditions to promote primary fracture healing [12]. On the other hand, secondary bone healing is defined as cortical union through the formation of a callus. Instead of direct osteoid production originating from the cortices themselves, secondary bone healing relies on a profound periosteal response, stabilization of the fracture gap through periosteal callus formed via endochondral ossification, bone healing through both endochondral and intramembranous ossification, and gradual remodeling of the bridged bone to return to its original morphology [13]. A relationship between interfragmentary strain and the type of healing that a fracture undergoes has been discovered, with strains <2% typically fostering primary bone healing, 2-10% strain encouraging secondary bone union, and >10% strain predisposing fracture nonunion [14]. In general, fixed beam constructs such as locking plates elicit secondary bone healing through stable fixation without the degree of interfragmentary compression that compression plating provides [15]. However, recent research posits that the mechanics of successful bone union are dynamic, with ideal strain, hydrostatic stresses, and interfragmentary motion changing throughout the course of bone healing [10, 16-19]. This may account for similar nonunion rates between compressive and fixed beam constructs.

Surgical fracture fixation serves several mechanical functions to foster bone healing. Fixations transmit force from one end of the bone to the other, allowing for necessary load-bearing functions without excessive motion at the fracture site [15]. These constructs maintain mechanical alignment of fractured bones, preserving not only the bone's original anatomy but also the integrity of associated muscles, tendons, and neurovascular tissues [12]. Current options for surgical fracture fixation include external fixation (i.e., Ilizarov-style fixators, hexapod-style fixators, and other circular, hybrid, or linear fixators), intramedullary nail/rod fixation (i.e., reamed nailing technique, interlocking nails, and Ender nails), internal plate fixation (i.e., neutralization plating, compression plating, locking plate fixation, and point-contact fixators), screw fixation (i.e., position screws, lag screws; either alone or in combination with other internal fixators), and other internal stabilizers such as pins and wires [20-23]. As mentioned above, surgical fixation aims to stabilize the fracture zone, preserving an anabolic strain environment and protecting fragile granulation tissue, microvasculature, and new cartilage/bone remodeling at the site of injury [24]. Advances in minimally

invasive surgical techniques and periosteal-sparing fracture fixations target the biologic factors of bone healing by preserving necessary periosteal and endosteal vascular supply, minimizing disruption to the fracture hematoma and associated signaling factors and reducing infection risk at the site of injury [25, 26]. Research into the systemic, patient-associated factors that influence bone healing such as patient age, sex, concurrent diseases (i.e., diabetes mellitus, cardiovascular disease, etc.), concurrent medications, body mass index (BMI), and lifestyle choices (i.e., smoking) has aided clinical decision making and allowed for refinement of patient-specific surgical techniques [27]. Delayed bone healing and fracture nonunion can arise from any mechanical, biological, or systemic dysfunction, and careful consideration of each nonunion case's history, presentation, and risk factors will aid clinicians in determining the proper treatment plan.

CLASSIFICATIONS OF FRACTURE NONUNION

Following surgical fracture fixation, bone healing is monitored through serial clinical and radiographic evaluation, and under normal circumstances, improvement should be apparent within three months [28-30]. In general, bone healing can be considered delayed between 3 and 6 months postoperative (case-dependent), and, per FDA guidelines, surgical nonunion can be diagnosed after 9 months postoperative [2]. However, due to the multifactorial nature of bone healing and the individual characteristics of each bone, clinical nonunion may be diagnosed earlier than 9 months [29]. On serial radiographic examinations, these cases exhibit a persistent fracture line without progression toward bone union, and patients with surgical nonunion often exhibit associated pain, loss of function, and reduced mobility [28]. Further radiographic classification of nonunion was first described by Drs. Weber and Cech, who classified three general radiographic morphologies of nonunion now termed atrophic, oligotrophic, and hypertrophic nonunions (Figure 1.1; all tables and figures are placed in appendices at the end of each chapter) [8, 31, 32]. Atrophic nonunions are characterized by a lack of periosteal callus formation and are hypothesized to be associated with impaired vascularity at the fracture site [4]. Oligotrophic nonunions exhibit mild periosteal callus formation and historically were considered to have preserved vascularity but reduced osteogenesis [8]. Hypertrophic nonunions are characterized by excessive periosteal callus formation, often termed "elephant's foot" or "horse's foot," and these nonunions have been associated with fixation instability [4]. Despite widespread use of the Weber-Cech classification system in clinical practice,

inference of vascular and/or metabolic activity of an individual nonunion based on radiographic appearance should be approached with caution [4]. Histological analyses comparing atrophic, oligotrophic, and hypertrophic nonunions, have documented similarities in vascular density and connective tissue ingrowth at the fracture site, and transcriptomic analyses of various tissue samples from nonunion cases yields similar transcriptomes regardless of Weber-Cech classification [4, 8, 33]. As advances continue in patient diagnostics, especially in transcriptomic and genomic profiling, fracture nonunions may be reclassified as either mechanical or biological in origin, aiding in successful, case-specific intervention [4, 8, 34].

NONUNION RISK FACTORS

Risk factors for delayed bone healing and eventual nonunion can be injury-related, patient-dependent, surgically related, or mechanical (Figure 1.2). As with all illnesses and injuries, the systemic health of the individual patient plays a substantial role in the outcome of a medical event. Retrospective patient outcome analyses have reported that fracture nonunions may be associated with pre-existing conditions such as diabetes mellitus, cardiovascular disease, immune-mediated disorders, renal insufficiency, cancer, and other immunosuppressive conditions [4, 11, 19, 27]. Certain concurrent medications including chemotherapeutics, anticoagulants, opioids, non-steroidal anti-inflammatory medications, and anabolic steroids have been associated with delayed or arrested bone healing [4, 35, 36]. In a meta-analysis of the association between a history of smoking and surgical nonunion, Mahajan et al. confirmed a strong association between smoking and complications in bone healing, utilizing data from 12 studies published between 1999 and 2020 (both prospective and retrospective) in their analysis [37]. Patient age has been associated with nonunion but not in a linear fashion. Several studies have noted a greater incidence of tibial and femoral nonunion in younger patients, who commonly present with high-energy, comminuted, and often open fractures [7, 8, 11, 38]. However, other studies have noted increased incidence of nonunion in middle-aged patients (aged 45-65 years) or in patients of advanced age often presenting with pre-existing conditions [3, 30]. Thus, patient age may not represent a risk factor for fracture nonunion in isolation, but age-related comorbidities should be considered.

Increased patient body mass index (BMI) has been identified as a risk factor for delayed bone healing and surgical nonunion of long bone fractures [4, 27, 39]. In a retrospective analysis of nonunions following lateral locking plate fixation of distal

femoral fractures, patients classified as obese (BMI > 30) were at significantly greater risk of undergoing a secondary surgical procedure to address delayed bone healing [39]. Additionally, a link between a patient's compensable/insurance status and hospital readmission for fracture healing complications was identified in a retrospective analysis of humeral, tibial, and femoral (excluding proximal) fractures registered by the Victoria Orthopedic Trauma Outcomes Registry between 2007 and 2011 [3]. Ekegren et al. noted that patients with compensable healthcare plans were 2.43 times more likely to be treated for fracture nonunion than those using Medicare or another non-compensable plan [3]. Although patients' insurance statuses do not directly affect bone healing, there is evidence that patient socioeconomic status affects healthcare, including the treatments provided, access to providers, routine follow-up, and patient-provider interactions [40, 41]. In a qualitative research study investigating American low-socioeconomic status patients' perceptions of hospitalization, discharge, and post-hospital transition, Kangovi et al. noted poor compliance to discharge instructions due to economic constraints, availability of care, lack of targeted follow-up, and initial misalignment of patient and care team goals [42]. Thus, patient socioeconomic status can be considered a risk factor for bone healing complications leading to nonunion.

Several fracture characteristics have been identified as risk factors for complications of bone healing leading to surgical nonunion. As noted above, younger patients more often present with high-energy-impact fractures characterized by extensive comminution, marked soft tissue damage, and open fracture status [43]. Open fractures are at significantly greater risk of infection-related nonunion, particularly in cases with severe vascular damage and/or segmental bone loss [44, 45]. Several studies have identified significant associations between the risk of fracture nonunion and increasing severity of comminution, as evaluated using the AO/OTA Fracture and Dislocation Classification system described by Meinberg et al. [7, 38, 46, 47]. Further investigation into the effects of fracture configuration was conducted using finite element analysis modeling of tibia fractures stabilized using intramedullary nail fixation [11]. When all other mechanical and surgical factors were held constant, wedge and complex (marked comminution) fracture geometries exhibited excessive strain patterns that delayed simulated healing, indicating that interfragmentary mechanics could directly affect bone healing regardless of external mechanical conditions [11]. In addition, both in vitro and in vivo analysis of fracture gap following intramedullary nail fixation of long bone fractures has shown a direct relationship between increasing fracture gap and risk of delayed bone healing [11, 48, 49]. Fracture gap and segmental bone loss form the foundation for determination of critically-sized defects in clinical

fracture management and in preclinical modeling of delayed bone healing [50-52]. These injury-related risk factors are inherently connected with both surgically related risk factors and fracture mechanics in the postoperative period.

Surgical risk factors for fracture nonunion include unstable fixation and inadequate fracture reduction [11]. Determination of the appropriate implant, proper surgical techniques, and optimal postoperative rehabilitation plan for each fracture is the foundation of modern fracture research, and this review will present several preventative and corrective surgical techniques targeting nonunion complications [53]. Changes in fixation stability through screw loosening, implant breakage, or implant displacement increase the risk of delayed union and often result in necessary revision surgery [2, 54]. Mechanical factors in the postoperative period also influence the quality of bone healing. Claes et al. described correlations between the hydrostatic strain and pressure conditions of a fracture and the types of tissues that will be deposited in the fracture callus [10]. Deviatoric stresses exert directional strain across a fracture gap, stimulating fibrous tissue production, whereas hydrostatic stresses exert pressure at the fracture site, stimulating cartilage formation [10]. Mechanical overload in the form of excessive weight-bearing or localized supra-physiologic strain concentrations on the bone itself will delay healing [55, 56]. These effects can be compounded by the type and placement of fracture fixation; for example, when locking plate fixations bridging FEA-modeled tibial fracture gaps were experimentally loaded, the greatest stress concentration occurred at the screws closest to the fracture gap, and in cases of short working lengths, stress dissipation led to mechanical overload at the fracture site [57]. In addition, multi-axial loading can contribute to delayed bone healing depending on the type and stability of fracture fixation; for example, intramedullary nail (IMN) fixation is less stable than other fixation methods under torsional stresses, and torsional instability has been identified as a risk factor for nonunion in IMN cases [7, 19]. The interplay between patient-specific, surgical, mechanical, and injury-related factors will determine the success of fracture healing, and increasing understanding of these risk factors has spurred development of several techniques and devices aimed at reducing nonunion prevalence in the future.

PREVENTATIVE TECHNIQUES AND ADVANCES

Dynamization

Dynamization of fracture fixation is an increase in interfragmentary motion delivered in a controlled manner to foster secondary bone healing [58]. It is based on the

theory that while marked fixation stiffness is beneficial to stabilize the fracture hematoma and developing granulation tissue, a degree of controlled motion is necessary to promote callus maturation and endochondral ossification [58, 59]. As the use of fixed-angle constructs has increased, an association between locking plate fixations and surgical nonunion has been identified [39, 60, 61]. In an analysis of the effects of locking plate construct stiffness on fracture healing, Bottlang et al. provided both in vitro mechanical and in vivo clinical evidence that locked-plate constructs may be too stiff to consistently promote fracture healing regardless of plate length or fixation working length [62]. Thus, dynamization aims to manipulate the biomechanical conditions of the fracture site, often in accordance with the stage of fracture healing [58]. Two simple examples of fracture dynamization are an increase in fixation working length and the use of semi-rigid locking screws during locking plate fixation of experimental 10 mm distal femoral osteotomies [63]. In this model, both working length (regardless of rigid or semi-rigid locking screws) and screw type contributed to axial interfragmentary motion, and substitution of semi-rigid locking screws during locking plate fixation of fractures provided auxiliary, controlled interfragmentary motion to stimulate healing [63]. Another example of fracture dynamization is the use of far-cortical locking screws (Figure 1.3B), introducing a degree of micromotion at the near-cortex while maintaining the stability of a fixed-angle construct [60, 64] Plate dynamization has been achieved through elastically suspended locking holes (termed active locking plates) which allow screws to independently slide within a small pocket in the plate, providing axial motion without significantly depreciating construct strength (Figure 1.3C and 1.3D). Dynamization using active locking plates and semi-rigid locking screws have reported success in animal models of delayed bone healing, but currently, only the far-cortical locking screw technique has been evaluated and successful in human clinical trials [60, 65, 66]. Related clinical trials are ongoing and further development and refinement of plate dynamization is expected with the current advances in additive manufacturing [59].

Recent research in bone mechanobiology has indicated that the ideal fracture mechanical environment changes over time, moving from greater stiffness and less strain to more interfragmentary motion as the fracture callus matures [67]. Thus, temporal dynamization aims to induce appropriate interfragmentary motion in accordance with the progression of fracture healing, moving from rigid fixation to more flexible over time [24, 65]. Three general methods of temporal dynamization are either in use or being developed at this time: staged surgical interventions, modifiable external fixation, and degradable biomaterials incorporated in surgical fixations [58, 59]. Staged

surgical interventions are the most simplistic form of temporal dynamization in which an initially rigid implant is surgically manipulated after initial callus formation to induce interfragmentary motion [59]. Examples of this include removal of a distal locking screw from an IMN fixation or removing paired screws adjacent to the fracture in a locking plate fixation to increase working length [68]. Modifiable external fixation originated as a form of staged surgical intervention, in which an external fixation could be converted from a static to a dynamic state with the removal stabilizing pins, screws, and/or connecting bars [69, 70]. However, external fixators provide an opportunity for more active control of interfragmentary motion, and additional forms of dynamization including use of sliding elements, dynamized pins and screws, and other external controls have been reported in research assessing the optimal timings and degrees of dynamization during fracture healing [59, 71, 72].

Temporal dynamization of internal fixators is also under development, and, currently, the most promising modality is the use of biodegradable polymers in plate fixation. Several methods have been described including the use of a threaded degradable polymer between locking screws and plate that degrades to induce motion around the screw head and the use of degradable coatings or composites in the locking plate itself that also induces motion around the screw heads with degradation [58, 73]. The Variable Fixation Locking Screw (VFLS, Biomech Innovations) combines the concepts of far-cortical locking screws with temporal dynamization [74]. It utilizes a biodegradable poly-(lactide-co-glycolide) (PLGA) sleeve positioned below the screw head to sit within the near cortex and induce near-cortical micromotion as it degrades (Figure 1.4) [75]. Initial results of temporal dynamization have been promising in animal models but further clinical use is limited by both the questions and the risks surrounding this technology [67, 69, 75]. First, the introduction of interfragmentary motion carries an inherent risk of delayed healing due to excessive motion or interfragmentary strain during early callus formation. Repeated disruption of the fibrous and cartilaginous portions of the fracture callus will impair intramembranous ossification, and the primary goal of fracture fixation is to stabilize the fracture site to promote bone healing [24]. Thus, both the degree and timing of induced interfragmentary motion is undetermined at this time [76]. Early dynamization in a rat femoral ostectomy model resulted in no difference in osteotomy volume, tissue mineral density, or bone mineral density between temporally dynamized and flexible control specimens, suggesting no benefit of early dynamization in this model [70]. On finite element analysis of temporally dynamized ostectomies, Fu et al. also noted delayed bone healing with early dynamization (within 1 week of experimental fixation), but this

effect could be reversed if the magnitude of early dynamization (amount of motion) was decreased, resulting in enhanced bone formation and biomechanical strength of new bone [77]. Further biomechanical and preclinical research aimed at identifying proper timing and degree of dynamization is ongoing, and clinical research utilizing both static and temporal dynamization techniques are in progress.

Reverse Dynamization

As the name suggests, reverse dynamization is a theory that, in contrast to dynamization, bone healing could be enhanced through early introduction of interfragmentary motion followed by conversion to more rigid fixation [59]. This stems from the idea that callus size is directly affected by the degree of interfragmentary motion during the inflammatory phase of healing, and if a fracture is stabilized early by a larger callus, it will remodel more effectively and quickly [78]. Glatt et al. reported accelerated and improved bone healing with reverse dynamization in a rat femoral ostectomy model comparing static low-stiffness external fixators to reverse dynamized fixations in the presence of implanted bone morphogenic protein-2 (BMP-2) [79]. However, in some cases, reverse dynamization resulted in persistence of a cartilaginous union in rat femoral ostectomies treated with BMP-2, indicating that, similar to dynamization, the timing and magnitude of interfragmentary motion will affect the quality of bone healing [78]. While additional reports of improved bone healing using reverse dynamization of external fixators have been published, further research into internal fixation options for reverse dynamization as well as the biologic and mechanical processes underlying this methodology is ongoing [59, 80, 81]. At this time, publications relating to in vivo use of reverse dynamization have been limited to preclinical segmental defect models, but clinical translation of these concepts to varying fracture configurations and fixations is a promising next step [59, 80, 82].

Genomics, Transcriptomics, and Proteomics

Extensive research has described the molecular nuances of fracture healing, but recent advances in genomic, transcriptomic, and proteomic analyses has expanded our understanding of the robust interplay of genetic up- and down-regulation at the site of fracture remodeling [83-87]. For example, single-cell transcriptomic analysis has characterized the differences in regulatory gene expression between chondroclasts and osteoclasts at the site of a fracture, and it identified several highly upregulated

chondroclast genes (PSMD2, ATP5B, MT-CO1, and GLUD1) that may maintain cellular metabolic activity, thus driving endochondral ossification within a callus [84]. While extensive analysis of genomic control of bone healing is outside the scope of this review, recent research targeting genetic or transcriptional markers of fracture nonunion provide promising data for future prognostic biomarkers or perioperative treatment targets [8, 85, 88, 89]. For example, Hadjiargyrou et al. compared the microRNAome of intact bone to fracture callus and nonunion tissue samples and identified both miRNAs unique to each tissue sample and miRNAs that were co-expressed in all circumstances [8]. This data allowed them to identify target genes differentially expressed between callus and nonunion samples, and these genes could serve as future targets for osteoregenerative therapeutics [8]. Another study utilized genomic analysis to try to understand the link between diabetes mellitus (Type II) and delayed bone healing; Liu et al. identified several modules and hub genes of interest, particularly ANXA3, that may serve as prognostic biomarkers for fracture nonunion in patients with diabetes [89]. As our understanding of the genetic controls of bone healing and transcriptional alterations associated with nonunion advances, we predict that more nonunion-risk biomarkers and preventative therapeutics will be developed for clinical use.

CORRECTIVE TECHNIQUES AND ADVANCES

Exchange Nailing

Exchange nailing has been an effective treatment for surgical nonunions following IMN fixation with success rates ranging from 78% to 86% in femoral shaft nonunions [4, 90]. An exchange nailing procedure consists of removal of the indwelling nail, longitudinal drilling of the intramedullary canal, and IMN replacement with a larger-diameter nail [91]. The thicker nail improves the biomechanical stability of fixation, and the reaming procedure stimulates both inflammatory and regenerative cell migration to the site of injury through vascular and tissue damage [4]. Exchange nailing is a relatively simple surgical procedure that does not expose the fracture site, it typically elicits minimal blood loss, and hospital stays for an exchange nail procedure are relatively short [43]. However, careful case selection is key to success as exchange nailing procedures alone have poor union rates in cases of septic nonunion or excessive fracture gaps (>5mm) [43, 91].

Intramedullary reaming represents a key step in exchange nailing, and it is often incorporated into original IMN surgical fixation as well [92]. However, the balance

between benefits and risks incurred by intramedullary reaming remains debated today [92]. Intramedullary reaming disrupts the endosteal blood supply to the bone in question through direct vascular damage and penetration of the central venous sinus within the medullary cavity [93]. Vascular injury directly stimulates tissue regeneration through chemotaxis of inflammatory cells and mediators, but for a period of time, vascular supply to the bone is impaired, driving rapid reorientation of blood flow to the periosteum [93]. Concerns regarding both compressive and thermal damage during reaming have been voiced, and risk of systemic embolization of bone marrow via venous outflow during reaming has been reported [93-95]. However, the value of intramedullary reaming to optimize bone-nail congruence and maximize fixation stability cannot be understated [93, 94]. At this time, consensus regarding the use of intramedullary reaming in initial IMN fixation has not been reached, and the majority of clinical studies display marked statistical fragility, with merely one or two event reversals necessary to reverse a binary conclusion [92]. On the other hand, intramedullary reaming during exchange nailing has been refined and augmented over time, serving as a valuable debridement tool for septic nonunions and a delivery method for intramedullary lavage and antibiotic therapy [96]. Clinical research utilizing exchange nailing in conjunction with biologic and regenerative therapies is ongoing and offers promising future paths for the treatment of both aseptic and septic nonunions [91, 96, 97].

Nail Dynamization

Nail dynamization involves the removal of proximally or distally locked screws from an intramedullary nail fixation to introduce a degree of interfragmentary motion at the fracture site [98]. As discussed above, this procedure can be staged as a preventative measure or enacted as a treatment for diagnosed delayed healing [4]. It represents a relatively simple and inexpensive treatment option for delayed bone healing, and historically, success rates following nail dynamization in tibial and femoral shaft nonunions (between 2011 and 2014) were reported between 55 and 65% [99]. In clinical practice, nail dynamization may be elected as an early intervention for cases with delayed bone healing and if bone union is not achieved, more invasive procedures such as exchange nailing may be warranted [100]. As with prophylactic dynamization, nail dynamization procedures carry risks of excessive motion at the fracture site, resulting in fixation failure, fracture shortening, and/or refracture [4, 99]. Modern advances in nail dynamization have centered around supplementary therapies such as

shock wave to improve bone healing following the dynamization procedure, but recent clinical studies have confirmed the value of nail dynamization as an early intervention for delayed bone healing, reporting improved success rates of 75-85% in tibial and femoral fracture cases [100-102].

Augmentation Plating

Augmentation plating describes the addition of an orthopedic plate to a pre-existing fracture fixation (most often IMN) to enhance stability and interfragmentary compression [103]. Augmentation plating can be used alone or in combination with exchange nailing, bone grafts, and/or other biologic therapeutics [4, 103, 104]. Since it is so versatile, success rates for union following augmentation plating vary based on the chosen methodology, but in a retrospective review of patients diagnosed with femoral shaft nonunion following IMN fixation and treated with plate augmentation (both dynamic compression and locking plates utilized), Uliana et al. reported an 86% union rate and excellent patient pain and mobility scores over two years of follow-up [105]. Similar successes in treating femoral nonunion with either locking or compressive augmentation plates has been reported in other prospective and retrospective analyses, and this modality has become increasingly popular in the management of femoral nonunion [106-108].

Strain Reduction Screws

Similar to augmentation plating, the use of strain reduction screws in the treatment of surgical nonunion avoids the removal of the initial fixation [109]. It involves the placement of standard cortical screws across a nonunion site to induce interfragmentary compression and reduce local strains [109]. Currently, clinical reports utilizing strain reduction screws are few, with use limited almost exclusively to lower limb aseptic nonunions [109-111]. However, clinical success has been reported following strain reduction screw placement across hypertrophic humeral nonunions in which the initial fixation exhibited no loss of stability [109]. Further large-scale clinical research is necessary to confirm the clinical efficacy of strain reduction screws and establish their indication for use, but this technique offers a promising minimally invasive option for surgical nonunion treatment.

External Fixation

External fixators are highly customizable and stable fixations that are widely used to treat surgical nonunion, particularly in cases of septic nonunion [112]. They operate percutaneously, and surgical stabilization using an external fixator results in minimal soft tissue and periosteal trauma [112]. External fixator designs allow for a wide range of mechanical stabilization, from linear, unilateral stabilization to circular, multiaxial support, and external fixators can be manipulated to act as fixed beam, compressive, or dynamized constructs [4, 71, 72]. External fixators are particularly suited for cases involving severe soft tissue damage, excessive bone loss, and/or infection [113]. Their versatility allows for staged soft tissue and bone reconstruction procedures, and percutaneous fixation minimizes the risk of implant-related bacterial dissemination or biofilm formation [112, 114]. Recent studies have highlighted the utility of the Ilizarov technique of external fixation, which utilizes the theory of distraction osteogenesis and applies controlled tensile stress to a fracture or nonunion site to encourage tissue regeneration [115]. Ilizarov external fixators stabilize and promote healing of large bone defects formed by high impact trauma, extensive resection of infected tissue, or osteotomy to address fracture shortening [115-117]. Although limited by surgical complexity, long treatment times, and general inconvenience to the patient, Ilizarov external fixators have reported success rates ranging from 76% to 100% in clinical case reports of long bone septic nonunion both as solo fixations and in conjunction with other nonunion treatments such as exchange nailing or bone grafting [115].

Bone Grafts

Bone grafts are widely used in the treatment of surgical nonunion with treatments ranging from cancellous autografts for osteoinduction and revascularization of an atrophic nonunion to large cortical allographs for osteoconduction and bridging of critically sized defect [104, 118]. While extensive discussion of bone grafting is outside of the scope for this review, we aim to highlight current advances and discussions related to bone graft treatment of surgical nonunions. To start, the topic of graft vascularization stems from a long-standing limitation of bone grafts, particularly allografts, in that the grafted bone lacks blood supply in the implantation site [118, 119]. The majority of grafted bone will necrose, serving more signaling and scaffold functions than direct incorporation, and impaired vascularity or diminished osteoprogenitor cell

populations at the implant site predispose the patient to graft failure or rejection [118, 119]. The use of vascularized autografts involves careful preservation of the graft's nutrient, metaphyseal, or other perforating vessel for anastomosis at the implant site. If the blood supply is preserved, the graft may incorporate by either primary or secondary bone healing, and vascularized bone grafts deliver donor osteocytes and osteoprogenitor cells more effectively than non-vascularized autografts [118, 120]. However, the balance between osteoinductive benefits of vascular grafting versus the technical difficulty and intensity of the procedure has been debated, spurring several recent, large-scale meta-analyses and systematic reviews of vascularized bone grafts to treat scaphoid nonunion [121-123]. These reviews documented favorable results of vascularized bone grafts (more rapid bone union) in cases with poor prognostic indicators such as systemic disease or avascular necrosis of the scaphoid [122, 123]. However, functional results were not as uniformly favorable, and questions remain as to the functional advantage of vascularized bone grafts over non-vascularized grafts in scaphoid nonunions [121].

Currently, the use of vascularized bone grafts is limited by donor site availability and graft viability during auto- or allotransplantation [118]. However, recently, Visser et al. described a technique for revascularization of cryopreserved bone allografts involving surgical placement of the host cranial tibial arteriovenous bundle within the intramedullary canal of the donor tissue (porcine tibia model) [119]. The goal was to supply and utilize the vascular channels already present within the graft tissue to encourage direct revascularization and incorporation of the graft. Seven of eight tibial defects treated with revascularized cryopreserved grafts healed within the 20-week experimental period, as compared to four of eight control defects treated with traditional cryopreserved grafts [119]. However, no differences in bone mineral density or biomechanical characteristics were noted between experimental and control bones, suggesting that while revascularization does not seem to impair bone healing, it cannot be proven to enhance bone density or strength from this study alone [119]. This theory of graft revascularization is a promising subject for future research and refinement and may address limitations such as donor site morbidity, graft availability, and graft rejection.

Tissue Engineering

As with bone grafts, extensive discussion of the numerous bioactive biomaterials, tissue regenerative therapeutics, and cell therapies developed to augment bone healing

is outside of the scope of this review. However, we would like to highlight some of the modern focuses of regenerative research targeting surgical nonunion. The field of regenerative bone biomaterials has undergone expansive growth in the last two decades following the approval of calcium phosphate cement for clinical use [124, 125]. Ceramic-, polymeric-, and composite- based bone biomaterials have been developed to serve numerous functions including osteoconductive filling of bone gaps, drug/hormone delivery, cellular activity direction, and extracellular matrix templating [124]. Bone biomaterials have been used to deliver concentrated and controlled doses of known anabolic (ie. parathyroid hormone analogues and bone morphogenic protein analogues) and anti-catabolic (ie. bisphosphonates, calcitonin, denosumab, and estrogen) therapeutics to the sites of nonunion, and modern considerations for bone biomaterial fabrication are presented in Figure 1.5 [124, 126-128]. Recent research regarding the use of teriparatide, a synthetic recombinant parathyroid hormone, delivered via a degradable biomaterial for the treatment of fracture nonunions has shown favorable results in both preclinical and clinical trials [127, 129]. Further development, refinement, and clinical evaluation of bone biomaterials for use in surgical nonunion cases is ongoing, and more commercial approval and widespread use is expected in the near future [125].

Stem cell therapy (alternatively termed stromal cell therapy) is another modality used in combination with other stabilizing and/or reconstructive procedures to address surgical nonunion [130, 131]. Similar to bone biomaterials, there are numerous types of cell therapies currently under research, varying in origin, cellular processing, preconditioning, delivery method, and supplementation (ie. co-delivery with growth factors or chemokines) [130, 132]. Despite the heterogeneity of treatment options, promising clinical results of stem cell therapy as a nonunion treatment have been reported [133]. Following implantation of autologous expanded human mesenchymal stromal cells (MSC) from bone marrow using a bioceramic delivery device to treat long bone nonunions; femoral, humeral, and tibial nonunions exhibited rapid, effective bone union following implantation with a 92.8% success rate at 12 months postoperative [133]. In another case series evaluating a combination therapy using autologous stomal cells loaded on collagen microspheres and delivered via platelet-rich plasma clots, rapid and effective bone union was seen following both tibial and femoral applications of the novel therapeutic [134]. However, the clinical efficacy of stem cell therapy in nonunion cases remains questionable, with no consensus as to the source, dosage, processing, or delivery of cells [130-132]. Current research exploring the paracrine effects of cell therapy and evaluating the efficacy of MSC exosome implantation aims to further refine

the therapeutic, and further development of cell therapy for clinical use is ongoing [130, 135].

CONCLUSIONS

Delayed healing and nonunion remain clinical challenges in the surgical management of fractures with nonunion prevalence ranging from 10 to 15% of fracture cases and costs associated with care averaging roughly $25,500 USD. Delayed bone healing arises from a combination of mechanical, biologic, and systemic factors acting on the site of tissue remodeling, and careful consideration of each case's injury-related, patient-dependent, surgical, and mechanical risk factors is key to successful bone union. Recent advances in fixation dynamization, both static and temporal, and reverse dynamization have the potential to reduce nonunion prevalence upon future refinement and implementation, and discoveries in the genomic, transcriptomic, and proteomic profiles of bone nonunion may direct development of risk-biomarkers and targeted therapeutics for delayed healing. Modern treatments for nonunion include exchange nailing, nail dynamization, augmentation plating, strain reduction screw placement, bone grafting, and external fixation. These modalities can be augmented by tissue engineered therapeutics including bioactive biomaterials, stem cell therapy, anabolic therapies, and anti-catabolic therapies. Thus, modern advances in the mechanics of fracture management combined with tissue engineering and biomaterial innovations provide promising options for both the prevention and treatment of surgical nonunions.

REFERENCES

1. Schlundt, C., et al., *Clinical and Research Approaches to Treat Non-union Fracture.* Curr Osteoporos Rep, 2018. **16**(2): p. 155-168.
2. Rupp, M., et al., *Do Systemic Factors Influence the Fate of Nonunions to Become Atrophic? A Retrospective Analysis of 162 Cases.* Biomed Res Int, 2019. **2019**: p. 6407098.
3. Ekegren, C.L., et al., *Incidence, Costs and Predictors of Non-Union, Delayed Union and Mal-Union Following Long Bone Fracture.* Int J Environ Res Public Health, 2018. **15**(12).
4. Rupp, M., et al., *Diaphyseal long bone nonunions - types, aetiology, economics, and treatment recommendations.* Int Orthop, 2018. **42**(2): p. 247-258.
5. Castillo, I.A., et al., *Where are we in 2022? A Summary of 11,000 Open Tibia Fractures over Four Decades.* J Orthop Trauma, 2023.
6. Antonova, E., et al., *Tibia shaft fractures: costly burden of nonunions.* BMC Musculoskeletal Disorders, 2013. **14**(1): p. 42.
7. Dailey, H.L., et al., *Tibial Fracture Nonunion and Time to Healing After Reamed Intramedullary Nailing: Risk Factors Based on a Single-Center Review of 1003 Patients.* J Orthop Trauma, 2018. **32**(7): p. e263-e269.
8. Hadjiargyrou, M., L. Salichos, and P. Kloen, *Identification of the miRNAome in human fracture callus and nonunion tissues.* J Orthop Translat, 2023. **39**: p. 113-123.
9. Hu, J., et al., *Spatial Bridge Locking Fixator versus Traditional Locking Plates in Treating AO/OTA 32-A3.2 Fracture: Finite Element Analysis and Biomechanical Evaluation.* Orthopaedic Surgery, 2022. **14**(8): p. 1638-1648.
10. Claes, L.E. and C.A. Heigele, *Magnitudes of local stress and strain along bony surfaces predict the course and type of fracture healing.* J Biomech, 1999. **32**(3): p. 255-66.
11. Ren, T. and H.L. Dailey, *Mechanoregulation modeling of bone healing in realistic fracture geometries.* Biomechanics and Modeling in Mechanobiology, 2020. **19**(6): p. 2307-2322.
12. Augat, P. and C. von Rüden, *Evolution of fracture treatment with bone plates.* Injury, 2018. **49**: p. S2-S7.
13. Bigham-Sadegh, A. and A. Oryan, *Basic concepts regarding fracture healing and the current options and future directions in managing bone fractures.* International Wound Journal, 2015. **12**(3): p. 238-247.
14. Egol, K.A., et al., *Biomechanics of locked plates and screws.* J Orthop Trauma, 2004. **18**(8): p. 488-93.
15. Larson, A.N. and M. Rizzo, *Locking plate technology and its applications in upper extremity fracture care.* Hand Clin, 2007. **23**(2): p. 269-78, vii.
16. Kim, S.D., O.J. Sohn, and B.H. Kwack, *The Comparison of LC-DCP versus LCP Fixation in the Plate Augmentation for the Nonunion of Femur Shaft Fractures after Intramedullary Nail Fixation.* jkfs, 2008. **21**(2): p. 117-123.
17. Hasami, N.A., et al., *Operative Fixation of Lateral Malleolus Fractures With Locking Plates vs Nonlocking Plates: A Systematic Review and Meta-analysis.* Foot Ankle Int, 2022. **43**(2): p. 280-290.
18. Fu, P., et al., *Optimal surgical treatment for periprosthetic distal femoral fractures after total knee arthroplasty: a Bayesian-based network analysis.* J Orthop Surg Res, 2023. **18**(1): p. 122.
19. Neradi, D., et al., *Locked Plating Versus Retrograde Intramedullary Nailing for Distal Femur Fractures: a Systematic Review and Meta-Analysis.* Arch Bone Jt Surg, 2022. **10**(2): p. 141-152.
20. Bliven, E.K., et al., *External fixation of the lower extremities: Biomechanical perspective and recent innovations.* Injury, 2019. **50 Suppl 1**: p. S10-s17.

21. Xiong, R., et al., *Intramedullary nailing for femoral shaft fractures in adults.* The Cochrane Database of Systematic Reviews, 2018. **2018**(2): p. CD010524.
22. Uhthoff, H.K., P. Poitras, and D.S. Backman, *Internal plate fixation of fractures: short history and recent developments.* Journal of Orthopaedic Science, 2006. **11**(2): p. 118-126.
23. Taljanovic, M.S., et al., *Fracture fixation.* Radiographics, 2003. **23**(6): p. 1569-90.
24. Glatt, V., C.H. Evans, and K. Tetsworth, *A Concert between Biology and Biomechanics: The Influence of the Mechanical Environment on Bone Healing.* Frontiers in Physiology, 2017. **7**.
25. Moens, N.M.M., *The Biology of Locking Plate Applications*, in *Locking Plates in Veterinary Orthopedics*. 2018. p. 13-24.
26. Schmierer, P. and A. Pozzi, *Minimally Invasive Plate Osteosynthesis*, in *Locking Plates in Veterinary Orthopedics*. 2018. p. 41-50.
27. Wang, M.T., V.V.G. An, and B.S. Sivakumar, *Non-union in lateral locked plating for distal femoral fractures: A systematic review.* Injury, 2019. **50**(11): p. 1790-1794.
28. Bishop, J.A., et al., *Assessment of compromised fracture healing.* J Am Acad Orthop Surg, 2012. **20**(5): p. 273-82.
29. Kostenuik, P. and F.M. Mirza, *Fracture healing physiology and the quest for therapies for delayed healing and nonunion.* J Orthop Res, 2017. **35**(2): p. 213-223.
30. Hak, D.J., et al., *Delayed union and nonunions: epidemiology, clinical issues, and financial aspects.* Injury, 2014. **45 Suppl 2**: p. S3-7.
31. Weber, B.G. and O. Cech, *Pseudarthrosis: pathophysiology, biomechanics, therapy, results*, in *Pseudarthrosis: pathophysiology, biomechanics, therapy, results*. 1976. p. 323-323.
32. Kloen, P., et al., *Bridging the gap: Compressing non-unions for proper cellular signaling.* Medical Hypotheses, 2022. **160**: p. 110794.
33. Bajada, S., et al., *Decreased osteogenesis, increased cell senescence and elevated Dickkopf-1 secretion in human fracture non union stromal cells.* Bone, 2009. **45**(4): p. 726-35.
34. Chen, H., et al., *miR-628-3p regulates osteoblast differentiation by targeting RUNX2: Possible role in atrophic non-union.* International Journal of Molecular Medicine, 2017. **39**(2): p. 279-286.
35. Liang, C., et al., *The Impact of Injury of the Tibial Nutrient Artery Canal on Type of Nonunion of Tibial Shaft Fractures: A Retrospective Computed Tomography Study.* Acad Radiol, 2023.
36. Al Farii, H., et al., *The effect of NSAIDs on postfracture bone healing: a meta-analysis of randomized controlled trials.* OTA Int, 2021. **4**(2): p. e092.
37. Mahajan, A., N. Kumar, and B. Gupta, *Delayed Tibial Shaft Fracture Healing Associated with Smoking: A Systematic Review and Meta-Analysis of Observational Studies Conducted Worldwide.* Int J Environ Res Public Health, 2021. **18**(19).
38. Mundi, R., et al., *Association of Three-Month Radiographic Union Score for Tibia Fractures (RUST) with Nonunion in Tibial Shaft Fracture Patients.* Cureus, 2020. **12**(5): p. e8314.
39. Rodriguez, E.K., et al., *Predictive factors of distal femoral fracture nonunion after lateral locked plating: a retrospective multicenter case-control study of 283 fractures.* Injury, 2014. **45**(3): p. 554-9.
40. Arpey, N.C., A.H. Gaglioti, and M.E. Rosenbaum, *How socioeconomic status affects patient perceptions of health care: a qualitative study.* Journal of primary care & community health, 2017. **8**(3): p. 169-175.
41. Kangovi, S., et al., *Understanding why patients of low socioeconomic status prefer hospitals over ambulatory care.* Health affairs, 2013. **32**(7): p. 1196-1203.
42. Kangovi, S., et al., *Challenges Faced by Patients with Low Socioeconomic Status During the Post-Hospital Transition.* Journal of General Internal Medicine, 2014. **29**(2): p. 283-289.
43. Tsang, S.T., et al., *Exchange nailing for nonunion of diaphyseal fractures of the tibia: our results and an analysis of the risk factors for failure.* Bone Joint J, 2016. **98-b**(4): p. 534-41.

44. Struijs, P.A., R.W. Poolman, and M. Bhandari, *Infected nonunion of the long bones.* Journal of orthopaedic trauma, 2007. **21**(7): p. 507-511.
45. Harvin, W.H., et al., *Working length and proximal screw constructs in plate osteosynthesis of distal femur fractures.* Injury, 2017. **48**(11): p. 2597-2601.
46. Meinberg, E.G., et al., *Fracture and Dislocation Classification Compendium-2018.* J Orthop Trauma, 2018. **32 Suppl 1**: p. S1-s170.
47. Kawasaki, N., et al., *Prediction of delayed union of tibial shaft fracture treated with intramedullary nailing: multicenter-study analysis and literature review -the TRON study.* Eur J Orthop Surg Traumatol, 2022. **32**(1): p. 129-135.
48. Nakagawa, T., et al., *Effect of postoperative fracture gap on bone union: A retrospective cohort analysis of simple femoral shaft fractures.* Journal of Orthopaedic Science, 2023.
49. McMillan, T.E. and A.J. Johnstone, *Technical considerations to avoid delayed and non-union.* Injury, 2017. **48 Suppl 1**: p. S64-s68.
50. Reichert, J.C., et al., *The challenge of establishing preclinical models for segmental bone defect research.* Biomaterials, 2009. **30**(12): p. 2149-2163.
51. Schemitsch, E.H., *Size matters: defining critical in bone defect size!* Journal of orthopaedic trauma, 2017. **31**: p. S20-S22.
52. Huang, E.E., et al., *Novel techniques and future perspective for investigating critical-size bone defects.* Bioengineering, 2022. **9**(4): p. 171.
53. Murphy, D., et al., *Modern management of paediatric tibial shaft fractures: an evidence-based update.* European Journal of Orthopaedic Surgery & Traumatology, 2021. **31**(5): p. 901-909.
54. Maresca, A., et al., *Why a surgically treated humeral shaft fracture became a nonunion: review of 11 years in two trauma centers.* Musculoskelet Surg, 2017. **101**(Suppl 2): p. 105-112.
55. Orth, M., et al., *Simulation-based prediction of bone healing and treatment recommendations for lower leg fractures: Effects of motion, weight-bearing and fibular mechanics.* Front Bioeng Biotechnol, 2023. **11**: p. 1067845.
56. Liu, C., et al., *Effects of mechanical loading on cortical defect repair using a novel mechanobiological model of bone healing.* Bone, 2018. **108**: p. 145-155.
57. Giordano, V., et al., *Mind the gap between the fracture line and the length of the working area: a 2-D finite element analysis using an extramedullary fixation model.* Revista Brasileira de Ortopedia (English Edition), 2018. **53**(1): p. 88-93.
58. Schultz, B.J., et al., *Locking Screws With a Threaded Degradable Polymer Collar Reduce Construct Stiffness Over Time.* J Orthop Trauma, 2020. **34**(3): p. 151-157.
59. Schmidt, E.C., et al., *Current concepts in fracture healing: temporal dynamization and applications for additive manufacturing.* OTA Int, 2022. **5**(1 Suppl): p. e164.
60. Henschel, J., et al., *Comparison of 4 Methods for Dynamization of Locking Plates: Differences in the Amount and Type of Fracture Motion.* Journal of Orthopaedic Trauma, 2017. **31**(10): p. 531-537.
61. Rodriguez, E.K., et al., *Mechanical Construct Characteristics Predisposing to Non-union After Locked Lateral Plating of Distal Femur Fractures.* J Orthop Trauma, 2016. **30**(8): p. 403-8.
62. Bottlang, M., et al., *Effects of Construct Stiffness on Healing of Fractures Stabilized with Locking Plates.* Journal of Bone and Joint Surgery, 2010. **92**(Supplement_2): p. 12-22.
63. Heyland, M., et al., *Semi-rigid screws provide an auxiliary option to plate working length to control interfragmentary movement in locking plate fixation at the distal femur.* Injury, 2015. **46 Suppl 4**: p. S24-32.
64. Bottlang, M. and F. Feist, *Biomechanics of Far Cortical Locking.* Journal of Orthopaedic Trauma, 2011. **25**(Supplement 1): p. S21-S28.

65. Bottlang, M., et al., *Dynamic Stabilization of Simple Fractures With Active Plates Delivers Stronger Healing Than Conventional Compression Plating.* J Orthop Trauma, 2017. **31**(2): p. 71-77.
66. Seo, J.-B., et al., *Assessment of the efficacy of the far cortical locking technique in proximal humeral fractures: a comparison with the conventional bi-cortical locking technique.* BMC Musculoskeletal Disorders, 2020. **21**(1).
67. Willie, B.M., et al., *Temporal variation in fixation stiffness affects healing by differential cartilage formation in a rat osteotomy model.* Clinical Orthopaedics and Related Research®, 2011. **469**: p. 3094-3101.
68. Yang, K.-H., C.-H. Lee, and Y.-C. Park, *Effect of Interlocking Mode on the Outcomes of Exchange Nailing for the Treatment of Aseptic Femoral Shaft Nonunion.* Clinics in Orthopedic Surgery, 2023. **15**(1): p. 13.
69. Durall, I., et al., *Effects of Static Fixation and Dynamization after Interlocking Femoral Nailing Locked with an External Fixator: An Experimental Study in Dogs.* Veterinary Surgery, 2004. **33**(4): p. 323-332.
70. Claes, L., et al., *Early dynamization by reduced fixation stiffness does not improve fracture healing in a rat femoral osteotomy model.* Journal of Orthopaedic Research, 2009. **27**(1): p. 22-27.
71. Iobst, C.A., et al., *A novel way to dynamize a spatial frame and optimize fracture healing.* Injury, 2021. **52**(1): p. 106-108.
72. Faria, F.F., et al., *Finite Element Analysis of a Controlled Dynamization Device for External Circular Fixation.* Rev Bras Ortop (Sao Paulo), 2021. **56**(1): p. 36-41.
73. Hutchinson, D.J., et al., *Highly Customizable Bone Fracture Fixation through the Marriage of Composites and Screws.* Advanced Functional Materials, 2021. **31**(41): p. 2105187.
74. Frank, A., et al., *Variable Fixation Technology Provides Rigid as Well as Progressive Dynamic Fixation: A Biomechanical Investigation.* J Bone Joint Surg Am, 2020. **102**(20): p. e115.
75. Plecko, M., et al., *Variable fixation promotes callus formation: an experimental study on transverse tibial osteotomies stabilized with locking plates.* BMC Musculoskeletal Disorders, 2020. **21**(1).
76. Schultz, B.J., et al., *Controversies in Fracture Healing: Early Versus Late Dynamization.* Orthopedics, 2020. **43**(3): p. e125-e133.
77. Fu, R., et al., *The combined effects of dynamization time and degree on bone healing.* Journal of Orthopaedic Research, 2022. **40**(3): p. 634-643.
78. Glatt, V., et al., *Reverse Dynamization.* Journal of Bone and Joint Surgery, 2016. **98**(8): p. 677-687.
79. Glatt, V., et al., *Improved Healing of Large Segmental Defects in the Rat Femur by Reverse Dynamization in the Presence of Bone Morphogenetic Protein-2.* The Journal of Bone and Joint Surgery-American Volume, 2012. **94**(22): p. 2063-2073.
80. Glatt, V., et al., *Reverse Dynamization Accelerates Bone-Healing in a Large-Animal Osteotomy Model.* J Bone Joint Surg Am, 2021. **103**(3): p. 257-263.
81. Evans, C.H., *Improved Healing of Large, Osseous, Segmental Defects by Reverse Dynamization: Evaluation in a Sheep Model*. 2017, Mayo Clinic Mayo Clinic United States.
82. Glatt, V., S. Tepic, and C. Evans, *Reverse dynamization: a novel approach to bone healing.* JAAOS-Journal of the American Academy of Orthopaedic Surgeons, 2016. **24**(7): p. e60-e61.
83. Tsiridis, E. and P.V. Giannoudis, *Transcriptomics and proteomics: advancing the understanding of genetic basis of fracture healing.* Injury, 2006. **37**(1): p. S13-S19.
84. Khan, N.M., et al., *Comparative transcriptomic analysis identifies distinct molecular signatures and regulatory networks of chondroclasts and osteoclasts.* Arthritis Research & Therapy, 2020. **22**(1).
85. Avin, K.G., et al., *Single-cell RNAseq provides insight into altered immune cell populations in human fracture nonunions.* Journal of Orthopaedic Research®, 2022.

86. Hadjiargyrou, M., et al., *Transcriptional Profiling of Bone Regeneration: INSIGHT INTO THE MOLECULAR COMPLEXITY OF WOUND REPAIR* 210.* Journal of Biological Chemistry, 2002. **277**(33): p. 30177-30182.
87. Bow, A.J., et al., *Temporal metabolic profiling of bone healing in a caprine tibia segmental defect model.* Frontiers in Veterinary Science, 2023. **9**.
88. Zheng, N., et al., *Magnesium facilitates the healing of atypical femoral fractures: A single-cell transcriptomic study.* Materials Today, 2022. **52**: p. 43-62.
89. Liu, C., et al., *Identification of Up-Regulated ANXA3 Resulting in Fracture Non-Union in Patients With T2DM.* Frontiers in Endocrinology, 2022. **13**.
90. Naeem-ur-Razaq, M., M. Qasim, and S. Sultan, *Exchange nailing for non-union of femoral shaft fractures.* J Ayub Med Coll Abbottabad, 2010. **22**(3): p. 106-9.
91. Bhan, K., et al., *Reamed Exchange Nailing in Nonunion of Tibial Shaft Fractures: A Review of the Current Evidence.* Cureus, 2020.
92. Minhas, A., et al., *The statistical fragility of intramedullary reaming in tibial nail fixation: a systematic review.* Eur J Trauma Emerg Surg, 2023.
93. Pfeifer, R., R. Sellei, and H.C. Pape, *The biology of intramedullary reaming.* Injury, 2010. **41 Suppl 2**: p. S4-8.
94. Kostic, I., M. Mitkovic, and M. Mitkovic, *The diaphyseal aseptic tibial nonunions after failed previous treatment options managed with the reamed intramedullary locking nail.* J Clin Orthop Trauma, 2019. **10**(1): p. 182-190.
95. Schemitsch, E.H., et al., *Pulmonary and systemic fat embolization after medullary canal pressurization: a hemodynamic and histologic investigation in the dog.* J Trauma, 1998. **45**(4): p. 738-42.
96. Zhang, H.-A., et al., *Intramedullary reaming and irrigation and antibiotic-loaded calcium sulfate implantation for the treatment of infection after intramedullary nailing: a retrospective study of 19 cases.* BMC Musculoskeletal Disorders, 2020. **21**(1).
97. Wu, C.-C., *Aseptic femoral nonunion treated with exchange locked nailing with intramedullary augmentation cancellous bone graft.* Journal of Orthopaedic Surgery and Research, 2022. **17**(1).
98. Perumal, R., et al., *Is nail dynamization beneficial after twelve weeks – An analysis of 37 cases.* Journal of Clinical Orthopaedics and Trauma, 2018. **9**(4): p. 322-326.
99. Vaughn, J., et al., *Nail Dynamization for Delayed Union and Nonunion in Femur and Tibia Fractures.* Orthopedics, 2016. **39**(6): p. e1117-e1123.
100. Vaughn, J.E., et al., *Systematic review of dynamization vs exchange nailing for delayed/non-union femoral fractures.* World Journal of Orthopedics, 2018. **9**(7): p. 92-99.
101. Stolberg-Stolberg, J., et al., *Addition of shock wave therapy to nail dynamization increases the chance of long-bone non-union healing.* Journal of Orthopaedics and Traumatology, 2022. **23**(1).
102. Ali, P., et al., *Effects of Dynamization on Delayed Union of Tibial Shaft Fractures After Reamed Intramedullary Interlocked Nailing.* Annals of Jinnah Sindh Medical University, 2023. **8**(2): p. 59-63.
103. Zhang, W., et al., *Clinical outcomes of femoral shaft non-union: dual plating versus exchange nailing with augmentation plating.* Journal of Orthopaedic Surgery and Research, 2018. **13**(1).
104. Mohamed, M.A., et al., *Plate augmentation and bone grafting in treatment of femoral shaft nonunion initially fixed by intramedullary nail.* SICOT-J, 2022. **8**: p. 19.
105. Uliana, C.S., et al., *Augmentation plating leaving the nail in situ is an excellent option for treating femoral shaft nonunion after IM nailing: a multicentre study.* European Journal of Trauma and Emergency Surgery, 2021. **47**(6): p. 1895-1901.
106. Perisano, C., et al., *Plate Augmentation in Aseptic Femoral Shaft Nonunion after Intramedullary Nailing: A Literature Review.* Bioengineering (Basel), 2022. **9**(10).

107. Jhunjhunwala, H.R. and A.A. Dhawale, *Is augmentation plating an effective treatment for non-union of femoral shaft fractures with nail in situ?* European Journal of Trauma and Emergency Surgery, 2016. **42**(3): p. 339-343.
108. Siavashi, B., et al., *The Effect of Augmentative Plating for the Treatment of Nonunion of Femoral Shaft Fractures after Intramedullary Nailing: A Case Series.* Journal of Orthopedic and Spine Trauma, 2022.
109. Bellringer, S.F., et al., *Strain reduction screws for nonunions following fixation around the elbow - A case series and review of the literature.* J Clin Orthop Trauma, 2023. **38**: p. 102129.
110. Bence, M., et al., *Percutaneous Strain Reduction Screws Are a Reproducible Minimally Invasive Method to Treat Long Bone Nonunion.* J Orthop Trauma, 2022. **36**(9): p. e343-e348.
111. Kothari, A., P. Monk, and R. Handley, *Percutaneous Strain Reduction Screws-A Safe and Simple Surgical Option for Problems With Bony Union. A Technical Trick.* J Orthop Trauma, 2019. **33**(4): p. e151-e157.
112. Simpson, A., et al., *Non-union: Indications for external fixation.* Injury, 2019. **50 Suppl 1**: p. S73-s78.
113. Yin, P., et al., *The treatment of infected tibial nonunion by bone transport using the Ilizarov external fixator and a systematic review of infected tibial nonunion treated by Ilizarov methods.* Acta Orthop Belg, 2014. **80**(3): p. 426-35.
114. Giannoudis, P.V., et al., *Masquelet technique for the treatment of bone defects: tips-tricks and future directions.* Injury, 2011. **42**(6): p. 591-8.
115. Li, J., et al., *Evolution and Development of Ilizarov Technique in the Treatment of Infected Long Bone Nonunion with or without Bone Defects.* Orthopaedic Surgery, 2022. **14**(5): p. 824-830.
116. Borzunov, D.Y. and S.N. Kolchin, *Nonunion of the femoral shaft associated with limb shortening treated with a combined technique of external fixation over an intramedullary nail versus the Ilizarov method.* Archives of Orthopaedic and Trauma Surgery, 2022. **142**(9): p. 2185-2192.
117. Borzunov, D.Y., S.N. Kolchin, and T.A. Malkova, *Role of the Ilizarov non-free bone plasty in the management of long bone defects and nonunion: Problems solved and unsolved.* World J Orthop, 2020. **11**(6): p. 304-318.
118. Roberts, T.T. and A.J. Rosenbaum, *Bone grafts, bone substitutes and orthobiologics.* Organogenesis, 2012. **8**(4): p. 114-124.
119. Visser, N., et al., *The effect of surgical revascularization on the mechanical properties of cryopreserved bone allograft in a porcine tibia model.* J Orthop Res, 2023. **41**(4): p. 815-822.
120. Winocour, S.J., et al. *Vascularized Posterior Iliac Crest Bone Grafting: Indications, Techniques, Clinical Outcomes, and Alternatives*. in *Seminars in plastic surgery*. 2021. Thieme Medical Publishers, Inc.
121. Zhang, H., et al., *Pedicled vascularized versus non-vascularized bone grafts in the treatment of scaphoid non-union: a meta-analysis of comparative studies.* ANZ Journal of Surgery, 2021. **91**(11): p. E682-E689.
122. Tsantes, A., et al., *The Efficacy of Vascularized Bone Grafts in the Treatment of Scaphoid Nonunions and Kienbock Disease: A Systematic Review in 917 Patients.* Journal of Hand and Microsurgery, 2019. **11**(01): p. 006-013.
123. Testa, G., et al., *Comparison between Vascular and Non-Vascular Bone Grafting in Scaphoid Nonunion: A Systematic Review.* Journal of Clinical Medicine, 2022. **11**(12): p. 3402.
124. Simpson, C.R., H.M. Kelly, and C.M. Murphy, *Synergistic use of biomaterials and licensed therapeutics to manipulate bone remodelling and promote non-union fracture repair.* Advanced Drug Delivery Reviews, 2020. **160**: p. 212-233.
125. Tang, G., et al., *Recent Trends in the Development of Bone Regenerative Biomaterials.* Frontiers in Cell and Developmental Biology, 2021. **9**.
126. Sales, A., et al., *Differential bioactivity of four BMP-family members as function of biomaterial stiffness.* Biomaterials, 2022. **281**: p. 121363.

127. Xie, Z., et al., *The fast degradation of β-TCP ceramics facilitates healing of bone defects by the combination of BMP-2 and Teriparatide.* Biomedicine & Pharmacotherapy, 2019. **112**: p. 108578.
128. Zhu, G., et al., *Bone physiological microenvironment and healing mechanism: Basis for future bone-tissue engineering scaffolds.* Bioactive Materials, 2021. **6**(11): p. 4110-4140.
129. Gariffo, G., et al., *Use of Teriparatide in preventing delayed bone healing and nonunion: a multicentric study on a series of 20 patients.* BMC Musculoskelet Disord, 2023. **24**(1): p. 184.
130. Thurairajah, K., G.D. Briggs, and Z.J. Balogh, *Stem cell therapy for fracture non-union: The current evidence from human studies.* Journal of Orthopaedic Surgery, 2021. **29**(3): p. 23094990211036545.
131. El-Jawhari, J.J., et al., *Defective Proliferation and Osteogenic Potential with Altered Immunoregulatory phenotype of Native Bone marrow-Multipotential Stromal Cells in Atrophic Fracture Non-Union.* Scientific Reports, 2019. **9**(1).
132. Khatkar, H. and A. See, *Stem Cell Therapy in the Management of Fracture Non-Union – Evaluating Cellular Mechanisms and Clinical Progress.* Cureus, 2021.
133. Gómez-Barrena, E., et al., *Early efficacy evaluation of mesenchymal stromal cells (MSC) combined to biomaterials to treat long bone non-unions.* Injury, 2020. **51**: p. S63-S73.
134. Wittig, O., et al., *A method of treatment for nonunion after fractures using mesenchymal stromal cells loaded on collagen microspheres and incorporated into platelet-rich plasma clots.* International Orthopaedics, 2016. **40**(5): p. 1033-1038.
135. Zhang, L., et al., *Exosomes from bone marrow mesenchymal stem cells enhance fracture healing through the promotion of osteogenesis and angiogenesis in a rat model of nonunion.* Stem Cell Research & Therapy, 2020. **11**(1): p. 1-15.

APPENDIX

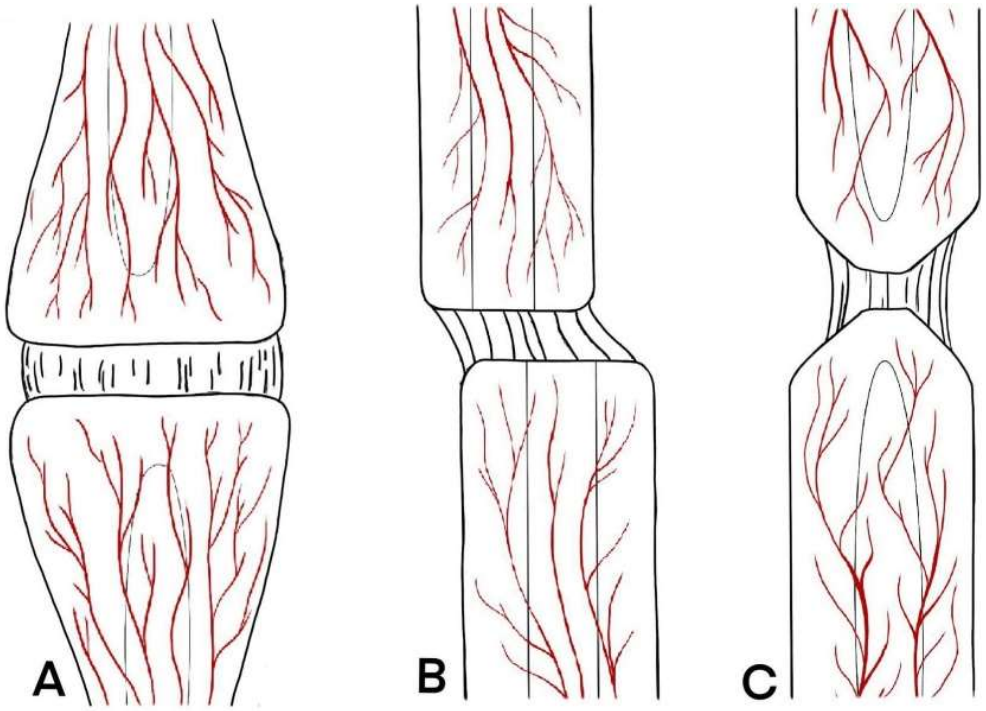

Figure 1.1: Illustration of Weber-Cech Classifications of Nonunion. (**A**) Hypertrophic nonunion is characterized by excessive periosteal callus formation without union of the fracture fragments. (**B**) Oligotrophic nonunion is characterized by mild periosteal callus formation without union of the fracture fragments. (**C**) Atrophic nonunion is characterized by no callus formation and often associated with impaired vascularity. Figure reprinted from "Figure 1" by Kloen et al. [32], licensed under CC BY 4.0.

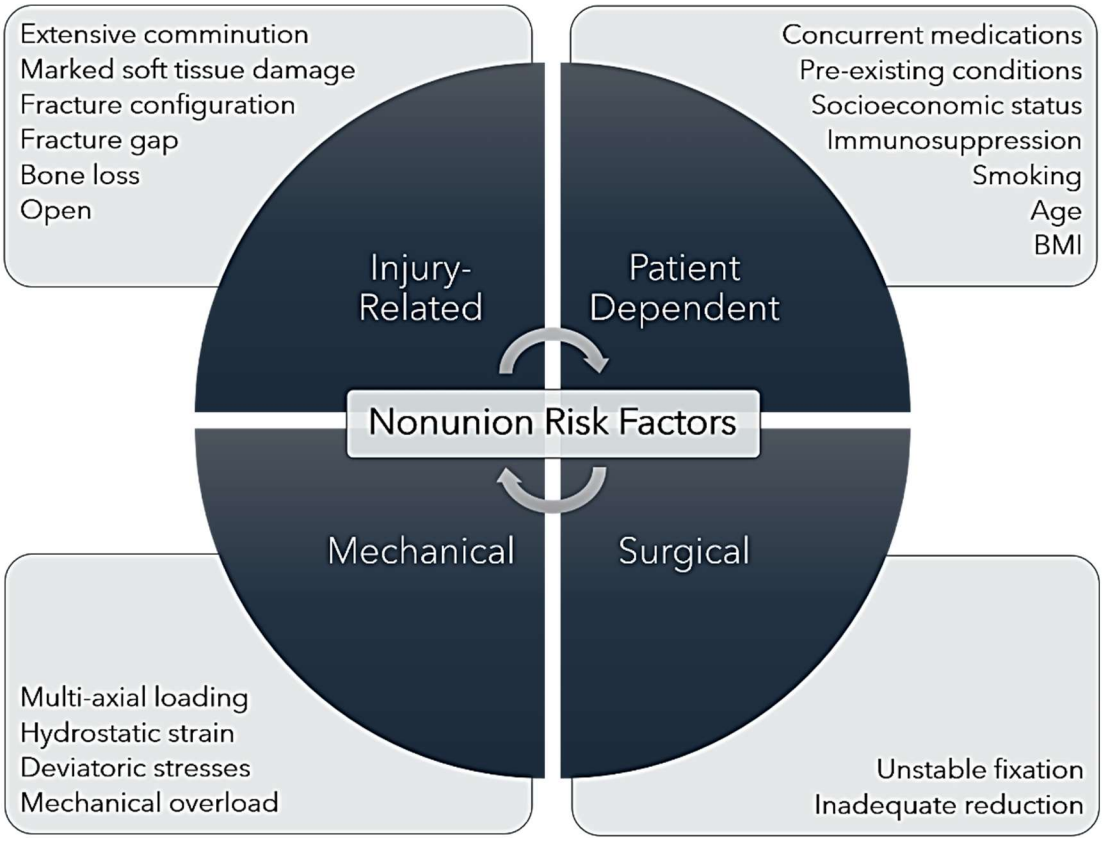

Figure 1.2: Nonunion Risk Factors. Illustration of the injury-related, patient dependent, mechanical, and surgical risk factors that contribute to fracture nonunion.

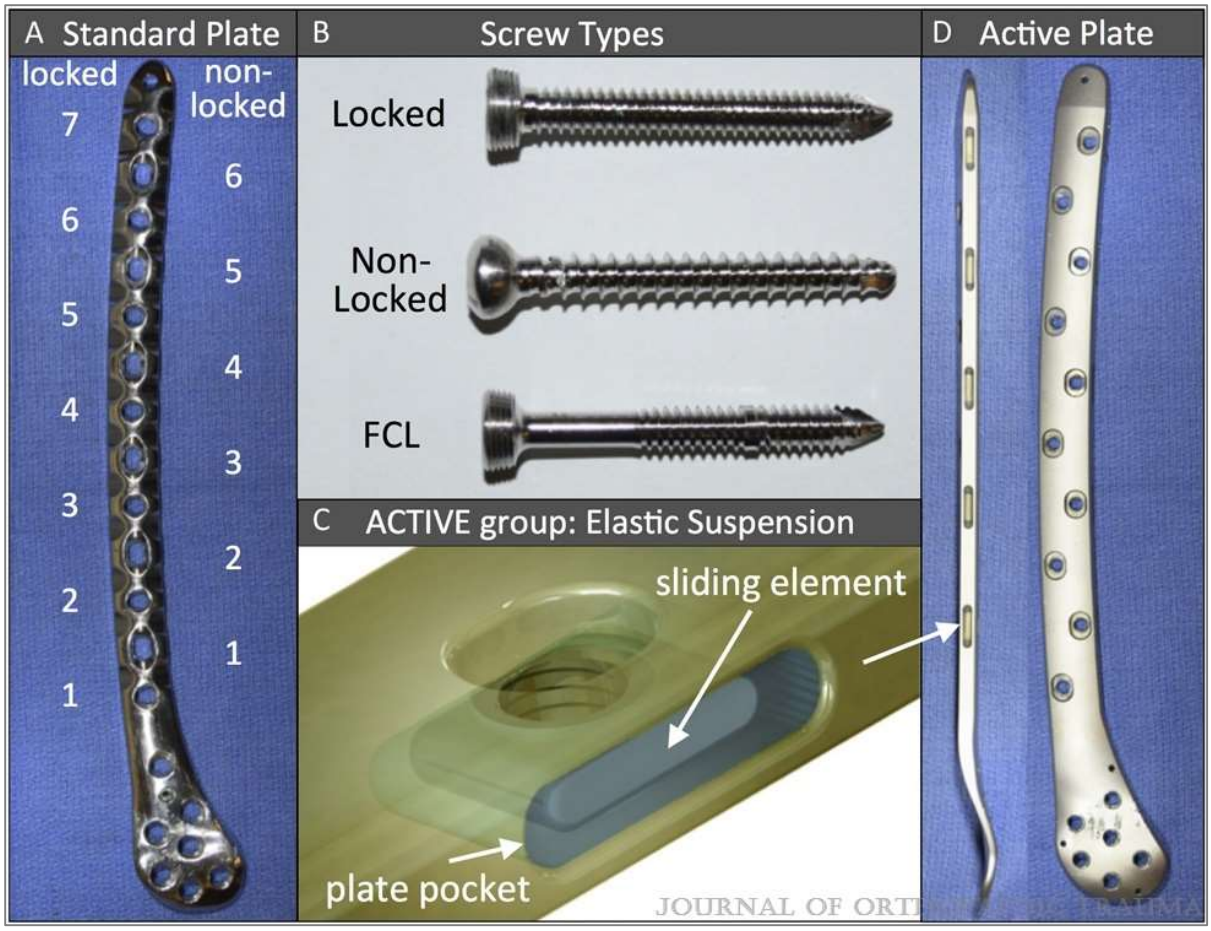

Figure 1.3: Illustration of Four Methods of Fixation Dynamization. Henschel et al. mechanically evaluated four methods of dynamization as compared to a non-dynamized locking plate control. (**A**) Distal femoral plates with alternating locked and non-locked holes for use in the locked control and non-locked treatment groups, respectively. (**B**) Images of locking, non-locking, and far cortical locking screws. (**C**) Schematic illustration of dynamized, active plate in which screws are locked into a sliding element within the plate. (**D**) Pictures of active locking plates; arrows point to the sliding element pockets within the plate. Figure reprinted from "Figure 2" by Henschel et al. [60]. Copyright © 2023 Wolters Kluwer Health, Inc. and/or its subsidiaries. All rights reserved.

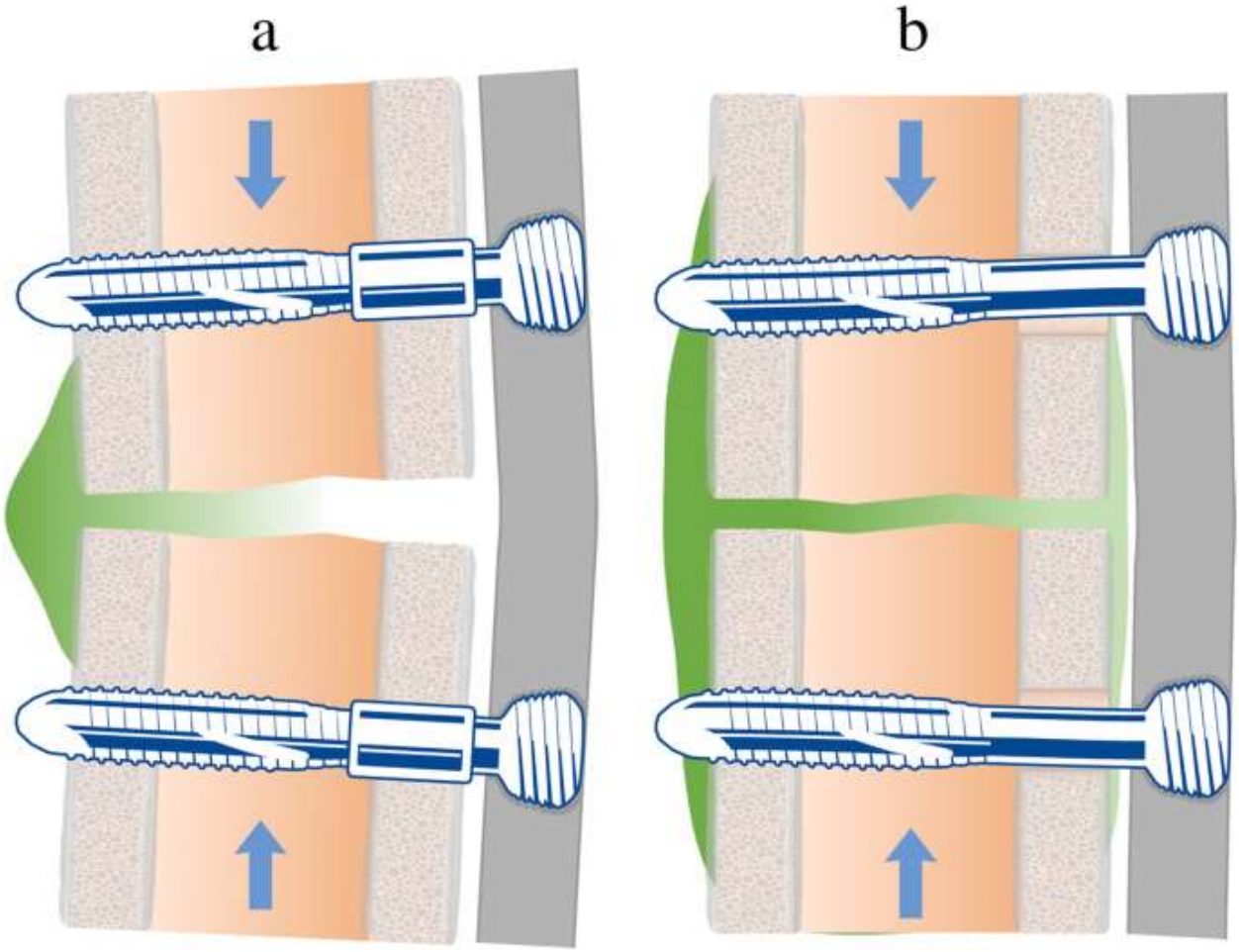

Figure 1.4: Schematic Representation of Variable Fixation Locking Screws. In these illustrations, solid grey represents the locking plate, green represents forming bone callus, and blue arrows indicate axial loads acting on the fracture site. (**A**) Initially, the VFLS is stabilized in the cis-cortex by a PLGA sleeve. (**B**) Once the sleeve degrades, the VFLS acts as a far-cortical locking screw, allowing for micromotion within the cis-cortex. Figure reprinted from "Figure 1" by Plecko et al. [75], licensed under CC BY 4.0.

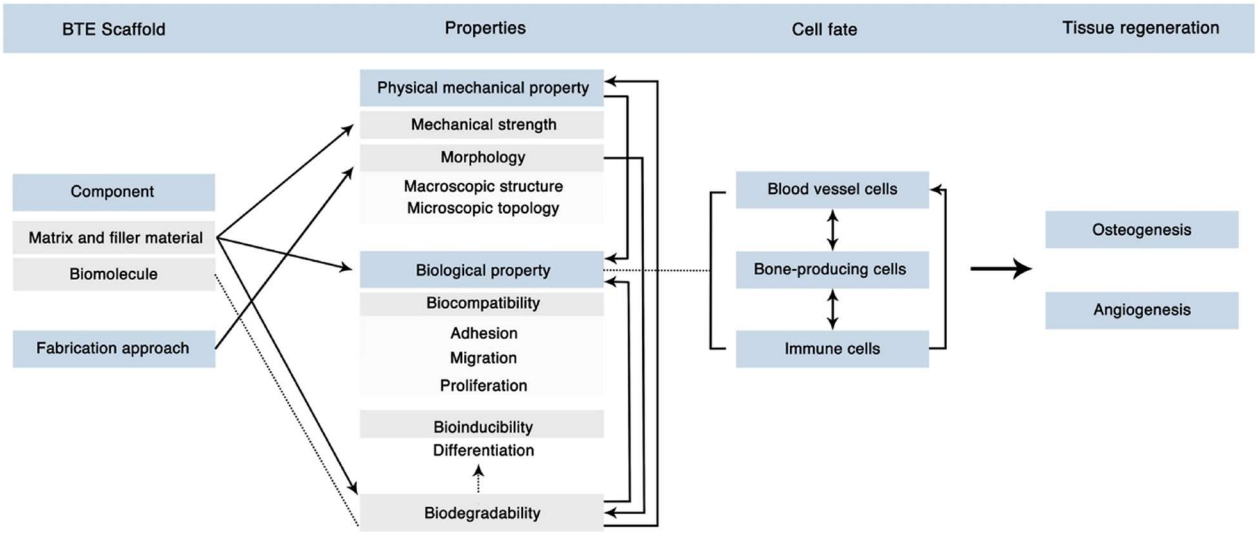

Figure 1.5: Modern Considerations for Bone Biomaterial Fabrication. Modern bone scaffolds combine biomimetic and biomolecule delivery designs, necessitating both mechanical and biological integrity for proper functionality in vivo. This figure illustrates the complexity and interconnectivity of biomaterial properties to achieve the final goals of bone and vascular regeneration. Figure reprinted from "Figure 12" by Zhu et al. [128], licensed under CC BY 4.0.

CHAPTER II:

MESENCHYMAL STEM CELL USE IN ACUTE TENDON INJURY: IN VITRO TENOGENIC POTENTIAL VS. IN VIVO DOSE RESPONSE

This chapter was previously published in *Bioengineering* by Kristin Marie Bowers:

Kristin Bowers[1*], Lisa Amelse[1], Austin Bow[1], Steven Newby[1], Amber MacDonald[1], Xiaocun Sun[1], David Anderson[1], and Madhu Dhar[1]

Affiliations:
[1] Large Animal Clinical Sciences, University of Tennessee College of Veterinary Medicine, Knoxville, Tennessee, USA

Corresponding Author:
Kristin Bowers, DVM, Large Animal Clinical Sciences, College of Veterinary Medicine, The University of Tennessee, 2407 River Dr., Knoxville, Tennessee, 37996, USA; email: kbower17@vols.utk.edu

This article was published by *Bioengineering*. 2022; 9(8):407. https://doi.org/10.3390/bioengineering9080407

ABSTRACT

Stem cell therapy for the treatment of tendon injury is an emerging clinical practice in the fields of human and veterinary sports medicine; however, the therapeutic benefit of intralesional transplantation of mesenchymal stem cells in tendonitis cases is not well designed. Questions persist regarding the overall tenogenic potential and efficacy of this treatment alone. In this study, we aimed to isolate a rat mesenchymal stem cell lineage for in vitro and in vivo use, to assess the effects of growth factor exposure in vitro on cell morphology, behavior, and tendon-associated glycoprotein production, and to assess the therapeutic potential of intralesional stem cells, as a function of dose, in vivo. First, rat adipose-derived (rAdMSC) and bone marrow-derived (rBMSC) stem cell lineages were isolated, characterized with flow cytometric analysis, and compared in terms of proliferation (MTS assay) and cellular viability (calcein-AM staining). Rat AdMSCs displayed superior proliferation and more homogenous CD 73, CD 44H, and CD 90 expression as compared to rBMSC. Next, the tenogenic differentiation potential of the rAdMSC lineage was tested in vitro through isolated and combined stimulation with reported tenogenic growth factors, transforming growth factor (TGF)-β3 and connective tissue growth factor (CTGF). We found that the most effective tenogenic factor in terms of cellular morphologic change, cell alignment/orientation, sustained cellular viability, and tendon-associated glycoprotein upregulation was TGF-β3, and we confirmed that rAdMSC could be induced toward a tenogenic lineage in vitro. Finally, the therapeutic potential of rAdMSCs as a function of dose was assessed using a rat acute Achilles tendon injury model. Amounts of 5×10^5 (low dose) and 4×10^6 (high dose) were used. Subjectively, on the gross morphology, the rAdMSC-treated tendons exhibited fewer adhesions and less scar tissue than the control tendons; however,
regardless of the rAdMSC dose, no significant differences in histological grade or tissue collagen I deposition were noted between the rAdMSC-treated and control tendons. Collectively, rAdMSCs exhibited appropriate stem cell markers and tenogenic potential in vitro, but the clinical efficacy of intralesional implantation of undifferentiated cells in acute tendonitis cases could not be proven. Further investigation into complementary therapeutics or specialized culture conditions prior to implantation are warranted.

INTRODUCTION

Stem cell therapy for the treatment of tendon injury is an emerging clinical practice in the fields of human and veterinary sports medicine. Intralesional stem cell implantation has been utilized for tendonitis treatment in sport horses for over a decade with promising results [1]. In a report of 105 National Hunt horses with over two years of follow-up, there was less recurrence of tendonitis in those horses treated with stem cells as opposed to traditional therapies [2]. An analysis of several case-control observational studies in equine sport horses indicated that treatment of tendonitis with bone marrow derived mesenchymal stem cells (BMSC) was associated with a reduction in the rate of reinjury [3-5]. Further clinical research is necessary to elucidate the potential of stem cell therapy in cases of acute or chronic tendon injury. In an experimental model of Achilles injury using rats, tissue treated with BMSCs exhibited superior biomechanical strength and histological evidence of healing when compared to control samples [6]. However, the therapeutic benefit of intralesional transplantation of mesenchymal stem cells in tendonitis cases is disputed in the literature with reports of no significant difference between BMSC-treated and control tendons in other Achilles injury trials [7-9]. Several strategies have been proposed to elevate the therapeutic potential of intralesional stem cell therapy including predifferentiation, biomaterial-based cell delivery, or concurrent growth factor injection [10-13], but uncertainty regarding the ideal therapeutic strategy in terms of cell source, expansion characteristics, and cell numbers persists [13-15].

Unlike osteogenic, chondrogenic, and adipogenic differentiation, a standardized, effective protocol for tenogenic differentiation of mesenchymal stem cells has not been established [16-18]. Methods include growth factor exposure, dynamic mechanical stimulation, biomaterial/ECM scaffold three-dimensional culture, and coculture with tendon-derived stem cells or tenocytes [17, 19, 20]. Growth factors that have been positively correlated with tendon associated biomarkers include transforming growth factor beta ligands (TGFβ), specifically TGF-β1 and TGF-β3, bone morphogenic protein (BMP) ligands, specifically BMP-12, BMP-13, and BMP-14, fibroblast growth factor (FGF) ligands, specifically FGF-2, and connective tissue growth factor (CTGF). These cytokines are inherently linked, and they exhibit significant co-expression through the mitogen-activated protein kinase (MAPK) pathway during embryonic development and active homeostasis/tissue turnover in adults [21, 22]. Recently, Yin et al. investigated the tenogenic effects of TGF-β1, BMP-12, and CTGF/ascorbic acid exposure on mesenchymal stem cells and noted superior morphologic changes, genetic

upregulations, and tendon-associated marker production using a stepwise protocol of initial TGF-β1 exposure, followed by CTGF/ascorbic acid [23]. In addition, several studies have reported similarly promising results following MSC exposure to TGF-β3 alone in either monolayer or three-dimensional culture [20, 24-27].
While uncertainty as to the ideal cell type and predifferentiation protocol for intralesional MSC therapy in tendon injury persists, another potential contributor to its inconsistent therapeutic benefit is the lack of an established therapeutic dose of mesenchymal stem cells [28-31]. Initially, MSCs were thought to aid healing directly through differentiation into tissue-appropriate cells, replication, and reestablishment of tissue architecture, but more recent research has suggested that their function is more immunomodulatory than direct repopulation [32]. Increasingly, experimental studies and clinical practice favor the use of allogenic MSCs, rather than autologous MSCs [28, 33]. Allogenic MSCs provide the benefits of proven cellular purity, multipotency, consistency, and ease of acquisition without the delays required for autologous cell isolation, characterization, and propagation [34, 35]. These benefits typically outweigh the risk of an inflammatory (rejection) reaction in response to foreign proteins, specifically major histocompatibility complexes (MHC) [32, 36]. However, too high of a dose of allogenic MSCs may impair their immunomodulatory functions by initiating an overwhelming MHC-mismatch inflammatory response [32, 37].

Dose-response studies to ascertain an effective dose or an adverse threshold for mesenchymal stem cell therapy are lacking. In one study, Saether et al. compared the effects of high dose (4×10^6 MSCs) and low dose (1×10^6 MSCs) stem cells used in a study of rat medial collateral ligament healing [37]. Improved strength and stiffness of the ligament and decreased inflammatory response in the low dose group was noted, but neither the high nor the low dose MSC treatments downregulated inflammatory cytokines or restricted inflammatory cell migration when compared to untreated controls [37]. This study was repeated using a rat Achilles tendon model and introduced the variables of preconditioning and genetic modification to promote production of anti-inflammatory modulators [32]. The authors reported that anti-inflammatory preconditioning through genetic engineering had a more significant effect on tendon healing than dosage in terms of M1 macrophage number and amount of inflammatory IL-12 cytokine. As of yet, the effect of MSC dose alone on tendon injury healing has not been described and an effective dose of MSC for use in treatment of acute tendonitis has not been established.

Our goals were to isolate a rat mesenchymal stem cell lineage for in vitro and in vivo use, to assess the effects of growth factor exposure in vitro on cell morphology,

behavior, and tendon-associated glycoprotein production, and to assess the therapeutic potential of intralesional stem cells as a function of dose in vivo. We aimed to characterize and establish the cells' tenogenic potential in vitro prior to implantation in vivo in a dosing trial. TGF-β3 was selected for this experiment based on promising published reports when used in vitro for tenogenic differentiation [20, 25-27]; CTGF with ascorbic acid was selected due to its reported synergy with TGF-β1 in a stepwise tenogenic differentiation protocol [23]. A rodent model of tendon injury is useful for assessment of the effect of mesenchymal stem cell dose on in vivo healing with achievement of appropriate endpoints in a time efficient manner [38-40]. The calcaneal tendon injury model is well characterized and provides guidelines specific to the duration of study, creation of defects, and analytical methods [6-8]. We hypothesized that concurrent exposure to TGF-β3, CTGF, and ascorbic acid would induce tenogenic differentiation of rat MSCs in vitro, and we hypothesized that intralesional MSC implantation would have a dose-dependent and beneficial effect on tendon healing in an acute injury model.

MATERIALS AND METHODS

Ethics

All studies were reviewed and approved by the University of Tennessee Institutional Animal Care and Use Committee and adhered to the National Institutes of Health's Guide for the Care and Use of Laboratory Animals [41].

Isolation, Culture, and Characterization of Rat Adipose-Derived MSCs

All MSCs were isolated from Sprague-Dawley rats (150-200 g, n = 2). BMSCs were collected from the bone marrow of the femurs as previously described [42-45]. Briefly, the femurs were rinsed with phosphate-buffered saline (PBS) before clipping the ends of the bone. An 18-gauge needle was used to extrude the bone marrow, and marrow was transferred to a collection tube using growth media flushes. After centrifugation at 1000 rpm for 5 minutes, the cell pellet was re-suspended in 5.5 mL growth media and filtered with a 70 μm strainer twice to ensure complete collection. AdMSCs were collected from perinephric and testicular adipose tissue as previously described [42, 43]. The tissue was minced and digested in PBS containing 0.1% Type I

Collagenase Buffer (Sigma-Aldrich, St. Louis, Mo, USA) at 37°C with intermittent mixing; incubation was discontinued when tissue appeared homogenous (roughly 60 minutes), and growth media was added to inactivate the collagenase. After centrifugation at 600 rpm for 5 minutes, the lipid layer and collagenase/media liquid fraction was removed, and the cell pellet was resuspended in PBS. Centrifugation and resuspension were repeated, and cells were filtered through a 70 μm strainer. Isolated bone marrow and adipose cells were cultured in complete medium consisting of Dulbecco's Modified Eagle Medium (DMEM-F12, Thermo Fisher Scientific, Waltham, MA, USA) containing 10% fetal bovine serum (FBS, Thermo Fisher Scientific, Waltham, MA, USA), 1% penicillin-streptomycin-neomycin (Thermo Fisher Scientific, Waltham, MA, USA), and 0.1% amphotericin B (Thermo Fisher Scientific, Waltham, MA, USA). Cells were grown to 80—90% confluency and then harvested with 0.05% trypsin for cryopreservation (80% FBS, 10% DMEM-F12, and 10% DMSO) or re-seeded for expansion in complete medium.

Immunophenotyping

Flow cytometry analysis was used as previously reported to characterize the isolated rAdMSC and rBMSC [45]. Cells were identified by the expression of the following cell-surface cluster-of-differentiation (CD) markers: CD29, CD73, CD44H, CD90, CD106, CD11b/c, CD45, and CD31. All markers tested are recognized by the Mesenchymal and Tissue Stem Cell Committee of the International Society for Cellular Therapy [42]. Anti-CD antibodies were used at the manufacturer's recommended concentrations (Biolegend, San Diego, CA). Labeled cells were assessed using a BD FACS Caliber Flow Cytometer (BD Biosciences, Haryana, India) and FlowJo software (FlowJo LLC, Ashland, OR, USA).

Proliferation Assay

Cell proliferation rates of rat adipose-derived and bone-marrow-derived mesenchymal stem cells were assessed at 1, 3, 5, and 7 days of culture using the CellTiter 96 Aqueous Non-Radioactive (MTS) assay (Promega, Madison, WI, USA) as previously described [46, 47]. Briefly, all experiments were performed using 24-well plates with 1.0×10^4 rBMSC or rAdMSC (passage 5 and passage 6, respectively) seeded in 500 μL complete growth medium as the seeding volume. The optical density of the cell and MTS reagent complex was measured using a microplate fluorescence reader

(BioTek, Winooski, VT, USA) at 490 nm. Medium without cells was used as a blank. Each timepoint was performed in triplicate, and average absorbance at 490 nm (corrected by the reference blank reading) of the three wells was utilized as data for further analysis. Absorbance data was analyzed for time effect and coefficients of determination (R^2 values) of linear regression were calculated for direct comparison. At each timepoint, an additional well was utilized for qualitative cell viability analysis using Calcein AM Viability Dye (Thermo Fisher, Waltham, MA, USA); stained cells were visualized after 5 minutes, and images were obtained using a laser scanning spectral confocal microscope (Leica Microsystems, Wetzlar, Germany).

Tenogenic Differentiation of Rat Adipose-Derived MSCs

Based on the results of proliferation assay, rAdMSC were utilized for the remainder of experimentation. Rat AdMSC (1.0×10^6 cells, passage 3) were thawed, suspended in complete growth medium, seeded into T175 flasks for expansion, and incubated at 37 °C in a humidified atmosphere with 5% CO_2. Medium was changed every two to three days until the cells reached 70-80% confluence. Upon reaching confluence, adherent cells were harvested using 0.25% trypsin EDTA (Thermo Fisher Scientific, Waltham, MA, USA) and transferred to 6-well plates for the tenogenic differentiation trial at a seeding density of 5.0×10^4 cells in 3 ml complete media per well. The rAdMSC were maintained in complete medium alone (Control) or supplemented with (a) 10 ng/ml TGF-β3 (Peprotech, Rocky Hill, NJ, USA), (b) 100 ng/ml CTGF (Peprotech, Rocky Hill, NJ, USA) with 50 μg/ml ascorbic acid (Sigma-Aldrich, St. Louis, MO, USA), or (c) 10 ng/ml TGF-β3, 100 ng/ml CTGF, and 50 μg/ml ascorbic acid. Growth factor concentrations were selected based on previously published reports regarding growth-factor-mediated tenogenic differentiation [15, 23, 25, 26, 48]. Conditioned media was changed every two days and cells were imaged daily using bright light phase-contrast microscopy (Leica Microsystems, Wetzlar, Germany). The cells were monitored for signs of differentiation including changes in cellular morphology, cell alignment/orientation, and cell-to-cell adherence/clumping, and cell culture was halted if marked cellular exfoliation (greater than 30% of previously adhered cells) was noted.

Immunofluorescence

For immunofluorescence assays, the previously described tenogenic differentiation experiment was repeated using the same growth factors and concentrations of each. Briefly, rAdMSC (passage 4) were harvested with 0.25% trypsin EDTA (Thermo Fisher Scientific, Waltham, MA, USA) and transferred to 12-well plates for the tenogenic differentiation trial at a seeding density of 1.5×10^4 cells in 1 ml complete media per well. The rAdMSC were maintained in complete medium alone (Control) or supplemented with (a) 10 ng/ml TGF-β3 (Peprotech, Rocky Hill, NJ, USA), (b) 100 ng/ml CTGF (Peprotech, Rocky Hill, NJ, USA) with 50 μg/ml ascorbic acid (Sigma-Aldrich, St. Louis, MO, USA), or (c) 10 ng/ml TGF-β3, 100 ng/ml CTGF, and 50 μg/ml ascorbic acid. Conditioned media was changed every two days and cell morphology was monitored daily using bright light phase-contrast microscopy. On days 1, 4, and 8, cells from each treatment group were fixed with 4% paraformaldehyde at room temperature for 10 minutes, permeabilized with 0.1% Triton X-100 in Hank's Balanced Salt Solution (HBSS), and blocked with Universal Blocking Reagent (BioGenex, Fremont, CA, USA) for 30 minutes at room temperature. Cytoskeletal organization and cellular morphology were assessed by evaluating expression of extracellular matrix proteins, F-actin and Collagen I, as previously described [45, 49]. Expression profiles of tendon-associated proteoglycans, tenascin C (TenC) and tenomodulin (Tnmd), were also evaluated at each timepoint as markers of tenogenic differentiation [17, 20, 24, 50]. Fixed cells were incubated with 1-2 μg of primary antibodies for F-actin (Alexa Fluor 594 phalloidin, Invitrogen, Waltham, MA, USA), Collagen I (Abcam, Cambridge, UK), TenC (Invitrogen, Waltham, MA, USA), and Tnmd (Biorbyt, Cambridge, UK) at 4°C for 24 hours. Subsequently, the cells were washed with HBSS and incubated with appropriate Alexa Fluor secondary anti-mouse or anti-rabbit antibodies at room temperature for 30 minutes in dark; Alexa Fluor 594 phalloidin was preconjugated and did not undergo secondary antibody exposure. Cells were mounted with Prolong Gold antifade reagent with 4′, 6-diamidino-2-phenylindole (DAPI) nuclear stain (Life Technologies, Carlsbad, CA, USA). Cells were analyzed and imaged using a laser scanning spectral confocal microscope (Leica Microsystems, Wetzlar, Germany). Images were further analyzed using Fiji image processing open-source software (ImageJ, Bethesda, MD, USA) to obtain DAPI-labeled cell counts, average nuclear size, TenC positive cell counts, and Tnmd positive cell counts [51, 52].

Fibrin Gel

In order to achieve local administration of stem cells in a controlled fashion, cells were suspended in fibrin gel, a viscous transport medium that will entrap but not inhibit the cells [53]. Fibrin gel was fabricated in our lab using fibrinogen and thrombin (MilliporeSigma, Burlington, MA) at a ratio of 0.2 U thrombin: 1 mg fibrinogen. This technique has been established and validated in our laboratory for cell uptake and suspension within the gel. Briefly, adequate cellular uptake and suspension in the gel was evaluated using equine mesenchymal stem cells stained with a fluorescent 1,1'-Dioctadecyl-3,3,3',3'-Tetramethylindocarbocyanine Perchlorate (DiI) marker available from the UTCVM Regenerative Medicine Laboratory. Adequate suspension in the gel with minimal residual cellular loss was confirmed using a laser scanning spectral confocal microscope at 600 nm wavelength (Leica Microsystems, Wetzlar, Germany).

Surgery

Twenty 12-week-old female Sprague Dawley rats each weighing between 208 and 242 g were acquired and maintained in a climate-controlled animal housing. Each rat underwent left hindlimb Achilles injury and was assigned intralesional treatment with fibrin gel alone (Control), 5×10^5 rAdMSC in fibrin gel (Low Dose), or 4×10^6 rAdMSC in fibrin gel (High Dose). Dosages were selected based on those previously employed in rat tendon or ligament injury models [7, 28, 54-56], and they reflect the lowest and highest reported dosages utilized in these models. Left hindlimb Achilles injury was induced as previously described [7, 8, 57]. Briefly, each rat was anesthetized using isoflurane gas and administered preoperative analgesics (buprenorphine 0.02 mg/kg SQ). A 1 cm longitudinal incision was made over the caudolateral aspect of the left hindlimb at the level of the Achilles tendon, terminating immediately proximal to the calcaneal insertion. Then, the central third of the Achilles tendon was isolated using blunt dissection and removed, resulting in a central defect that extended from the myotendinous junction to immediately proximal to the calcaneal insertion. Following defect creation, the appropriate treatment was administered intralesional using forceps to transfer the semi-solid fibrin gel into the lesion site. The skin incision was closed in a single layer using a full thickness, interrupted cruciate pattern.

Postoperative Management

The animals were individually housed with free cage activity during the postoperative period. Dietary intake, body weight, fecal/urine output, incisional healing, and subjective lameness were monitored routinely, and postoperative analgesia was provided for the first three days as needed (buprenorphine 0.02 mg/kg subcutaneously every twelve hours). At thirty days postoperatively, all animals were humanely euthanized via anesthetic overdose (isoflurane) and both Achilles tendons were harvested. Gross appearances of the left Achilles tendons were documented and photographed.

Histological Analysis

Tendon tissue was placed in 10% formalin solution for 48 hours, embedded in paraffin, cut into coronal sections, and stained. Each tendon sample underwent hematoxylin and eosin (H&E), Masson's Trichrome (MT), and Gomori's Reticulin (GR) staining. All H&E and MT samples were imaged, randomized by rat, and graded as previously described (Figure 2.1, please see chapter appendix for all figures) [7, 8, 57-59]. A minimum of six images (two at the tendon origin, two at the tendon mid-body, and two at the tendon insertion site) were acquired per stain per rat. Briefly, a histologic grading scale was employed that assessed H&E sections on the criteria of fiber structure and arrangement, cellular density, cellular appearance, inflammation, neovascularization, and fatty deposits. Images were randomized and histological grading was conducted by one reviewer blinded to treatment group assignment. Histological grades in each category were averaged for each rat and included in statistical analysis as separate variables. The same grading methodology was repeated for MT sections. GR samples were randomized by rat and graded on the same scale, but only the variable of fiber structure and arrangement was assessed.

Immunohistochemistry

The distribution and quality of Collagen I deposition was assessed by immunohistochemical (IHC) staining. Briefly, coronal sections of tendon tissue were deparaffinized, rehydrated, and subjected to antigen retrieval using 0.25% trypsin at 37°C for 30 minutes. After blocking with 5% bovine serum, the sections were incubated with diluted anti-collagen type 1 (1:50; Bio Rad, Hercules, CA, USA) overnight. Goat

anti-rabbit antibody served as the secondary antibody and all sections were counterstained with Nova Red, hematoxylin, and a bluing agent prior to dehydration and mounting. The sections were examined using bright field microscopy and imaged (Leica Microsystems, Wetzlar, Germany). Sections were quantitatively analyzed with the TWOMBLI macro for Fiji (ImageJ, Bethesda, MD, USA) [60, 61].

Statistical Analysis

Immunofluorescence quantitative data was summarized for mean, standard deviation, median, and range, and the effects of growth factor exposure over time were evaluated using two-way ANOVA. Categorical histological grades were summarized as counts and percentages. The effects of treatment on histological grades were screened using logistic regression analysis for a completely randomized design with subsamples. Numeric outcomes including nuclear counts as a measure of tissue cellularity and TWOMBLI output metrics were summarized for mean, standard deviation, median and range. The effects of treatment on tissue cellularity and TWOMBLI output metrics were analyzed using a general linear model for a completely randomized design with subsamples. Ranked transformation was applied when diagnostic analysis on residuals exhibited violation of normality and equal variance assumptions using Shapiro–Wilk test and Levene's test. Post hoc multiple comparisons were performed with Tukey's adjustment. Statistical significance was identified at the level of 0.05. Analyses were conducted in SAS 9.4 TS1M7 for Windows 64x (SAS institute Inc., Cary, NC, USA).

RESULTS

Rat Mesenchymal Stem Cell Isolation, Characterization, and Tenogenic Differentiation

Isolation, Expansion, and Immunophenotyping of rAdMSCs and rBMSCs

Lineages of rAdMSCs and rBMSCs were successfully isolated and characterized with flow cytometry (Figure 2.2). Immunophenotypic surface marker analysis revealed that the rAdMSCs expressed CD29, CD73, CD 44H, CD90, and CD106, and they did not express CD11b/c, CD45, and CD31. Isolated rBMSCs expressed CD29 and CD106 and did not express CD11b/c, CD45, and CD31; however, widened peaks and mixed positive and negative expression were noted on CD73, CD44H, and CD90 analysis, suggesting a heterogenous population of cells at the tested passage.

Cell Proliferation

Cellular proliferation of rBMSCs and rAdMSCs was assessed over a period of 7 days using MTS assays, and cellular viability was qualitatively assessed using calcein AM cellular staining (Figure 2.3). In the presence of the standardized growth medium provided, both cell types were viable and cell numbers increased linearly over time. The proliferation rate and overall cellular viability of rAdMSCs was superior to that of rBMSCs so all further analyses and experimentation was conducted using rAdMSCs.

Tenogenic Differentiation – Morphological Changes

Prior to exposure with enriched media, all wells were confirmed to contain adherent rAdMSC with minimal debris or cellular exfoliation. Twelve hours following exposure to enriched media, marked changes in cellular distribution and morphology were evident in all treatment groups (Figure 2.4). Cells exposed to TGF-β3 alone displayed apparent migration and clumping while maintaining adherence to the wells while cells exposed to CTGF/ascorbic acid (AA) and TGF-β3/CTGF/AA exhibited elongated, spindle-like morphology and, subjectively, a burst of proliferation. Two days following initial exposure to enriched media, the TGF-β3/CTGF/AA cells exhibited distinct spindle morphology and had migrated into clumps with a mix of parallel and intersecting cell-to-cell alignment within the well; similar changes in cell morphology and alignment were noted in the remaining two treatment groups at Day 3 of enriched media exposure (Figure 2.4). No apparent change in the TGF-β3/CTGF/AA cells was noted between Days 4 and 6 with the exceptions of gradual, cumulative exfoliation of cells present and accumulation of a granular extracellular byproduct visualized in all wells; a threshold of roughly 30% of cells exfoliated was reached on Day 6 of enriched media exposure and further culture of the TGF-β3/CTGF/AA group was halted. Cells exposed to TGF-β3 exhibited distinct spindle-morphology by Day 4 of culture and had migrated into independently oriented clumps of parallel-arranged cells; between Days 4 and 8 of culture, these cells remained relatively static but extracellular-matrix deposition (in the form of tendrils of extracellular material) could be visualized at cell-to-cell contact points (Figure 2.4). Cells exposed to CTGF/AA remained static between Days 4 and 8 of culture, but beginning on Day 6, a granular extracellular byproduct was visualized in all wells, increasing in amount over the remainder of the differentiation

trial. Both the TGF-β3 and CTGF/AA wells reached >30% cellular exfoliation on Day 8 of culture and further culture was discontinued.

Immunofluorescence

Tenogenic differentiation was characterized by immunofluorescence staining for cytoskeletal proteins, collagen I and F-actin, and for tendon-associated extracellular matrix (ECM) glycoproteins, tenascin C and tenomodulin. Morphological changes observed through phase contrast light microscopy were confirmed with F-actin and collagen I immunofluorescence (Figure 2.5). Briefly, cells treated with TGF-β3, CTGF/AA, and TGF-β3/CTGF/AA displayed filipodia extension, overall cell elongation, and parallel cytoskeletal conformation at cell junctions on Days 1 and 4 of culture. Concurrently, a qualitative increase in collagen I expression was seen in all three groups with distinct points of high intensity fluorescence indicative of collagen bundle formation most apparent on Day 4. On Day 8, cells treated with TGF-β3 remained adhered with robust cytoskeletal morphology, characterized by parallel F-actin orientation with a high degree of cell-to-cell contact. However, cells treated with CTGF/AA and TGF-β3/CTGF/AA displayed qualitatively poor cytoskeletal morphology on Day 8 of culture, characterized by retraction of filipodia, reduction in cytoskeletal size, and apparent decrease in cell numbers; the number of DAPI stained nuclei significantly decreased between Day 1 and Days 4 and 8 of culture in the TGF-β3/CTGF/AA group (Figure 2.5, $p<0.001$ and $p<0.001$ respectively).

No significant differences in the proportion of cells displaying tenascin C immunofluorescence to total cell counts were observed between treatment groups on Days 1 and 4 (Figure 2.6). However, both the TGF-β3 and CTGF/AA groups exhibited increased tenascin C expression on Day 8 when compared to unexposed controls ($p=0.0185$ and $p=0.0188$ respectively). In addition, cells exposed to TGF-β3 exhibited a unique but consistent tenascin C immunofluorescent signature characterized by high intensity fluorescence encircling the nucleus and moderate intensity fluorescence adjacent to the cell membrane; this signature was most apparent at Day 4 of culture but could be noted at all timepoints in the TGF-β3 group.

Rat AdMSC displayed temporal upregulation of tenomodulin expression in response growth factor exposure (Figure 2.7). Cells exposed to CTGF/AA exhibited significantly increased tenomodulin expression on Day 1 compared to unexposed controls ($p=0.0420$), and the relative magnitude expression remained consistent throughout the culture period. Cells exposed to TGF-β3 displayed delayed but marked

upregulation of tenomodulin expression on Day 4 ($p<0.001$). Cells exposed to TGF-β3, CTGF/AA, and TGF-β3/CTGF/AA displayed significantly greater tenomodulin expression compared to unexposed controls on Day 8 ($p=0.0130$, $p=0.0013$, and $p=0.0041$ respectively).

Fibrin Gel

Equine mesenchymal stem cells were suspended within the fibrin gel with minimal residual cells noted in the liquid fraction surrounding the gel clot. Images of cellular suspension are provided in Figure 2.8.

Intralesional Rat Mesenchymal Stem Cell Use in Achilles Tendon Injury

Gross Morphology

On gross morphologic analysis, control tendons exhibited marked adhesions to surrounding soft tissue and overlying skin, and thick scar tissue overlying and fusing the remaining medial and lateral thirds of the Achilles tendon was observed in four of six rats. Adhesions were rarely observed in the high dose and low dose groups ($n=1$ and $n=0$, respectively) and the overall appearance of the stem cell treated Achilles tendons more closely resembled uninjured controls with subjectively less scar tissue formation (Figure 2.9). No evidence of infection or further tendon injury/rupture was noted in any operated limbs.

Histological Analysis

At thirty days post-injury, all treatment groups displayed marked hypercellularity, fiber disruption, and disorganization of fiber arrangement compared to uninjured tendon. Histological grading of both H&E stained and Masson's Trichrome (MT) stained tendon samples revealed no statistically significant differences in terms of fiber structure and arrangement, cell density, cell appearance, inflammation, fatty deposits, or neovascularization grades (Figure 2.10). However, qualitative review of fiber arrangement and macroscopic structure revealed marked matrix disruption with complete loss of parallel structure and polar orientation of matrix fibers in Achilles tendons treated with fibrin gel alone (Figure 2.11). In addition, on a macroscopic scale, Achilles tendons treated with both high and low doses of stem cells displayed more

widespread neovascularization without concurrent perivascular inflammation or fat deposition.

Despite morphologic signs of healing, Achilles tendons treated with high dose rAdMSCs, low dose rAdMSCs, and fibrin gel alone had significantly greater cellularity (mean cell counts) than uninjured tendon ($p=<0.001$ for each pairwise comparison). While normal tendon samples were not included in blinded histological analysis, macroscopic differences from normal tendon in terms of cellularity, fiber pattern, and cell appearance were appreciated on qualitative review (Figure 2.11).

Immunohistochemistry

Results of immunohistochemical staining for Collagen I are presented in Figure 2.12. The TWOMBLI metrics of high-density matrix (HDM, the proportion of pixels in an image corresponding to stained matrix) and alignment (the extent to which fibers within the field of view are oriented in a similar direction) were considered for quantification of global collagen fiber pattern. No statistically significant differences in quantitative analysis of Collagen I IHC were noted between treatment groups.

DISCUSSION

This study sought to evaluate the potential of allogenic rat MSCs for tenogenic differentiation in vitro and intralesional application in vivo. First, rat adipose-derived and bone marrow derived stem cells were isolated, expanded, and characterized using flow cytometry. According to the International Society for Cellular Therapy, the minimum criteria for mesenchymal stem cells include cells that are plastic adherent in standard culture conditions, express CD106, CD73 and CD90, and must not express CD45, CD11b, or CD31 [14, 62]. Additional MSC markers include CD29, which should be present in both bone marrow and adipose tissue, and CD44H, which is more specific to bone marrow but can be found in adipose-derived stem cells [62]. In the current project, rAdMSC exhibited clear positive expression of CD29, CD73, CD44H, CD90, and CD106 and negative expression of CD11 b/c, CD45, and CD31 (Figure 2.2), but rBMSC only exhibited apparent positive CD29 and CD106 expression; while these differences could be a function of cell source or the specific isolation procedure, rBMSC flow cytometric results for CD73, CD44H, and CD90 suggested a heterogenous cell line, as indicated by the bimodal positive and negative peaks for each of these cell surface markers [62]. The rBMSC lineage also produced inferior results when compared to

rAdMSC in a proliferation assay (Figure 2.3). Adipose-derived mesenchymal stem cells have been extensively utilized in tissue engineering due to their relative ease of acquisition and expansion, and positive results in terms of tenogenic differentiation potential have been reported in rat, equine, and human cell lineages [19, 25, 26, 62]. However, in a tenogenic differentiation trial testing cell response to BMP-12-enriched differentiation media, similar isolation, characterization, and proliferation assays of three rat mesenchymal cell lines (rBMSC, rAdMSC, and rat synovial membrane MSCs) was conducted [43]. While all three lineages displayed upregulation of tendon-associated markers including *Scleraxis* expression and Tnmd, TenC, and Col I production, rBMSC displayed the highest degree of upregulation in response to BMP-12, and the authors concluded that rBMSC exhibited superior tenogenic differentiation capability as compared to rAdMSC and rat synovial membrane MSCs [43]. In the current experiment, based on the suspected heterogenous nature of isolated rBMSC and apparent differences in cellular proliferation, the decision was made to move forward with isolated rAdMSC for further use in vitro and in vivo.

Two potential tenogenic factors, TGF-β3 and CTGF, were chosen to evaluate their isolated and combined effects on rAdMSCs in monolayer cell culture. The TGF-β family of cytokines plays key roles in cell proliferation and tissue morphogenesis during embryogenesis and loss of TGF-β3 specifically (null mutants) directly correlates with a loss of normal tendon phenotype [20]. Several studies have reported on the tenogenic potential of TGF-β3 with significant upregulation of tendon associated markers including *Scleraxis* and Mohawk expression and Tnmd, TenC, cartilage oligomeric matrix protein (COMP), and thrombospondin production in both two-dimensional and three-dimensional culture [20, 24, 26, 27, 50]. One study compared the tenogenic potential of TGF-β1, TGF-β2, and TGF-β3 exposure on equine embryonic stem cells as compared to equine tenocytes; while all three TGF-β ligands upregulated *Scleraxis* expression in vitro, further upregulation of tendon-associated glycoprotein and Col I production was only observed in embryonic stem cells cultured in TGF-β3 differentiation media [24]. Following evaluation of isolated and combined exposure of rBMSC to TGF-β1, BMP-12, and CTGF/AA, Yin et al. proposed a stepwise tenogenic differentiation protocol that consisted of isolated TGF-β1 stimulation for three days followed by combined TGF-β1/CTGF/AA stimulation for an additional seven days [23]. The current study aimed to expand upon these previous experiments by testing the synergistic potential of TGF-β3 and CTGF/AA in two-dimensional culture. Similar to the results described in Barsby et al., TGF-β3 was the most effective single tenogenic factor in terms of cell morphological changes, cytoskeletal structure/integrity, and

tendon-associated glycoprotein production [24]. While morphological changes and upregulation of TenC and Tnmd were detected in all groups within eight days of induction, a subjective loss of cell-to-cell connections (F-actin immunofluorescence) and cytoskeletal integrity (F-actin and Col I immunofluorescence) was observed between Days 4 and 8 of CTGF/AA and TGF-β3/CTGF/AA exposure (Figure 2.5).

Previous studies have identified several key cellular morphology and orientation changes that are associated with a tenogenic lineage including elongation of the cell into a fibroblast-like morphology, orientation along a polar axis, and parallel alignment of clustered cells in monolayer culture [17, 19, 25]. Several culture conditions have been described to directly enhance MSC orientation and alignment during tenogenic differentiation, including dynamic mechanical stimulation such as cyclic uniaxial stretching or culture environment manipulation such as cellular attachment on an ECM scaffold or microgrooved matrix [19, 63-65]. In a study assessing the effects of both biochemical (TGF-β3 and BMP-12) and environmental (three-dimensional culture on decellularized tendon ECM scaffolds) stimulation of equine AdMSC toward a tenogenic lineage, TGF-β3 exposure in monolayer culture conditions elicited similar effects to the current study, including cellular elongation, migration resulting in parallel alignment, and marked proliferation (see Figure 2.4) [25]; concurrently, equine AdMSC cultured in TGF-β3-enriched media displayed widespread upregulation of Col I-A2, TenC, and *Scleraxis* expression [25]. However, cellular alignment and uniform orientation along a polar axis was superior in scaffold cultures compared to their monolayer counterparts, and TGF-β3 exposure in scaffold culture resulted in only a transient upregulation of *Scleraxis* and concurrent upregulation of osteopontin, an osteogenic marker. In the current study, rAdMSC exposed to TGF-β3 in monolayer culture exhibited distinct spindle morphology by Day 4 of enriched media culture and migrated into independently oriented clumps of parallel aligned cells. It is probable that environmental stimuli, in the form of mechanical stimulation or manipulation of the culture matrix, would enhance the observed tenogenic effects of TGF-β3 and yield more uniform orientation and superior ECM organization in future tenogenic differentiation trials.

In contrast, cells in the CTGF/AA and TGF-β3/CTGF/AA, while notably exhibiting a spindle-like morphology earlier than cells in the TGFβ3 group, did not achieve the same degree of cellular alignment and organization (Figure 2.4). F-actin and Col I immunofluorescence was utilized to assess the cytoskeletal integrity, ECM organization, and overall cellular health of MSCs in this differentiation trial. The actin cytoskeleton plays a role in cell migration, cytokinesis, endocytosis, and polarization

and visualization of the interplay between filamentous actin networks in a cell can give insight into active cellular mechanisms such as division, migration, growth, or apoptosis [66]. Collagen Type I, while the primary component of tendon matrix, is a non-specific, structural ECM component and visualization of Col I immunofluorescence will allow for qualitative comparison of ECM deposition between treatment groups [16]. Cells treated with TGF-β3, CTGF/AA, and TGF-β3/CTGF/AA displayed filipodia extension, overall cell elongation, and parallel cytoskeletal conformation at cell junctions on Days 1 and 4 of culture, but by Day 8 of culture, cells exposed to CTGF/AA and TGF-β3/CTGF/AA exhibited reduction in cytoskeletal size and loss of apparent cell-to-cell connections. Qualitative review of Col I immunofluorescence revealed superior collagen deposition in the TGF-β3 group with a robust cytoskeletal network persisting through Day 8 of culture. Most apparent as green hyperintense fluorescent artifact in Figures 5 and 6 (CTGF/AA and TGF-β3/CTGF/AA groups), a granular extracellular byproduct was observed in all wells exposed to CTGF/AA, either alone or in combination. This result was not described in previous studies utilizing CTGF/AA in tenogenic differentiation and further characterization of the byproduct was outside of the scope of this project [15, 23]; however, detrimental effects of byproduct accumulation cannot be ruled out as a contributing factor to the poor survival and relatively inferior tenogenic differentiation results in this group.

Immunofluorescent staining and quantification of the glycoproteins, tenomodulin and tenascin C, served as downstream markers of effective tenogenic differentiation. Tenascin C functions in tendon ECM to aid collagen fiber alignment and orientation [17]; other tenogenic differentiation trials have reported a transient burst of TenC production in the first few days of differentiation, followed by a gradual decline in ECM concentration for the remainder of culture [50, 67]. Tenomodulin is a transmembrane glycoprotein vital to tenocyte proliferation and tendon maturation [17]; it is a downstream product of the pathway activated by the *Scleraxis* transcription factor, a well-accepted marker of tenogenic lineage, and increasing tenomodulin concentrations in vitro are directly correlated to *Scleraxis* upregulation [68, 69]. In the current experiment, significant upregulation of TenC immunofluorescence was noted on Day of 8 culture in the TGF-β3 and CTGF/AA groups compared to matched controls, and significant upregulation of Tnmd immunofluorescence was first noted on Days 1, 4, and 8 in the CTGF/AA, TGF-β3, and TGF-β3/CTGF/AA groups respectively. In addition, cells in the TGF-β3 group exhibited a unique but consistent tenascin C immunofluorescent signature characterized by high intensity fluorescence encircling the nucleus and moderate intensity fluorescence adjacent to the cell membrane, first

noted on Day 4 of culture. Similar patterns and relative intensity of TenC immunofluorescence have been documented in other tenogenic differentiation or tenocyte characterization trials [70, 71], and in an experiment assessing the effect of BMSC coculture with mechanically stretched ligament fibroblasts, hyperintense TenC immunofluorescent signature was directly correlated with TenC mRNA expression quantified using reverse-transcription-quantitative polymerase chain reaction (RT-qPCR) [72]. Therefore, based on superior tendon-associated glycoprotein expression upregulation and appropriate morphologic, behavioral, and proliferative changes, we can conclude that TGF-β3 alone was the most effective tenogenic factor in this experiment, and we can confirm that the rAdMSC lineage can be effectively directed toward a tenogenic lineage in vitro.

Following characterization of the rAdMSC and confirmation of their tenogenic potential in experimental conditions, we sought to evaluate the rAdMSC therapeutic potential in vivo in an acute tendon injury model. Fibrin gel (fibrinogen/factor XIII combined with thrombin/calcium chloride) was selected as the delivery vehicle for intralesional MSC therapy to ensure the safety and proper localization of delivered cells within the injured tissue [11]; widely used in cardiac, neurological, and plastic surgery, fibrin gel is a biocompatible, biopolymeric substrate that allows for cell suspension for delivery and facilitates cell adhesion, proliferation, and differentiation after implementation [50, 53, 73]. To allow for accurate evaluation of the effect of rAdMSC dose in the current experiment, control rats underwent Achilles injury as described and received fibrin gel without mesenchymal stem cells; a potential therapeutic benefit of fibrin gel cannot be ruled out and serves as a limitation to the current study.

Thirty days following left Achilles injury and intralesional rAdMSC implantation, all rats were euthanized, and the left Achilles tendons were evaluated for gross pathology, structurally assessed using histopathology, and compositionally assessed using immunohistochemistry. On gross morphologic analysis, control tendons exhibited marked adhesions to surrounding soft tissue and overlying skin and apparent thickening of the remaining Achilles tendon was noted in four of six control rats; adhesions were rarely observed in rAdMSC treated tendons and the overall appearance of the stem cell treated Achilles tendons more closely resembled uninjured controls with subjectively less scar tissue formation. Tendon has a comparatively poor capacity for repair following injury, and primary healing is often prolonged and scar mediated as opposed to regenerative [16]. Manifestations of scar tissue, adhesions, or fibrotic scars on gross pathology give insight into ineffective remodeling on a microscopic scale, including lack of compartmental collagen organization, chronic tissue inflammation,

and loss of gliding functionality [74]. Qualitative structural and compositional differences were noted on histopathology, including marked matrix disruption with complete loss of parallel structure and polar orientation of matrix fibers in control tendons and notable neovascularization without concurrent perivascular inflammation or fat deposition in rAdMSC-treated tendons. However, no significant differences in histological grades or quantitative assessment of Col I deposition (IHC) were noted between rAdMSC-treated and control tendons, regardless of rAdMSC dose. Several reports of intralesional MSC therapy in acute tendon injury models corroborate these findings [7, 54, 75, 76]; for example, in an analysis of the therapeutic potential of stem-cell-derived extracellular vesicles as compared to rBMSCs in a rat Achilles defect model, tendons treated with rBMSCs alone yielded no significant difference in histological grade or quantitative Col I:Col III ratio from control tendons [8]. In a chronic model of equine superficial digital flexor tendon injury, intralesional injection of autologous AdMSC suspended in serum (three weeks after lesion induction) yielded no significant differences from controls in terms of gross histology, histological grade, vascularization, or Col I deposition at 12- and 24-weeks post-injury [77]. Similar to previous publications, no effect of MSC dose was appreciated in this experiment, either on gross morphology or histopathologic evaluation [28, 29, 31]; this challenges the notion that more cells are indeed better, and in this experiment, suspension and delivery of 4×10^6 rAdMSC into a subjectively small lesion without significant cellular loss or compromise was difficult. Saether et al. noted a MSC-dose dependent difference in innate immune response characterized by higher concentrations of pro-inflammatory cytokines and M1 macrophages in rat medial collateral ligaments treated with high dose (4×10^6) MSCs as compared to those treated with low dose (1×10^6) MSCs [28]. It has been suggested that the immunomodulatory potential of MSCs may not be unconditional, and high doses of MSCs can still induce an immune response through MCH II upregulation in certain environmental conditions or direct stimulation through toll-like receptor recognition of pathogen-associated molecular patterns [13, 14]. Based on this and previous studies, we suggest that increasing MSC dose may not be therapeutically beneficial and future studies to elucidate an optimal therapeutic dose for intralesional MSC implantation are necessary.

CONCLUSIONS

Rat adipose-derived and bone marrow-derived stem cell lineages were isolated and compared using flow cytometry for stem cell surface markers and using

proliferation (MTS) assays. Rat AdMSC displayed superior proliferation and more homogenous CD73, CD44H, and CD90 expression as compared to rBMSC. Tenogenic differentiation potential of the rAdMSC lineage was tested through isolated and combined TGF-β3 and CTGF/AA stimulation, and the most effective tenogenic factor in terms of cellular morphology change, cell alignment/orientation, sustained cellular viability, and tendon-associated glycoprotein upregulation was TGF-β3. Therapeutic potential of undifferentiated rAdMSC were assessed using a rat acute Achilles tendon injury model; on gross morphology, rAdMSC treated tendons exhibited fewer adhesions and subjectively less scar tissue and tissue thickening, but no significant differences in histological grade or tissue Col I deposition was noted between rAdMSC and control tendons. No effect of mesenchymal stem cell dose was noted on gross pathology or histopathological analysis.

REFERENCES

1. Schnabel, L.V.; Fortier, L.A.; McIlwraith, C.W.; Nobert, K.M. Therapeutic use of stem cells in horses: Which type, how, and when? *Vet. J.* **2013**, *197*, 570–577.
2. Godwin, E.E.; Young, N.J.; Dudhia, J.; Beamish, I.C.; Smith, R.K.W. Implantation of bone marrow-derived mesenchymal stem cells demonstrates improved outcome in horses with overstrain injury of the superficial digital flexor tendon. *Equine Vet. J.* **2012**, *44*, 25–32.
3. O'Meara, B.; Bladon, B.; Parkin, T.; Fraser, B.; Lischer, C.J. An investigation of the relationship between race performance and superficial digital flexor tendonitis in the Thoroughbred racehorse. *Equine Vet. J.* **2010**, *42*, 322–326.
4. Dyson, S.J. Medical management of superficial digital flexor tendonitis: A comparative study in 219 horses (1992–2000). *Equine Vet. J.* **2004**, *36*, 415–419.
5. Pacini, S.; Spinabella, S.; Trombi, L.; Fazzi, R.; Galimberti, S.; Dini, F.; Carlucci, F.; Petrini, M. Suspension of Bone Marrow–Derived Undifferentiated Mesenchymal Stromal Cells for Repair of Superficial Digital Flexor Tendon in Race Horses. *Tissue Eng.* **2007**, *13*, 2949–2955.
6. Al-Ani, M.K.A.; Xu, K.; Sun, Y.; Pan, L.; Xu, Z.; Yang, L. Study of Bone Marrow Mesenchymal and Tendon-Derived Stem Cells Transplantation on the Regenerating Effect of Achilles Tendon Ruptures in Rats. *Stem Cells Int.* **2015**, *2015*, 984146.
7. Oliva, F.; Maffulli, N.; Gissi, C.; Veronesi, F.; Calciano, L.; Fini, M.; Brogini, S.; Gallorini, M.; Passeri, C.A.L.; Bernardini, R.; et al. Combined ascorbic acid and T3 produce better healing compared to bone marrow mesenchymal stem cells in an Achilles tendon injury rat model: A proof of concept study. *J. Orthop. Surg. Res.* **2019**, *14*, 54.
8. Gissi, C.; Radeghieri, A.; Passeri, C.A.L.; Gallorini, M.; Calciano, L.; Oliva, F.; Veronesi, F.; Zendrini, A.; Cataldi, A.; Bergese, P.; et al. Extracellular vesicles from rat-bone-marrow mesenchymal stromal/stem cells improve tendon repair in rat Achilles tendon injury model in dose-dependent manner: A pilot study. *PLoS ONE* **2020**, *15*, e0229914.
9. Schnabel, L.V.; Lynch, M.E.; Van Der Meulen, M.C.H.; Yeager, A.E.; Kornatowski, M.A.; Nixon, A.J. Mesenchymal stem cells and insulin-like growth factor-I gene-enhanced mesenchymal stem cells improve structural aspects of healing in equine flexor digitorum superficialis tendons. *J. Orthop. Res.* **2009**, *27*, 1392–1398.
10. Leong, N.L.; Kator, J.L.; Clemens, T.L.; James, A.; Dds, M.E.; Jiang, J. Tendon and Ligament Healing and Current Approaches to Tendon and Ligament Regeneration. *J. Orthop. Res.* **2020**, *38*, 7–12.
11. Bianco, S.T.; Moser, H.L.; Galatz, L.M.; Huang, A.H. Biologics and stem cell-based therapies for rotator cuff repair. *Ann. New York Acad. Sci.* **2019**, *1442*, 35–47.
12. Guo, D.; Li, H.; Liu, Y.; Yu, X.; Zhang, X.; Chu, W.; She, Y.; Wang, D.; Chen, G. Fibroblast growth factor-2 promotes the function of tendon-derived stem cells in Achilles tendon restoration in an Achilles tendon injury rat model. *Biochem. Biophys. Res. Commun.* **2020**, *521*, 91–97.
13. Brandt, L.; Schubert, S.; Scheibe, P.; Brehm, W.; Franzen, J.; Gross, C.; Burk, J. Tenogenic Properties of Mesenchymal Progenitor Cells Are Compromised in an Inflammatory Environment. *Int. J. Mol. Sci.* **2018**, *19*, 2549.
14. De Miguel, M.P.; Fuentes-Julian, S.; Blazquez-Martinez, A.; Pascual, C.Y.; Aller, M.A.; Arias, J.; Arnalich-Montiel, F. Immunosuppressive Properties of Mesenchymal Stem Cells: Advances and Applications. *Curr. Mol. Med.* **2012**, *12*, 574–591.
15. Liu, L.; Hindieh, J.; Leong, D.J.; Sun, H.B. Advances of stem cell based-therapeutic approaches for tendon repair. *J. Orthop. Transl.* **2017**, *9*, 69–75.
16. Durgam, S.; Stewart, M. Cellular and Molecular Factors Influencing Tendon Repair. *Tissue Eng. Part B: Rev.* **2017**, *23*, 307–317.

17. Liu, Y.; Suen, C.-W.; Zhang, J.-F.; Li, G. Current concepts on tenogenic differentiation and clinical applications. *J. Orthop. Transl.* **2017**, *9*, 28–42.
18. Grafe, I.; Alexander, S.; Peterson, J.R.; Snider, T.N.; Levi, B.; Lee, B.; Mishina, Y. TGF-β Family Signaling in Mesenchymal Differentiation. *Cold Spring Harb. Perspect. Biol.* **2018**, *10*, a022202.
19. Long, C.; Wang, Z.; Legrand, A.; Chattopadhyay, A.; Chang, J.; Fox, P.M. Tendon Tissue Engineering: Mechanism and Effects of Human Tenocyte Coculture With Adipose-Derived Stem Cells. *J. Hand Surg.* **2018**, *43*, 183.e1–183.e9.
20. Barsby, T.; Bavin, E.P.; Guest, D.J. Three-dimensional culture and transforming growth factor beta3 synergistically promote tenogenic differentiation of equine embryo-derived stem cells. *Tissue Eng. Part A* **2014**, *20*, 2604–2613.
21. Guo, X.; Wang, X.-F. Signaling cross-talk between TGF-β/BMP and other pathways. *Cell Res.* **2008**, *19*, 71–88.
22. Chang, L.; Karin, M. Mammalian MAP kinase signaling cascades. *Nat.* **2001**, *410*, 37–40.
23. Yin, Z.; Guo, J.; Wu, T.-Y.; Chen, X.; Xu, L.-L.; Lin, S.-E.; Sun, Y.-X.; Chan, K.-M.; Ouyang, H.; Li, G. Stepwise Differentiation of Mesenchymal Stem Cells Augments Tendon-Like Tissue Formation and Defect Repair In Vivo. *STEM CELLS Transl. Med.* **2016**, *5*, 1106–1116.
24. Barsby, T.; Guest, D. Transforming growth factor beta3 promotes tendon differentiation of equine embryo-derived stem cells. *Tissue Eng. Part A* **2013**, *19*, 2156–2165.
25. Roth, S.P.; Schubert, S.; Scheibe, P.; Groß, C.; Brehm, W.; Burk, J. Growth Factor-Mediated Tenogenic Induction of Multipotent Mesenchymal Stromal Cells Is Altered by the Microenvironment of Tendon Matrix. *Cell Transplant.* **2018**, *27*, 1434–1450.
26. Yang, G.; Rothrauff, B.B.; Lin, H.; Yu, S.; Tuan, R.S. Tendon-Derived Extracellular Matrix Enhances Transforming Growth Factor-β3-Induced Tenogenic Differentiation of Human Adipose-Derived Stem Cells. *Tissue Eng. Part A* **2017**, *23*, 166–176.
27. Yu, Y.; Lee, S.Y.; Yang, E.-J.; Kim, H.Y.; Jo, I.; Shin, S.-J. Expression of tenocyte lineage-related factors from tonsil-derived mesenchymal stem cells. *Tissue Eng. Regen. Med.* **2016**, *13*, 162–170.
28. Saether, E.E.; Chamberlain, C.S.; Leiferman, E.M.; Kondratko-Mittnacht, J.R.; Li, W.-J.; Brickson, S.L.; Vanderby, R. Enhanced Medial Collateral Ligament Healing Using Mesenchymal Stem Cells: Dosage Effects on Cellular Response and Cytokine Profile. *Stem Cell Rev. Rep.* **2014**, *10*, 86–96.
29. Awad, H.A.; Boivin, G.P.; Dressler, M.R.; Smith, F.N.L.; Young, R.G.; Butler, D.L. Repair of patellar tendon injuries using a cell–collagen composite. *J. Orthop. Res.* **2003**, *21*, 420–431.
30. Lee, S.Y.; Kim, W.; Lim, C.; Chung, S.G. Treatment of Lateral Epicondylosis by Using Allogeneic Adipose-Derived Mesenchymal Stem Cells: A Pilot Study. *Stem Cells* **2015**, *33*, 2995–3005.
31. Kwon, D.R.; Park, G.-Y.; Lee, S.C. Regenerative effects of mesenchymal stem cells by dosage in a chronic rotator cuff tendon tear in a rabbit model. *Regen. Med.* **2019**, *14*, 1001–1012.
32. Centeno, C.J. Clinical challenges and opportunities of mesenchymal stem cells in musculoskeletal medicine. *PM&R* **2014**, *6*, 70–77.
33. Meirelles, S.; Fontes, A.M.; Covas, D.T.; Caplan, A.I. Mechanisms Involved in the Therapeutic Properties of Mesenchymal Stem Cells. *Cytokine Growth Factor Rev.* **2009**, *20*, 419–427.
34. Steinert, A.F.; Rackwitz, L.; Gilbert, F.; Nöth, U.; Tuan, R.S. Concise Review: The Clinical Application of Mesenchymal Stem Cells for Musculoskeletal Regeneration: Current Status and Perspectives. *STEM CELLS Transl. Med.* **2012**, *1*, 237–247.
35. Chamberlain, C.S.; Saether, E.E.; Vanderby, R.; Aktas, E. Mesenchymal Stem Cell Therapy on Tendon/Ligament Healing. *J. Cytokine Biol.* **2017**, *2*, 112.
36. Ursini, T.L.; Amelse, L.L.; Elkhenany, H.A.; Odoi, A.; Carter-Arnold, J.L.; Adair, H.S.; Dhar, M.S. Retrospective analysis of local injection site adverse reactions associated with 230 allogenic

administrations of bone marrow-derived mesenchymal stem cells in 164 horses. *Equine Vet. J.* **2019**, *51*, 198–205.
38. Ryan, J.M.; Barry, F.P.; Murphy, J.M.; Mahon, B.P. Mesenchymal Stem Cells Avoid Allogenic Rejection. *J. Inflam.* **2005**, *2*, 8.
39. Hast, M.W.; Zuskov, A.; Soslowsky, L.J. The role of animal models in tendon research. *Bone Jt. Res.* **2014**, *3*, 193–202.
39. Carpenter, J.E.; Thomopoulos, S.; Soslowsky, L.J. Animal Models of Tendon and Ligament Injuries for Tissue Engineering Applications. *Clin. Orthop. Relat. Res.* **1999**, *367*, S296–S311.
40. Thomopoulos, S.; Parks, W.C.; Rifkin, D.B.; Derwin, K.A. Mechanisms of tendon injury and repair. *J. Orthop. Res.* **2015**, *33*, 832–839.
41. National Research Council Committee for the Update of the Guide for the Care and Use of Laboratory Animals. The National Academies Collection: Reports funded by National Institutes of Health. In *Guide for the Care and Use of Laboratory Animals*; National Academies Press: Washington, DC, USA, 2011.
42. Dominici, M.; Le Blanc, K.; Mueller, I.; Slaper-Cortenbach, I.; Marini, F.C.; Krause, D.S.; Deans, R.J.; Keating, A.; Prockop, D.J.; Horwitz, E.M. Minimal criteria for defining multipotent mesenchymal stromal cells. The International Society for Cellular Therapy position statement. *Cytotherapy* **2006**, *8*, 315–317.
43. Dai, L.; Hu, X.; Zhang, X.; Zhu, J.; Zhang, J.; Fu, X.; Duan, X.; Ao, Y.; Zhou, C. Different tenogenic differentiation capacities of different mesenchymal stem cells in the presence of BMP-12. *J. Transl. Med.* **2015**, *13*, 200.
44. Labora, J.A.F.; Fernández-Pernas, P.; Fuentes, I.; De Toro, J.; Oreiro, N.; Sangiao-Alvarellos, S.; Mateos, J.; Arufe, M. Influence of age on rat bone-marrow mesenchymal stem cells potential. *Sci. Rep.* **2015**, *5*, 16765–16765.
45. Alghazali, K.M.; Newby, S.D.; Nima, Z.A.; Hamzah, R.N.; Watanabe, F.; Bourdo, S.E.; Masi, T.J.; Stephenson, S.M.; Anderson, D.E.; Dhar, M.S.; et al. Functionalized gold nanorod nanocomposite system to modulate differentiation of human mesenchymal stem cells into neural-like progenitors. *Sci. Rep.* **2017**, *7*, 16654.
46. Zayed, M.; Caniglia, C.; Misk, N.; Dhar, M.S. Donor-Matched Comparison of Chondrogenic Potential of Equine Bone Marrow- and Synovial Fluid-Derived Mesenchymal Stem Cells: Implications for Cartilage Tissue Regeneration. *Front. Vet. Sci.* **2017**, *3*, 121.
47. Carter-Arnold, J.L.; Neilsen, N.L.; Amelse, L.L.; Odoi, A.; Dhar, M.S. In vitro analysis of equine, bone marrow-derived mesenchymal stem cells demonstrates differences within age- and gender-matched horses. *Equine Vet. J.* **2014**, *46*, 589–595.
48. Shojaee, A.; Parham, A. Strategies of tenogenic differentiation of equine stem cells for tendon repair: Current status and challenges. *Stem Cell Res. Ther.* **2019**, *10*, 1–13.
49. Newby, S.D.; Masi, T.; Griffin, C.D.; King, W.J.; Chipman, A.; Stephenson, S.; Anderson, D.E.; Biris, A.S.; Bourdo, S.E.; Dhar, M. Functionalized Graphene Nanoparticles Induce Human Mesenchymal Stem Cells to Express Distinct Extracellular Matrix Proteins Mediating Osteogenesis. *Int. J. Nanomed.* **2020**, *15*, 2501–2513.
50. Bottagisio, M.; Lopa, S.; Granata, V.; Talò, G.; Bazzocchi, C.; Moretti, M.; Lovati, A.B. Different combinations of growth factors for the tenogenic differentiation of bone marrow mesenchymal stem cells in monolayer culture and in fibrin-based three-dimensional constructs. *Differentiation* **2017**, *95*, 44–53.
51. Handala, L.; Fiore, T.; Rouillé, Y.; Helle, F. QuantIF: An ImageJ Macro to Automatically Determine the Percentage of Infected Cells after Immunofluorescence. *Viruses* **2019**, *11*, 165.

52. Pemberton, K.; Mersman, B.; Xu, F. Using ImageJ to Assess Neurite Outgrowth in Mammalian Cell Cultures: Research Data Quantification Exercises in Undergraduate Neuroscience Lab. *J. Undergrad. Neurosci. Educ. : JUNE: A Publ. FUN, Fac. Undergrad. Neurosci.* **2018**, *16*, A186–A194.
54. Wu, X.; Ren, J.; Li, J. Fibrin glue as the cell-delivery vehicle for mesenchymal stromal cells in regenerative medicine. *Cytotherapy* **2012**, *14*, 555–562.
55. Xu, K.; Al-Ani, M.K.; Sun, Y.; Xu, W.; Pan, L.; Song, Y.; Xu, Z.; Pan, X.; Yang, L. Platelet-rich Plasma Activates Tendon-Derived Stem Cells to Promote Regeneration of Achilles Tendon Rupture in Rats. *J. Tissue Eng. Regen. Med.* **2017**, *11*, 1173–1184.
56. Devana, S.K.; Kelley, B.V.; McBride, O.J.; Kabir, N.; Jensen, A.R.; Park, S.J.; Eliasberg, C.D.; Dar, A.; Mosich, G.M.; Kowalski, T.J.; et al. Adipose-derived Human Perivascular Stem Cells May Improve Achilles Tendon Healing in Rats. *Clin. Orthop. Relat. Res.* **2018**, *476*, 2091–2100.
56. Wagner, J.R.; Taguchi, T.; Cho, J.Y.; Charavaryamath, C.; Griffon, D.J. Evaluation of Stem Cell Therapies in a Bilateral Patellar Tendon Injury Model in Rats. *J. Vis. Exp.* **2018**, *133*, e56810.
57. Yang, Z.; Cao, H.; Gao, S.; Yang, M.; Lyu, J.; Tang, K. Effect of Tendon Stem Cells in Chitosan/β-Glycerophosphate/Collagen Hydrogel on Achilles Tendon Healing in a Rat Model. *Med Sci. Monit.* **2017**, *23*, 4633–4643.
58. Chen, C.; Zhang, T.; Liu, F.; Qu, J.; Chen, Y.; Fan, S.; Chen, H.; Sun, L.; Zhao, C.; Hu, J.; et al. Effect of Low-Intensity Pulsed Ultrasound After Autologous Adipose-Derived Stromal Cell Transplantation for Bone-Tendon Healing in a Rabbit Model. *Am. J. Sports Med.* **2019**, *47*, 942–953.
59. de Girolamo, L.; Morlin Ambra, L.F.; Perucca Orfei, C.; McQuilling, J.P.; Kimmerling, K.A.; Mowry, K.C.; Johnson, K.A.; Phan, A.T.; Whited, J.L.; Gomoll, A.H. Treatment with Human Amniotic Suspension Allograft Improves Tendon Healing in a Rat Model of Collagenase-Induced Tendinopathy. *Cells* **2019**, *8*, 1411.
60. Schneider, C.A.; Rasband, W.S.; Eliceiri, K.W. NIH Image to ImageJ: 25 Years of image analysis. *Nat. Methods* **2012**, *9*, 671–675.
61. Wershof, E.; Park, D.; Barry, D.J.; Jenkins, R.P.; Rullan, A.; Wilkins, A.; Schlegelmilch, K.; Roxanis, I.;Anderson, K.I.; Bates, P.A.; et al. A FIJI macro for quantifying pattern in extracellular matrix. *Life Sci. Alliance* **2021**, *4*, e202000880.
62. Rojewski, M.T.; Weber, B.M.; Schrezenmeier, H. Phenotypic Characterization of Mesenchymal Stem Cells from Various Tissues. *Transfus. Med. Hemotherapy* **2008**, *35*, 168–184.
63. Liu, G.-M.; Pan, J.; Zhang, Y.; Ning, L.-J.; Luo, J.-C.; Huang, F.-G.; Qin, T.-W. Bridging Repair of Large Rotator Cuff Tears Using a Multilayer Decellularized Tendon Slices Graft in a Rabbit Model. *Arthrosc. J. Arthrosc. Relat. Surg.* **2018**, *34*, 2569–2578.
64. Morita, Y.; Yamashita, T.; Toku, T.; Ju, Y. Optimization of differentiation time of mesenchymal-stem-cell to tenocyte under a cyclic stretching with a microgrooved culture membrane and selected measurement cells.. *Acta Bioeng. Biomech.* **2018**, *20*, 3–10.
65. Morita, Y.; Sato, T.; Higashiura, K.; Hirano, Y.; Matsubara, F.; Oshima, K.; Niwa, K.; Toku, Y.; Song, G.; Luo, Q.; et al. The optimal mechanical condition in stem cell-to-tenocyte differentiation determined with the homogeneous strain distributions and the cellular orientation control. *Biol. Open* **2019**, *8*, bio039164.
66. Kadzik, R.S.; Homa, K.E.; Kovar, D.R. F-Actin Cytoskeleton Network Self-Organization Through Competition and Cooperation. *Annu. Rev. Cell Dev. Biol.* **2020**, *36*, 35–60.
67. Yang, F.; Zhang, A.; Richardson, D.W. Regulation of the tenogenic gene expression in equine tenocyte-derived induced pluripotent stem cells by mechanical loading and Mohawk. *Stem Cell Res.* **2019**, *39*, 101489–101489.

68. Shukunami, C.; Takimoto, A.; Nishizaki, Y.; Yoshimoto, Y.; Tanaka, S.; Miura, S.; Watanabe, H.; Sakuma, T.; Yamamoto, T.; Kondoh, G.; et al. Scleraxis is a transcriptional activator that regulates the expression of Tenomodulin, a marker of mature tenocytes and ligamentocytes. *Sci. Rep.* **2018**, *8*, 1–17.
69. Shukunami, C.; Takimoto, A.; Oro, M.; Hiraki, Y. Scleraxis positively regulates the expression of tenomodulin, a differentiation marker of tenocytes. *Dev. Biol.* **2006**, *298*, 234–247.
70. Jackson, J.E.; Kopecki, Z.; Anderson, P.; Cowin, A.J. In vitro analysis of the effect of Flightless I on murine tenocyte cellular functions. *J. Orthop. Surg. Res.* **2020**, *15*, 1–14.
71. Gonçalves, A.; Rodrigues, M.; Lee, S.J.; Atala, A.; Yoo, J.J.; Reis, R.L.; Gomes, M.E. Understanding the Role of Growth Factors in Modulating Stem Cell Tenogenesis. *PLoS ONE* **2013**, *8*, e83734.
72. Zhao, B.; Hu, M.; Wu, H.; Ren, C.; Wang, J.; Cui, S. Tenascin-C expression and its associated pathway in BMSCs following co-culture with mechanically stretched ligament fibroblasts.. *Mol. Med. Rep.* **2017**, *15*, 2465–2472.
73. Li, Y.; Meng, H.; Liu, Y.; Lee, B.P. Fibrin Gel as an Injectable Biodegradable Scaffold and Cell Carrier for Tissue Engineering. *Sci. World J.* **2015**, *2015*, 685690.
74. O'Brien, C.; Marr, N.; Thorpe, C. Microdamage in the equine superficial digital flexor tendon. *Equine Vet. J.* **2021**, *53*, 417–430.
75. Khan, M.R.; Dudhia, J.; David, F.H.; De Godoy, R.; Mehra, V.; Hughes, G.; Dakin, S.G.; Carr, A.J.; Goodship, A.E.; Smith, R.K.W. Bone marrow mesenchymal stem cells do not enhance intra-synovial tendon healing despite engraftment and homing to niches within the synovium. *Stem Cell Res. Ther.* **2018**, *9*, 1–14.
76. Khan, M.R.; Smith, R.K.; David, F.; Lam, R.; Hughes, G.; De Godoy, R.; Carr, A.J.; Goodship, A.E.; Dudhia, J. Evaluation of the Effects of Synovial Multipotent Cells on Deep Digital Flexor Tendon Repair in a Large Animal Model of Intra-Synovial Tendinopathy. *J. Orthop. Res.* **2020**, *38*, 128–138.
77. Ahrberg, A.B.; Horstmeier, C.; Berner, D.; Brehm, W.; Gittel, C.; Hillmann, A.; Josten, C.; Rossi, G.; Schubert, S.; Winter, K.; et al. Effects of mesenchymal stromal cells versus serum on tendon healing in a controlled experimental trial in an equine model.. *BMC Musculoskelet. Disord.* **2018**, *19*, 230.

APPENDIX

Score	Fiber Structure and Arrangement	Cell Density	Cell Appearance	Inflammation	Neovascularization	Fatty Deposits
0	Normal; compact, parallel, and long fibers	Normal	Long, spindle-shaped cells with elongated nuclei	<10%	Normal appearance and number of vascular bundles	Normal; no lipid deposits
1	Slight fragmentation; mildly wavy, disorganized fibers	Slightly increased	Slightly rounded cells	10-20%	Slight increase in vascularity	Slight increase in lipid deposits
2	Moderate fragmentation and disorganization; crossed, wavy, and short fibers	Moderately increased	Moderately rounded cells	20-30%	Moderate increase in vascularity	Moderate increase in lipid deposits
3	Severe disorganization with no appreciable pattern; short and fragmented fibers	Markedly increased	Markedly rounded cells with distinctly round nuclei	>30%	Marked increase in vascularity	Marked increase in lipid deposits

Figure 2.1: Histological Grading Scale as Described by Girolamo et al. (2019).

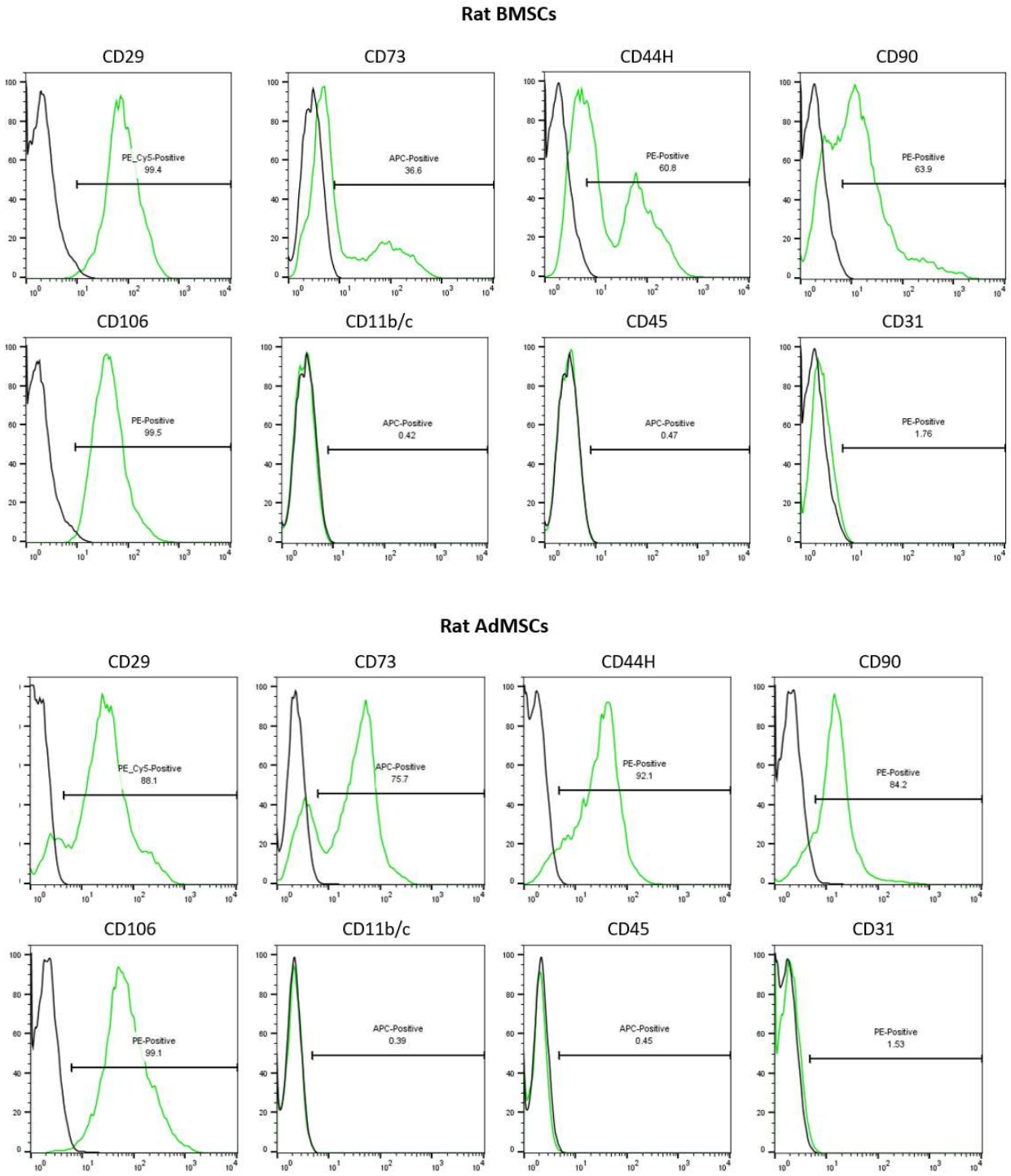

Figure 2.2: Flow Cytometry Results for rAdMSC and rBMSC. These results illustrate a homogenous population of CD29, CD73, CD44H, and CD90 positive rAdMSCs and a heterogenous population of rBMSCs with mixed positive and negative results at the same foci.

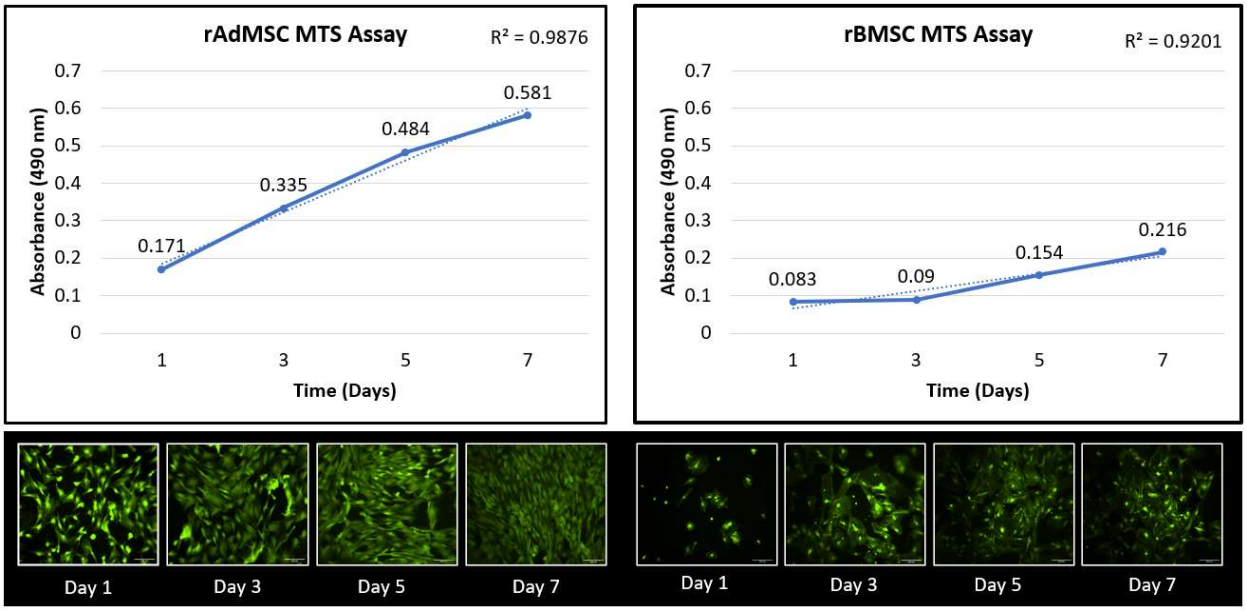

Figure 2.3: Proliferation and Viability Assays of rAdMSCs and rBMSCs. The solid line represents average absorbance at 490 nm at Days 1, 3, 5, and 7, and the dashed line represents the linear trendline for the respective data; the coefficients of determination (R^2 values) of linear regression are reported in the upper right corner of each graph. Representative confocal images of calcein AM stained cells at each timepoint are included below the respective cell lineage's graph. Scale bar = 100 μm.

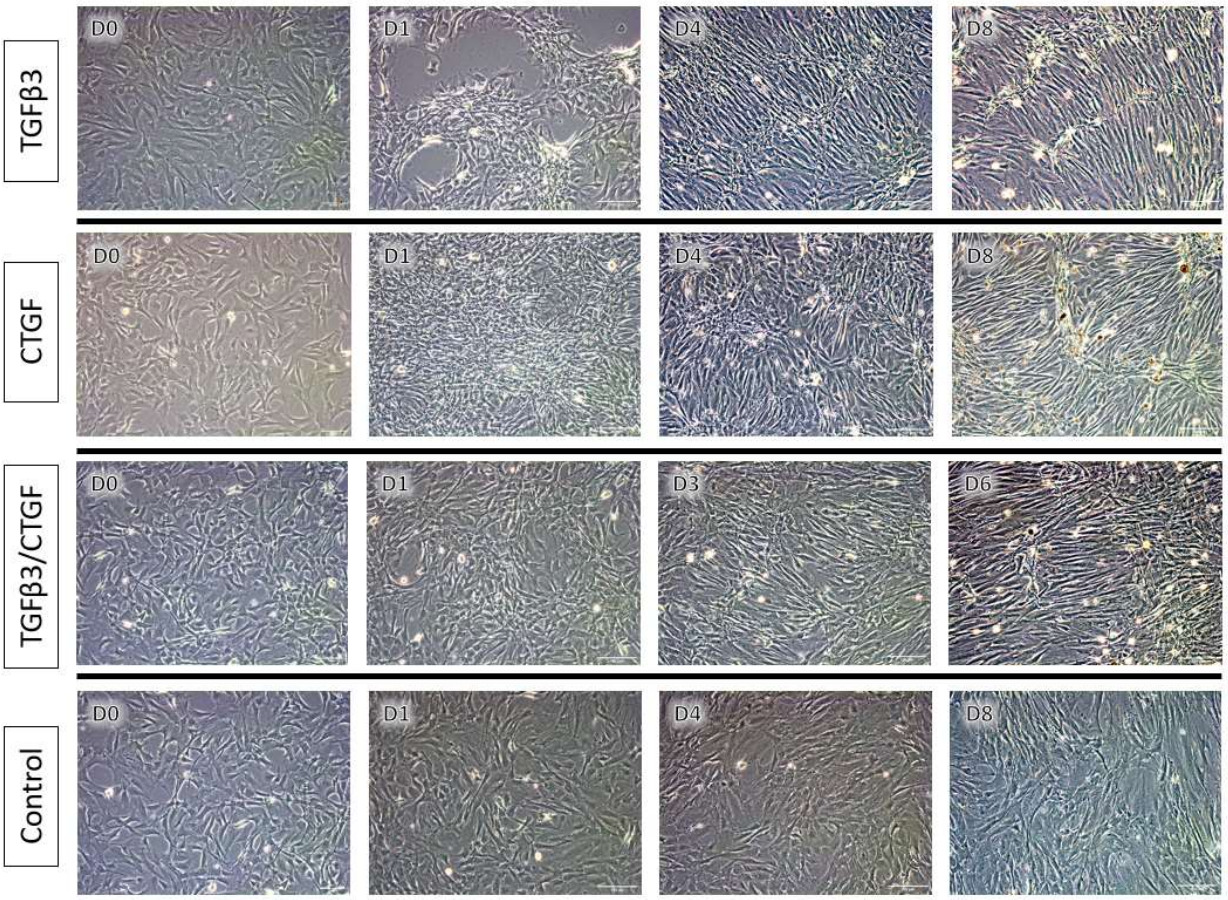

Figure 2.4: Tenogenic Differentiation Trial, Bright Light Phase-Contrast Microscopy. rAdMSCs were maintained in complete medium alone (Control) or were exposed to either TGF-β3 (10 ng/ml), CTGF (100 ng/ml) with 50 μg/ml ascorbic acid, or TGF-β3 (10 ng/ml), CTGF (100 ng/ml), and 50 μg/ml ascorbic acid. Representative images from Days 0, 1, 4, and 8 of the Control, TGF-β3, and CTGF groups and Days 0, 1, 3, and 6 of the TGF-β3/CTGF group are depicted above to illustrate the change in cellular morphology, orientation, alignment, and extracellular matrix. Scale bar = 100 μm.

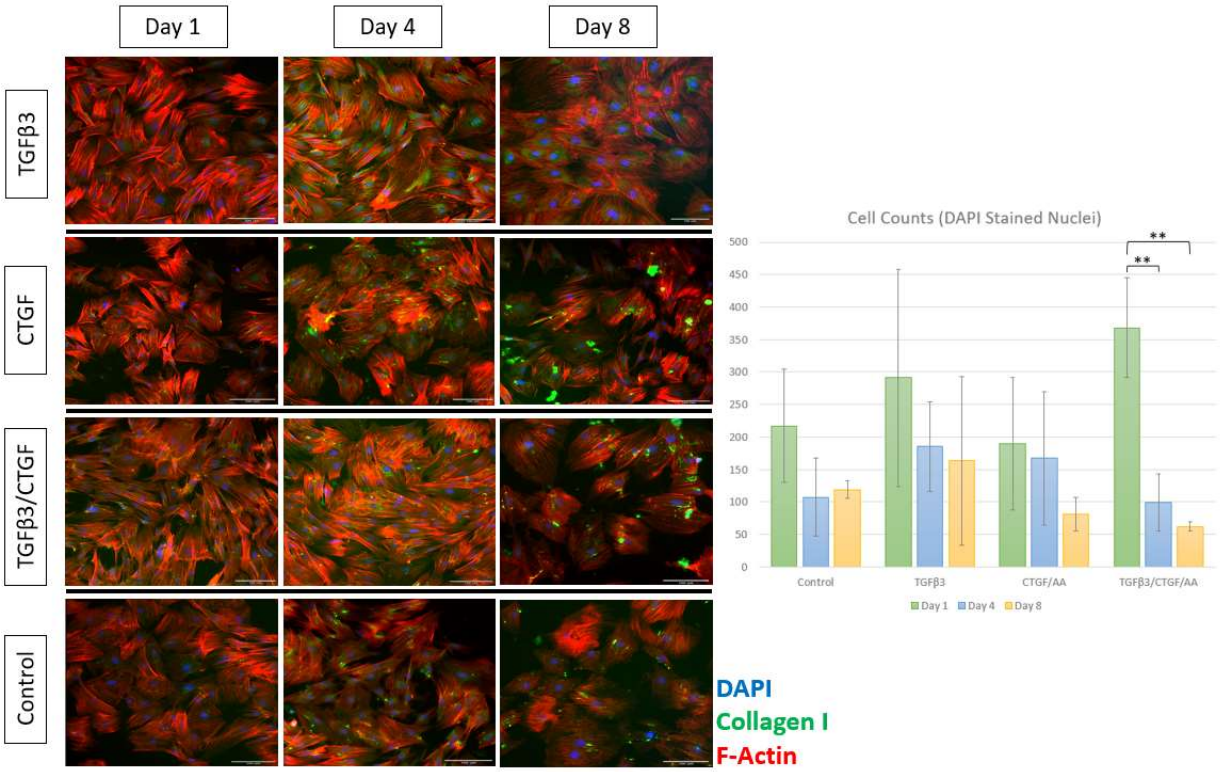

Figure 2.5: Collagen Type I and F-Actin Immunofluorescence and Cellular Quantification. Expression of collagen Type I (green) and F-actin (red) in rAdMSCs exposed to various growth factor enriched media at Days 1, 4, and 8 of culture; cell nuclei counterstained with DAPI (blue). Mean values of DAPI stained nuclei counts are depicted in the accompanying chart; cell counts significantly decreased between Day 1 and Days 4 and 8 in the group treated with TGFβ3/CTGF/AA. Scale bar = 100 μm. "**" represents $p<0.01$ in pairwise comparison.

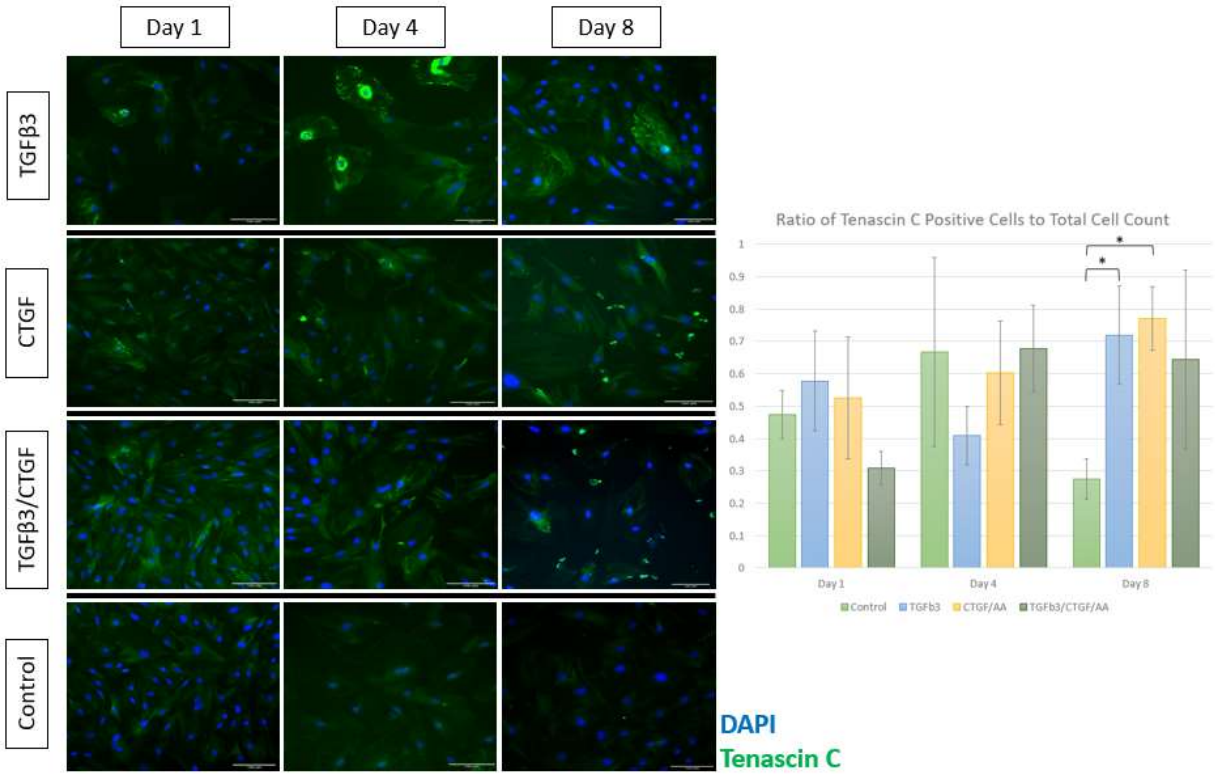

Figure 2.6: Tenascin C Immunofluorescence and Quantification. Expression of tenascin C (green) in rAdMSCs exposed to various growth factor enriched media at Days 1, 4, and 8 of culture; cell nuclei counterstained with DAPI (blue). Immunofluorescence staining of tenascin C was significantly upregulated in the groups treated with CTGF/ascorbic acid (AA) and with TGFβ3 on Day 8. Scale bar = 100 μm. "*" represents $p<0.05$ in pairwise comparison.

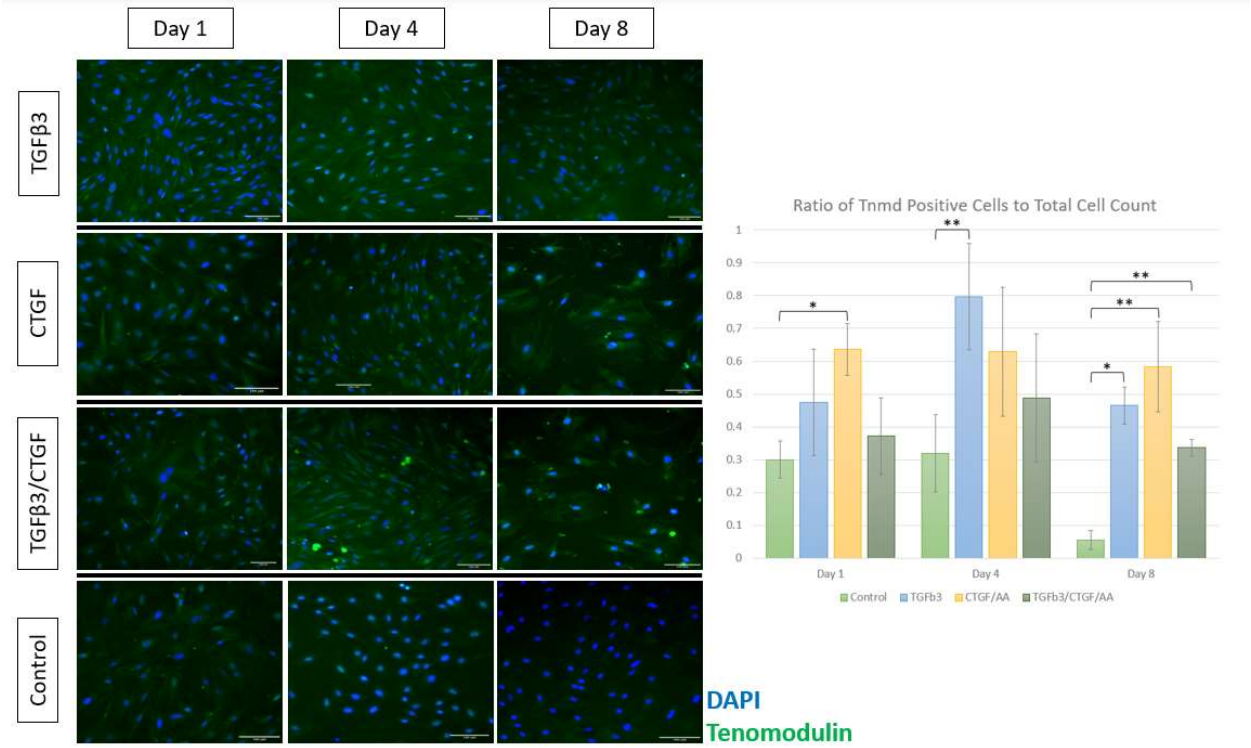

Figure 2.7: Tenomodulin Immunofluorescence and Quantification. Expression of tenomodulin (green) in rAdMSCs exposed to various growth factor enriched media at Days 1, 4, and 8 of culture; cell nuclei counterstained with DAPI (blue). Immunofluorescence staining of tenomodulin was significantly upregulated in the group treated with CTGF/ascorbic acid (AA) on Day 1, in the group treated with TGFβ3 on Day 4, and in the groups treated with CTGF/AA, TGFβ3, and TGFβ3/CTGF/AA on Day 8. Scale bar = 100 μm. "*" represents $p<0.05$ and "**" represents $p<0.01$ in pairwise comparison.

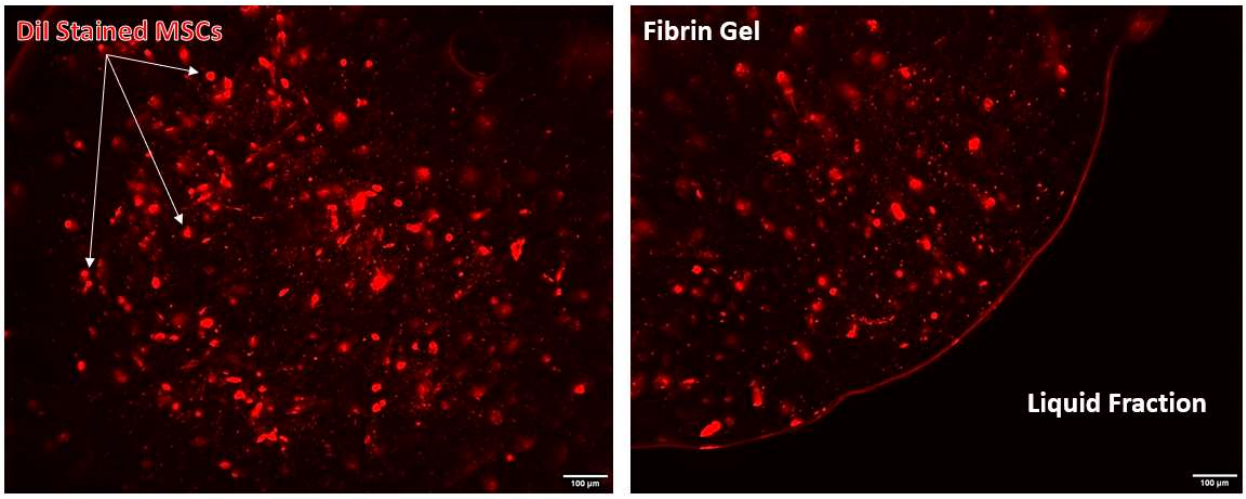

Figure 2.8: Fibrin Gel Cellular Uptake. Immunofluorescent images of equine mesenchymal stem cells (red) suspended in fibrin gel. The image on the left highlights cellular suspension within the gel and the image on the right highlights the relative concentrations of cells entrapped in the gel compared to those remaining in the liquid fraction residual from fibrin gel fabrication. Scale bar = 100 μm.

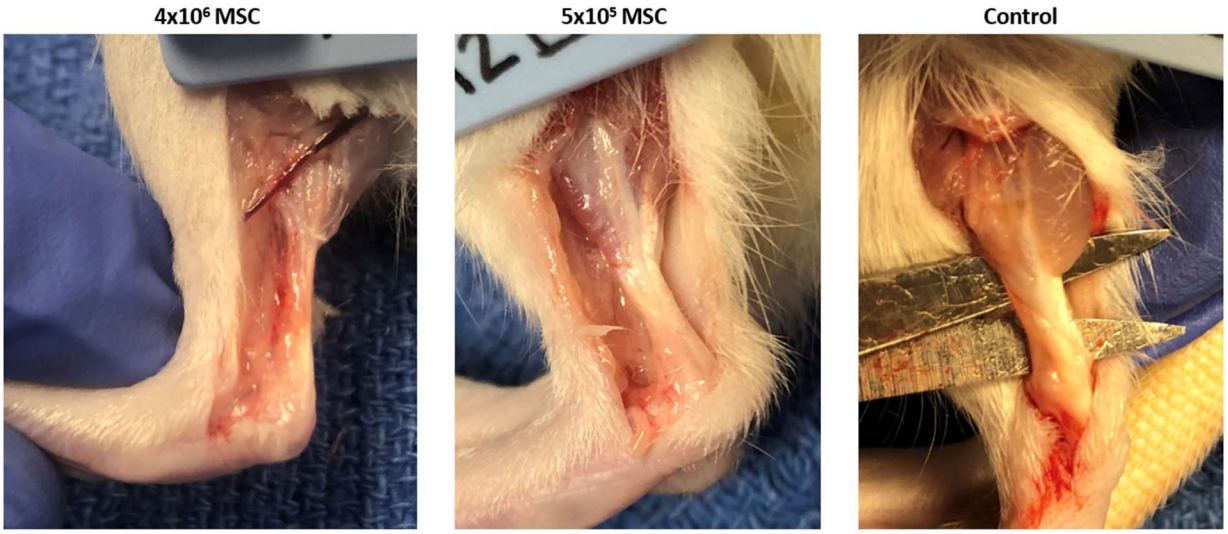

Figure 2.9: Gross Pathology. Gross appearance of the rat Achilles tendon 30 days after tendon injury and intralesional rAdMSC treatments at the indicated dosages

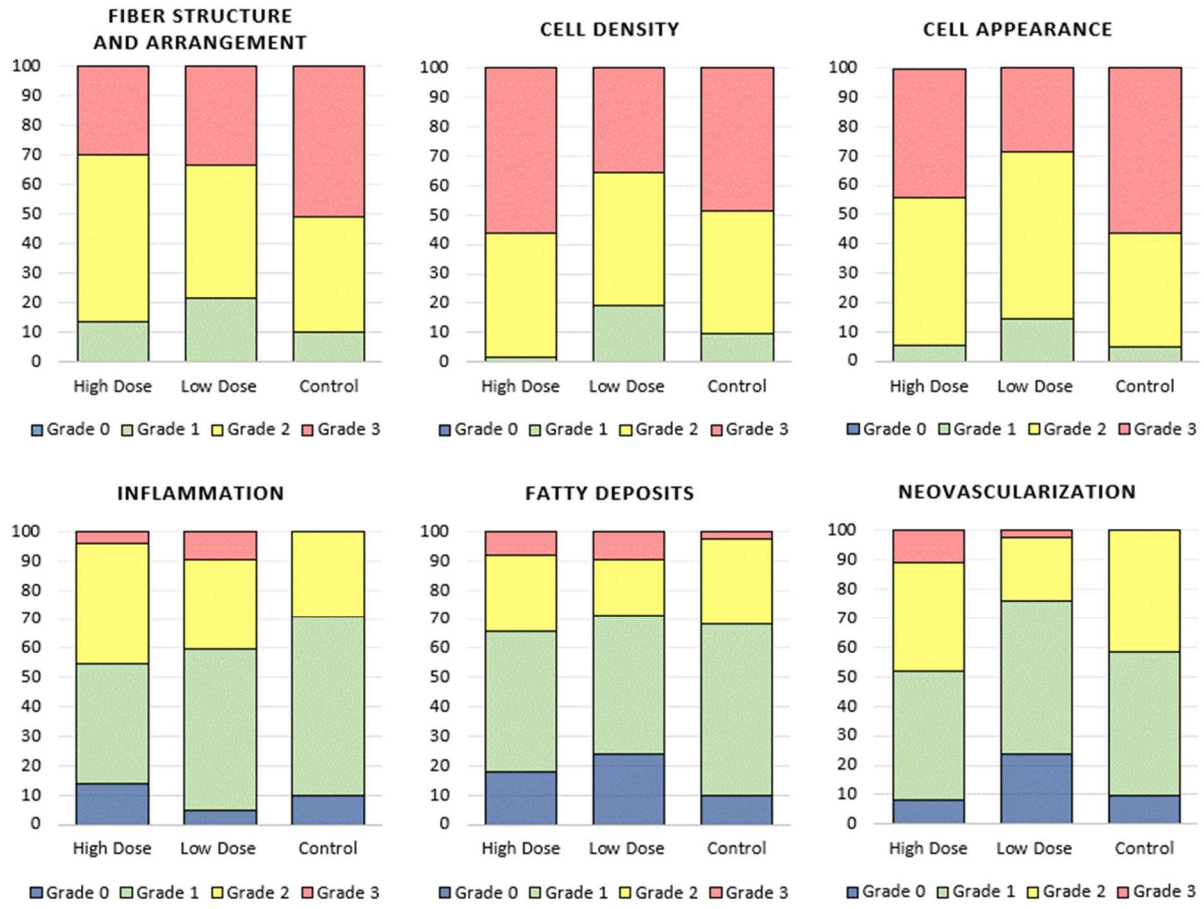

Figure 2.10: Histological Grading. Results of histological grading (H&E) in terms of fiber structure, cell density, cell appearance, inflammation, neovascularization, and fatty deposits; color corresponds to histological grade and color bar height indicates the percentage of the indicated treatment group assigned that histological grade. No statistically significant differences in histological grade were detected between the high dose, low dose, and control groups in any category.

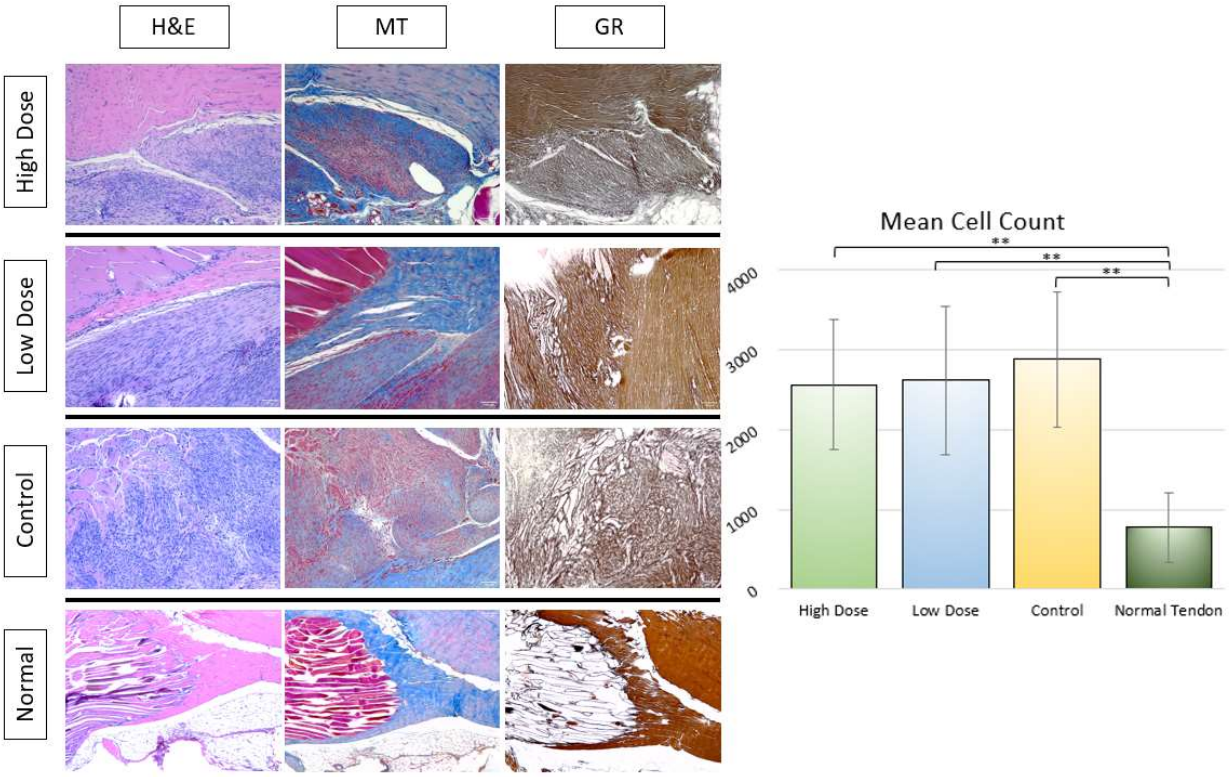

Figure 2.11: Histological Staining and Quantification. Histological staining of rat Achilles tendon 30 days after tendon injury and treatment compared to uninjured rat Achilles tendon. H&E staining highlights cellular density, architectural changes to the tendon matrix, cellular morphology, and abnormal vascularization or fat deposition within the tissue. Masson's Trichrome staining highlights changes in the tendon extracellular matrix with more normal tendon tissue (blue) and muscle (bright red) differentiated from abnormal matrix (dull red). Gomori's Reticulin stain highlights abnormal reticular fiber conformation and overall organization of fibrous tissue within the tendon. Scale bar = 100 μm. Mean cell counts on H&E-stained samples are depicted to the right. "**" represents $p<0.01$ in pairwise comparison.

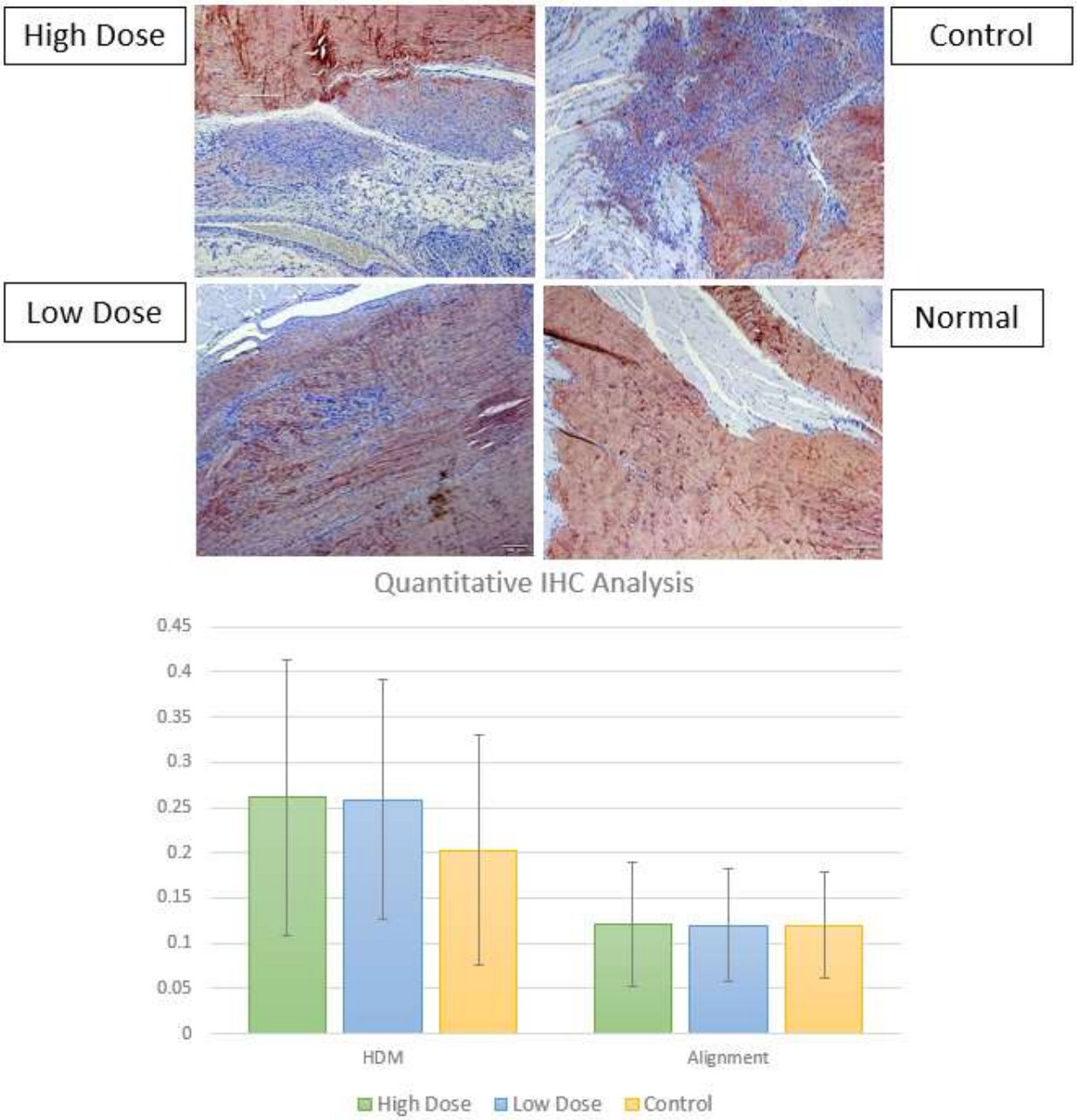

Figure 2.12: Collagen Type I Immunostaining and TWOMBLI Analysis. Collagen Type I immunostaining of rat Achilles tendon 30 days after tendon injury and treatment compared to normal, uninjured rat Achilles tendon. Scale bar = 100 μm. Quantitative TWOMBLI metrics of high-density matrix and matrix alignment are presented in the chart above. No significant differences in quantitative analysis of collagen I IHC were noted between treatment groups.

CHAPTER III:

ASSESSMENT OF GAIT FOLLOWING LOCKING PLATE FIXATION OF A TIBIAL SEGMENTAL DEFECT AND CAST IMMOBILIZATION IN GOATS

This chapter was previously published in *Biomechanics* by Kristin Marie Bowers:

Kristin M. Bowers[1*], Lori D. Terrones[1], Elizabeth G. Croy[1], Pierre-Yves Mulon[1], Henry S. Adair[1], and David Anderson[1]

Affiliations:
[1] Large Animal Clinical Sciences, University of Tennessee College of Veterinary Medicine, Knoxville, Tennessee, USA

Corresponding Author:
Kristin Bowers, DVM, Large Animal Clinical Sciences, College of Veterinary Medicine, The University of Tennessee, 2407 River Dr., Knoxville, Tennessee, 37996, USA; email: kbower17@vols.utk.edu

This article was published by *Biomechanics*. 2022; 2(4), 575–590. https://doi.org/10.3390/biomechanics2040045

ABSTRACT

The purpose of this study was to analyze the effects of locking plate fixation used for bridging of tibial segmental ostectomy and of cast immobilization on gait biomechanics in goats. We hypothesized that stable fixation of a segmental bone defect, using a locking plate construct, would result in minimal changes in biomechanical variables of gait in goats, but full-limb immobilization would result in lasting alterations in the immobilized limb's gait kinetics. A pressure-sensing walkway was used to measure biomechanical characteristics for stride, gait, and walking vertical force. Thirteen, non-lame adult Boer-cross goats were trained to walk over a pressure-sensing walkway prior to instrumentation. Segmental ostectomy was performed on the right hind tibia of each goat and the defect was stabilized using bridging plate fixation with a locking compression plate. Per the protocol of an ongoing orthopedic study, the same goats underwent right hindlimb cast immobilization between one and four months postoperatively. Data was collected preoperatively and then over twelve months postoperatively in goats with unrestricted mobility. Statistical analysis revealed no significant alterations in hindlimb kinematics or maximum force when comparing the period after surgery with that after cast immobilization; significant decreases in forelimb stride length and velocity were noted postoperatively but normalized prior to cast placement, suggesting the overall functional stability of fixation. Cast immobilization had a profound and sustained effect on gait with significant alterations in both forelimb kinetics and hindlimb kinetics and kinematics for the remainder of the trial period; increased hindlimb asymmetry characterized by greater weight distribution and impulse to the left hindlimb was observed, suggesting the potential for long-term and/or permanent detrimental effects of prolonged limb immobilization.

INTRODUCTION

Small ruminants such as sheep and goats remain an important species model for translational bone healing research, effectively modeling human osteoporosis, osteoarthritis, bony trauma, and fracture physiology [1-4]. The caprine tibial segmental defect model of bone healing is well described and offers the opportunity to model multiple in vivo healing prognostic factors such as defect size, anatomic location, and soft tissue coverage [2, 5, 6]. Benefits of the caprine model include clinically relevant body weight and long bone dimensions to human subjects allowing use of human implants, bone tissue macro- and microstructural similarities to human bone, similar metabolic and bone remodeling rates to those of human bone, subject trainability, and affordable housing and upkeep in normal group social structure [1, 5, 7, 8]. The caprine model of segmental ostectomy also allows for translational capability in biomaterials and tissue engineering research when combined with plate fixation [9]. Plate osteosynthesis with rigid fixation (ie. dynamic compression plate, limited contact dynamic compression plate, and locking plate) represents the standard treatment for metaphyseal fractures, and it provides long-term stabilization while leaving an open space for biomaterial/ construct implantation [5, 7, 10]. However, at the early stages of fixation, this technique diverts load eccentrically from the tibial shaft to the plate, and the balance of fixation rigidity and mechanical stimulation across the fracture/ostectomy site remains a focus of biomedical research [10-12]. The dynamic compression plate (DCP) offers adequate biomechanical stiffness of fixation, but it is associated with potential complications from excessive periosteal contact and pressure including potential avascular necrosis and/or impaired healing [7, 13, 14]. The limited contact DCP (LC-DCP) reduces the area of periosteal contact and inherent contact-related risks, but it still relies on the plate-bone interface for fixation stability [13]. Conversely, locking plate fixation relies on the screw plate interface for fixation stability and can maintain sufficient strength in cases with weak metaphyseal bone (ie. osteoporosis, osteomalacia, or severe fracture comminution) that would warrant tissue engineering or biomaterial-based intervention [12, 15]. This construct carries similar mechanical stability to external fixation but reduces risks associated with long-term external fixation including infection or patient-associated trauma to the fixation [6, 10-12]. Studies have confirmed similar rates and quality of fracture healing between DCP and locking plate fixation, despite a significant increase in fixation rigidity with the locking plate [13, 16]. However, few studies describe biomechanical analysis of gait following locking plate fixation of segmental ostectomy, assessing the subject's perceived stability of fixation and subsequent weight distribution [17, 18]. Given the translational importance of the caprine and ovine tibial segmental ostectomy models in

biomaterials research, further characterization of the subject's biomechanical response to surgery is necessary.

Cast immobilization is a common clinical practice in both human and veterinary medicine, allowing for necessary immobilization and stability for bone, ligament, tendon, and other soft tissue healing [19, 20]. However, prolonged cast immobilization is associated with common, severe complications including muscle atrophy, intramuscular fibrosis, joint contracture, central and peripheral neural impairment, venous thromboembolism, tendon atrophy, cartilage degeneration, hyperalgesia, and osteoporosis [19-25]. Despite ample research into the biomechanical changes in gait induced during joint immobilization and into the physiologic effects of cast placement on bone, muscle, tendon, and nervous tissue, few studies document long-term alterations in gait following long-term immobilization [23, 26-29]. Caplan et al. described significantly reduced plantar-flexor strength and overall balance impairment after only seven days of ankle immobilization in a prospective human trial [26]. In an equine prospective trial testing the effect of distal limb cast immobilization for 56 days, Stewart et al. observed a 24-fold increase in the likelihood of lameness after cast placement, and complications such as lameness, deep digital flexor tendonitis, decreased metacarpophalangeal joint range of motion, and increased sensitivity to flexion that did not resolve during a 12-week rehabilitation period after cast removal [19]. We aimed to further add to the body of knowledge regarding the effects of extended full limb cast immobilization using serial biomechanical assessment of gait in goat models used in orthopedic research.

Biomechanical assessment of gait via plantar pressure sensing technology provides an objective tool for use in orthopedic research to monitor response to treatment, lameness, and animal welfare [30]. Historically, both subjective and objective measurements of gait have been employed to detect pain in goats. Subjective modalities include visual lameness scores, behavior scoring, and numeric rating scales, but these methods are variable and prone to biases including observer effect and categorical bias (in which an increase in lameness score does not correspond to an equivalent degree of behavioral change) [31-33]. Objective modalities include biomechanical assessment of gait, infrared thermography of an area of interest, pedometer and accelerometer tracking, and biochemical analysis such as plasma cortisol [30-32, 34]. The number of studies utilizing two-dimensional and three-dimensional biomechanical investigation of gait in veterinary research are rapidly increasing, and implementation of biomechanical gait analysis adds weight to both veterinary and translational interpretation of results [35, 36]. In particular, biomechanical analysis of gait via pressure sensing systems is a portable, time-efficient and affordable option for quantitative and serial evaluation of orthopedic pain, and, as opposed to ground reaction force measurement with force plates, it allows the observer to evaluate multiple steps within and among strides in the

same pass [30, 37, 38]. Multi-step analysis enables determination of paired limb symmetry in quadrupedal research species, and calculated asymmetry indices, described as a percentage of paired-limb symmetry, allow for subject-to-subject comparison without confounding factors of heterogenous body size, conformation, body mass, and gait velocity [38-41]. The current study utilizes long-term monitoring of plantar pressure to evaluate goats' biomechanical responses to surgical stabilization of tibial segmental ostectomy and to extended full limb cast immobilization. We hypothesized that stable fixation of a segmental bone defect, using a locking plate construct, would result in minimal changes in biomechanical variables of gait, but full-limb immobilization would result in alterations in gait kinetics of the affected limb.

MATERIALS AND METHODS

Goats

The goats involved in this study were part of an orthopedic research project assessing bone healing over 12 months. Thirty-two female, Boer-cross adult goats were purchased from a licensed, commercial vendor. Criteria for inclusion in this study were goats who completed the 12-month duration orthopedic research study of segmental defects that are non-load sharing and who had complete sets of biomechanical data at the desired time points. All study procedures were approved by the University of Tennessee Animal Care and Use Committee (protocol number 2741) and adhered to the National Institute of Health's Guide for the Care and Use of Laboratory Animals [42]. Of the thirty-two goats enrolled in the ongoing orthopedic research project, thirteen female Boer-cross, adult goats weighing 52.8 ± 7.9 kg (range 29-67 kg) met inclusion criteria for this study. Preoperatively, goats were judged to be free of lameness based on a visual lameness score of 0 out of 4. Hooves and feet were inspected and trimmed to ensure consistent, normal balance and conditioning. Preoperatively, goats were housed in small group pens in groups of four to six (≥17 ft^2 per goat); postoperatively, goats were housed individually in adjacent pens (≥20 ft^2 per goat). Flooring included a layer of wood shavings laid on top of rubber mats over concrete flooring in a conditioned housing facility for the duration of the study. The goats were fed a balanced ration of grass hay, supplemental grain mix, and alfalfa as needed based on body condition and weight change. Free choice fresh water was provided via automatic waterers in group housing and in water buckets in individual pens. Goats were weighed at study entry, weekly for the first thirty days postoperatively, and monthly for the remainder of the study.

Surgery

A mid-diaphyseal segmental ostectomy was performed on the right hind tibia of each goat, and it was stabilized using a custom-designed low contact round double threaded 8-hole, 4.5-mm thick locking plate (Veterinary Orthopedic Implants, St. Augustine, FL, USA) with a solid central portion between the screw holes [5]. The plate was stabilized with eight 4.0-mm diameter locking-head self-tapping screws (Veterinary Orthopedic Implants, St. Augustine, FL, USA), four in the proximal segment and four in the distal segment.

Surgical procedures were as follows. Goats received perioperative antibiotics (ceftiofur sodium 2.2 mg/kg IV, q12h, Zoetis®, Parsippany, NJ., USA, and oxytetracycline 20 mg/kg IV, single dose, Zoetis®, Parsippany, NJ., USA), non-steroidal anti-inflammatory medication (flunixin meglumine 1.1 mg/kg IV, q12h, Merck®, Keniworth, NJ, USA), and opioid analgesic (fentanyl transdermal patch 75 mcg/h, placed 12 hours preoperatively, Mallinckrodt, Surrey, UK). After placement of a jugular intravenous catheter (18GA x 2 in polyurethane catheter, Terumo Medical Corporation, Somerset, NJ., USA), goats were sedated with xylazine (0.05 mg/kg IV, MWI Animal Health, Boise, ID, USA) and induced into general anesthesia using a mixture of ketamine hydrochloride (5 mg/kg IV, MWI Animal Health, Boise, ID, USA) and midazolam (0.25 mg/kg IV, West-Ward Pharmaceuticals, Eatontown, NJ, USA) titrated to effect. The goats were intubated, and general anesthesia was maintained using isoflurane vaporized into oxygen (1-2 L/min, MWI Animal Health, Boise, ID, USA) and administered via endotracheal intubation. Goats were placed in dorsal recumbency and the right hindlimb was suspended in an extended position, clipped, cleaned, and aseptically prepped. A roughly 20 cm incision was made along the medial surface of the tibia, extending from immediately proximal to the medial malleolus to immediately distal to the medial condyle of the tibia. The periosteum was stripped from the bone surface using periosteal elevators (Veterinary Orthopedic Implants, St. Augustine, FL, USA). The locking plate was applied to the craniomedial surface of the tibia and stabilized with screws. Screws were placed using standard techniques, in brief: a 3.2 mm diameter locking-head drill sleeve (Veterinary Orthopedic Implants, St. Augustine, FL, USA) was secured in the intended hole of the locking plate, a guide hole was drilled using a battery-powered orthopedic drill (Model Number: ND-1001, Anhui, China) and 3.2-mm diameter drill bit (Veterinary Orthopedic Implants, St. Augustine, FL, USA) with continuous lavage with sterile saline for cooling and debris clearance, depth and appropriate screw length were determined using a depth gauge (Veterinary Orthopedic Implants, St. Augustine, FL, USA), and each self-tapping screw was manually driven into the bone using a hand-held screwdriver (Veterinary Orthopedic Implants, St. Augustine, FL, USA). After initial placement of screws in the 1st, 4th, 5th, and 8th position with unicortical engagement, the plate was distracted away from the bone to allow for ostectomy using an oscillating bone saw (DEJUN, Shenzhen, China) to create a

2.0 cm segmental defect in the mid-diaphysis. The plate was realigned in contact with the bone and all screws were hand tightened until tight engagement between the screw and plate threads. Soft tissues were closed in a routine fashion and a full limb bandage with medial and lateral plastic splints (Premier1Supplies, Washington, IA, USA) that spanned the limb from foot to stifle was applied for recovery. Postoperatively, the goats were continued on an antibiotic (ceftiofur sodium 2.2 mg/kg IV, q12h, Zoetis®, Parsippany, NJ., USA) and nonsteroidal anti-inflammatory medication (flunixin meglumine 1.1 mg/kg IV, q12h, Merck®, Keniworth, NJ, USA) for three days. Supplemental analgesia was provided via a transdermal opioid (fentanyl patch 75 mcg/h, q72h, Mallinckrodt, Surrey, UK) and/or a non-steroidal anti-inflammatory medication (meloxicam 0.5-1 mg/kg PO, q24h, MWI Animal Health, Boise, ID, USA) at the discretion of the attending veterinarian. Immediately after surgery, goats were maintained in full limb bandages with medial and lateral plastic splints (Premier1Supplies, Washington, IA, USA) that spanned the limb from foot to stifle for the first month. Bandage changes occurred every two days for the first two weeks, then twice weekly for the remainder of the month.

Cast Immobilization

Based on the ongoing research protocol, goats included in this study had full limb casts placed on the treated limbs for a period of three months, beginning one month after surgery. Casts were changed monthly. Briefly, each goat was sedated using midazolam (0.25 mg/kg IV, West-Ward Pharmaceuticals, Eatontown, NJ, USA) and xylazine (0.01-0.02 mg/kg IV, MWI Animal Health, Boise, ID, USA) and placed in left lateral recumbency. A fiberglass cast was placed on the right hindlimb encasing the hoof and extending proximally to the level of the femorotibial joint. Goats were maintained in individual housing (≥20 ft^2 per goat) throughout the immobilization period. Following cast removal, the goats were transitioned to a full limb bandage with medial and lateral plastic splints that spanned the limb from foot to stifle. Bandages were changed twice weekly for a minimum of two weeks and then the goats were returned to unrestricted activity. Biomechanical data collection was reinitiated when the goat had returned to unrestricted mobility.

Biomechanical Data Collection

Gait parameters were objectively assessed using an automated, real-time pressure sensing system (Walkway Pressure Mapping System, Tekscan Inc., South Boston, MA, USA) with a sensor matrix of 87.1 cm by 36.9 cm and a sensor density of 1.4 sensors/cm2. The mat was calibrated and equilibrated according to the manufacturer's instructions. Recordings were manually triggered and ended by the

investigator based on the goat's approach and exit from the mat. Maximum recorded frames were set at 1000 frames with a recording rate of 15 frames per second. Goats were trained to walk on a halter through an alleyway that housed the mat into a small pen (~20 sq. ft.). The mat was placed at the midpoint of the alley and covered with a soft, rubber overlay for device protection and to avoid slipping during ambulation. One side of the alleyway was formed using a single plexiglass barrier to allow for perpendicular video recording of each pass (Figure 3.1, please see chapter appendix for all figures and tables). Prior to training, goats were weighed on a digital scale and the weight was recorded in the computer system software for future data. Prior to surgery, the goats were trained to walk at a uniform pace across the mat from a starting handler to a second handler holding a halter with long lead. The lead was held without tension applied to the halter during the pass to allow for free movement at a normal pace. The investigator was positioned at the midpoint of the mat and each pass was recorded using a digital video camera (Microsoft LifeCam Cinema, Microsoft Corporation, Redmond, WA, USA) with the same frame rate of 15 frames per second and positioned at the same location as the investigator to allow for accurate determination of extremity strike and overall gait.

Biomechanical assessment of gait was collected from the three best-fit recordings in one direction, on each of the following timepoints: preoperative (Day -1) and Days 1, 7, 30, 180, 240, 300, and 360 postoperative. The Day 1, Day 7, and Day 30 timepoints were obtained after surgery and without external coaptation. The remaining postoperative timepoints occurred after goats had reached unrestricted mobility following cast immobilization of the treated hindlimb. During each data collection session, each goat was walked across the mat until at least three valid walking passes were obtained. A valid walking pass was defined as traversal of the mat at a progressive and calm walking gait with all four limbs having at least one contact with the pressure sensing surface and without stopping, excessive lateral or medial deviation, distraction, or tension applied on the halter. The data from the first three valid passes on each day were recorded and averaged for each goat and this averaged data was used for further analysis. On Days 1, 7, and 30 postoperatively, each goat's splint bandage was removed prior to pressure mat analysis and replaced immediately after each day's data collection was completed. At the completion of each session, pressure-sensing data was exported from the Tekscan software to Microsoft Excel (Microsoft, Redmond, WA, USA) for backup and storage within an external hard drive (Seagate Technology, Cupertino, CA, USA).

Kinematic variables of interest included the number of stances, gait time-front (sec), gait distance-front (cm), gait velocity-front (cm/sec), cycles per minute, stance time (sec), swing time (sec), stride time (sec), stride length (cm), and stride velocity (cm/sec). Kinetic variables of interest included maximum vertical force (kg), maximum vertical force normalized to body weight (%BW), vertical impulse (kg*sec), vertical impulse normalized to body weight (%BW*sec), and maximum peak pressure (kPa). These

variables were defined as previously reported [30]. Maximum force (kg) and maximum force normalized to body weight (%BW) were collected during the stance phase of each extremity, and when multiple stances were present within the same pass, the values were averaged for further data analysis. Impulse (kg*sec) and impulse normalized to body weight (%BW*sec) utilized the average impulse for a given extremity.

Asymmetry Indices

To further characterize the effects of surgery and cast immobilization on gait, asymmetry indices (ASI) were employed for both the forelimbs and hindlimbs as previously described [40,41]. Briefly, data was transformed using the following equation:

$$ASI = \frac{1}{2} \times \frac{RL - LL}{RL + LL} \times 100$$

where RL is the right limb and LL is the paired left limb. Asymmetry indices were calculated for the variables of limb stance time, stride length, stride velocity, normalized maximum vertical force, normalized maximum impulse, and maximum peak pressure. Variable-specific ASI values, expressed as percent asymmetry, with a value of 0 reflecting perfect symmetry between paired limbs, were generated for each timepoint for each goat and were utilized for statistical analysis.

Statistical Analysis

Descriptive statistics for each kinematic and kinetic variable of interest were generated, including the mean, standard deviation, range, minimum, and maximum values. The effects of time and limb on kinematic and kinetic variables were analyzed using mixed model analysis for randomized block design, respectively, with the individual animal as the block effect. Ranked transformation was applied when diagnostic analysis using Shapiro–Wilk test and Levene's test on residuals exhibited violation of normality and equal variance assumption. Post hoc multiple comparisons were performed with Tukey's adjustment.

Asymmetry indices were calculated for limb stance time, stride length, stride velocity, normalized maximum vertical force, normalized maximum impulse, and maximum peak pressure as described above for all timepoints completed by each goat. Descriptive statistics were generated including mean, standard deviation, and range. ASI were analyzed using repeated-measures analysis of variance and post hoc comparisons were performed with Tukey's adjustment. All biomechanical and asymmetry analyses were conducted in SAS 9.4 TS1M7 (SAS Institute Inc., Cary, NC, USA), and statistical significance was identified at the level of 0.05.

RESULTS

Goats

All goats completed the study to the 12-month endpoint. Due to a software error, data loss was sustained for five goats, affecting the Day 1, Day 7, and Day 30 timepoints. The adjusted sample sizes are reported in Tables 3.1–3.3. Briefly, data from 12 of 13 goats was included in the Day 1 and Day 7 subsets, and data from 10 of 13 goats was included in the Day 30 subset.

Post-Surgical Biomechanics (Days 1-30)

Limb-specific kinematics are presented in Table 3.1 and the variables of stance time, stride length, and stride velocity are illustrated in Figure 3.2 (forelimbs) and Figure 3.3 (hindlimbs). During the initial postoperative period, prior to limb immobilization, significant shortening of stride length was noted in the right forelimb ($p = 0.010$) and left forelimb ($p = 0.026$) on Day 1 compared to preoperative baseline, but stride length normalized by the Day 7 and Day 30 timepoints. No significant changes in hindlimb kinematics were appreciated during the first thirty days postoperative.

Limb-specific kinetics are presented in Table 3.2 and the variables of weight-normalized maximum vertical force, weight-normalized impulse, and maximum peak pressure are illustrated in Figure 3.2 (forelimbs) and Figure 3.3 (hindlimbs). No significant alterations in forelimb kinetics were appreciated in the first thirty days postoperative. Right hindlimb impulse (%BW*s) and maximum peak pressure decreased postoperatively compared to preoperative baseline, reaching significance on Day 30 ($p = 0.041$ and $p = 0.001$, respectively), but no significant change in left hindlimb kinetics was noted.

Post-Immobilization Biomechanics (Days 180-360)

Post-immobilization limb-specific kinematics are included in Table 3.1 and Figures 2 and 3. Significant shortening of forelimb stride length compared with preoperative baseline was found at all post-immobilization timepoints ($p < 0.003$). In addition, average right forelimb stride lengths on Days 240 and 360 were significantly shorter than that on Day 30 ($p = 0.006$ and $p = 0.025$, respectively). Similarly, average left forelimb stride lengths on Days 180, 240, and 360 were significantly shorter as compared with that on Days 7 ($p = 0.020$, $p = 0.003$, and $p = 0.010$, respectively) and 30 ($p = 0.042$, $p = 0.008$, and $p = 0.025$, respectively). Significant decreases in forelimb stride velocity compared with Day 30 were found for the right forelimb on Days 240, 300, and 360 ($p = 0.024$, $p = 0.049$, and $p = 0.029$, respectively) and for the left forelimb on Days 180, 240, 300, and 360 ($p = 0.003$, $p = 0.014$, $p = 0.037$, and $p = 0.018$, respectively).

Throughout the entire postoperative period, no significant alterations in forelimb stance time, swing time, or stride time were noted.

Hindlimb stride length was significantly shortened compared to preoperative baseline at all post-immobilization timepoints with the exception of Day 300 for the left hindlimb ($p < 0.015$ for RH Days 180, 240, 300, and 360 and LH Days 180, 240, and 360). In addition, left hindlimb average stride lengths on Days 180, 240, and 360 were significantly shorter than that of Day 30 ($p = 0.018$, $p < 0.001$, and $p = 0.020$, respectively). Left hindlimb stance time was significantly less on Days 180 and 240 compared to preoperative baseline ($p = 0.010$ and $p = 0.029$). Both left and right hindlimb stride velocity was significantly less on Day 240 compared to their respective preoperative baselines ($p = 0.020$ and $p = 0.003$, respectively). In addition, left hindlimb average stride velocities on Days 180, 300, and 360 were significantly less than that of Day 30 ($p = 0.007$, $p < 0.001$, and $p = 0.034$, respectively). Finally, left hindlimb stance times on Days 180 and 240 were significantly greater than preoperative baseline ($p = 0.010$ and $p = 0.029$, respectively). Although reciprocal lessening of right hindlimb stance time can be appreciated in Table 3.1, these differences were not statistically significant. Throughout the entire postoperative period, no significant differences in left hindlimb stride time and in right hindlimb stance, swing, and stride times were noted.

Post-immobilization limb-specific kinetics are included in Table 3.2 and Figures 3.2 and 3.3. No significant alterations in forelimb kinetics were noted post-immobilization. For the left hindlimb, normalized impulse (%BW*s) on Day 240 was significantly greater than preoperative baseline ($p = 0.019$), but no significant changes in maximum vertical force (%BW) or maximum peak pressure (kPa) were appreciated. Significant alterations of right hindlimb kinetics were noted for all variables throughout the post-immobilization period. Right hindlimb maximum vertical force (%BW) and maximum peak pressure values were significantly less than preoperative baseline on Days 180, 240, 300, and 360 ($p < 0.005$). Right hindlimb impulse (%BW*s) was significantly less than preoperative baseline on Days 180, 300, and 360 ($p < 0.005$).

Asymmetry Indices

Asymmetry index values, expressed as % asymmetry for stance time, stride length, stride velocity, maximum vertical force, impulse, and maximum peak pressure, are presented in Table 3.3 and illustrated in Figure 4. No significant changes in forelimb asymmetry indices were found. No significant differences in stride length, stride velocity, and maximum peak pressure asymmetry indices were found. Hindlimb stance time ASI was significantly greater than baseline on Days 1, 180, 240, 300, and 360 ($p = 0.006$, $p < 0.001$, $p = 0.026$, $p = 0.004$, and $p = 0.006$, respectively). Hindlimb maximum force ASI was significantly greater than preoperative baseline on Days 180 and 300 ($p = 0.028$ and $p = 0.022$, respectively), and hindlimb impulse ASI was significantly greater

than baseline on Days 180, 240, 300, and 360 ($p < 0.001$, $p = 0.013$, $p < 0.001$, and $p = 0.002$, respectively).

DISCUSSION

This study is the first of its kind to characterize the effects of locking plate stabilization of tibial segmental ostectomy and extended cast immobilization on the biomechanical characteristics of gait in goats. The results of this study showed that goats recovered substantially from creation of the surgical model in the first 30 days after surgery; however, prolonged immobilization of the limb resulted in profound alterations in gait kinetics of the affected limb. Notable findings can be categorized temporally into two postoperative periods: pre-immobilization and post-immobilization. Pre-immobilization biomechanical analysis supported our hypothesis and documented the short-term functional stability of locking plate fixation of bone defects. However, marked alterations in gait kinetics and kinematics were noted post-immobilization, suggesting the potential for long-term and/or permanent detrimental effects of prolonged limb immobilization. Unfortunately, the study design of the ongoing orthopedic research project limited our ability to define or control the factors associated with alterations in gait. However, the results reported here could be used to design more specific studies in which risk factors can be isolated.

An important finding in this study is that the transient significant alterations in gait kinematics associated with the locking plate model used in goats normalized by 30 days postoperative. Initially, forelimb stride length significantly decreased bilaterally despite increased stance time. Interestingly, concurrent significant changes in hindlimb kinematics were not present on Day 1, but a significant increase in hindlimb stance time asymmetry was detected. Taken together, these kinematic alterations describe voluntary gait alteration to compensate for surgically induced lameness. Similar shortening of forelimb stride length and increase in forelimb stance time in response to hindlimb lameness were observed in an ovine segmental ostectomy model stabilized with external fixators [17,18]. These kinematic alterations create an offloading effect, allowing for more weight to be distributed across the three unoperated limbs. Although postoperative reductions in right hindlimb maximum vertical force, impulse, and maximum peak pressure were mirrored by increases on the forelimbs and left hindlimb, these compensatory kinetic changes did not reach significance. Kinematic alterations in gait normalized by Day 30 postoperative, supporting the overall functional stability of ostectomy fixation using the locking plate.

Kinetic depreciations in right hindlimb impulse and maximum peak pressure were noted in the pre-immobilization period. This represented an offloading effect similar to that described in an ovine model of tibial segmental ostectomy stabilized by a rigid external fixator, with maximal offloading (defined as local minima in maximum vertical force on the operated limb) occurring at two weeks postoperative and with

normalization by nine weeks postoperative [17,18]. However, as interfragmentary stability was experimentally decreased, the offloading effect became more pronounced and rapid, reaching maximal offloading between 2–7 days postoperative [18]. A notable limitation of the current study is the short pre-immobilization period of 30 days compared to six months post-immobilization. Due to the nature of the ongoing study, long term effects of surgical fixation without cast immobilization could not be assessed, but the timing of maximal offloading may give insight into the functional rigidity of fixation. Unlike that observed by Schell et al., significant decreases in right hindlimb maximum vertical force were not observed in the first thirty days postoperative, and the observed offloading pattern more closely resembles that of the stable, rigid external fixation documented by Seebeck et al. [17,18]. In contrast to both ovine studies, no significant changes in left hindlimb (unoperated paired limb) kinetics or in hindlimb kinetic asymmetry were observed in the current trial's pre-immobilization period. Therefore, the normalization of forelimb kinematics, the lack of significant alterations to hindlimb symmetry, and the gradual and relatively minor changes to hindlimb kinetics support the use of locking plate osteosynthesis as a functionally stable fixation for tibial segmental ostectomy in goats.

Long-term full limb cast immobilization in goats had marked and prolonged effects on gait kinematics and kinetics following cast removal. Both forelimbs exhibited significantly shortened stride lengths and slower stride velocities throughout the post-immobilization period, without apparent normalization. To the authors' knowledge, previous biomechanical analysis of the long-term effects of hindlimb cast immobilization in small ruminants has not been documented. These seemingly permanent alterations in forelimb kinematics may reflect the true treatment effect of hindlimb immobilization, representing an adaptation during cast immobilization, or they may be the result of training effect, with the goats' gait variability and overall stride frequency altered as the number of biomechanical data collection sessions increased. Follow-up studies analyzing either the long-term biomechanical effects of cast immobilization in small ruminants or the trends in normal goat biomechanics over a year of data collection are necessary. However, in this study, a return to preoperative baseline forelimb kinematics post-immobilization was not achieved, and these findings in conjunction with the hindlimb kinetic alterations discussed below suggest potentially permanent detrimental effects of prolonged limb immobilization on gait in goats.

Cast immobilization had significant, lasting effects on hindlimb kinetics and kinematics. Similar to the forelimbs, both hindlimbs exhibited significantly shorter stride lengths compared to preoperative baseline, but unlike in the forelimbs, hindlimb stride velocity was not as consistently affected. Notably, right hindlimb stride velocity did not differ significantly from preoperative baseline during the post-immobilization period. A consistent, concurrent decrease in velocity on all four limbs would explain the significant reductions in stride lengths, but the documented changes in forelimb and left hindlimb kinematics, without concurrent alteration in right hindlimb velocity, suggests

a true treatment effect of cast immobilization. Marked decreases in right hindlimb maximum vertical force, impulse, and maximum peak pressure throughout the post-immobilization period support this treatment effect and emphasize the clinical impact that cast immobilization can have on a limb. Previous studies have extensively documented the physiologic changes that cast immobilization can elicit, including muscle atrophy, neuromuscular impairment, cartilage degeneration, tendon atrophy, and joint stiffness [20–23]. These physiologic changes manifest as functional impairment, as measured by impulse, weight distribution, and muscular strength (isometric force); in a study assessing the effect of one week of hindlimb immobilization in rats, significant reductions in the immobilized limb's strength, load before irreversible deformation (ex vivo), and stiffness were documented following remobilization [20]. In a meta-analysis comparing results of internal fixation and cast immobilization for scaphoid fractures (a non-loadbearing carpal bone) in humans, no difference in overall healing or reported pain was noted between modalities, but functional parameters such as grip strength were impaired in the cast-immobilized group [43].

The current study provides further evidence of functional impairment following immobilization through biomechanical analysis of gait. The immobilized right hindlimb exhibited significant kinematic alterations throughout the post-immobilization period, including reduced stride length and increased asymmetry favoring the left hindlimb in stance time. Marked, significant increases in hindlimb impulse ASIs, reaching over 24% asymmetry favoring the left hindlimb, were noted at all post-immobilization timepoints, and concurrent significant depreciations in right hindlimb impulse, reaching almost a 50% decrease in impulse compared to preoperative baseline, were appreciated. Weight bearing was shifted away from the right hindlimb, as shown by significant decreases in maximum vertical force and maximum peak pressure as well as significant increases in hindlimb maximum force ASI. One limitation of this study is that further characterization of the muscular, neural, and soft tissue changes in both the immobilized and contralateral limb were outside of the scope of the ongoing orthopedic research project. We can hypothesize that the biomechanical changes documented in both hindlimbs were secondary to the physiologic complications described above, but quantification and characterization of atrophy or other degenerative process was not performed. However, the most consistently and significantly affected kinetic variable in this study was impulse; directly related to muscular force and the time over which the motion was completed, a significant drop in impulse without concurrent drop in stride velocity or stride time, as seen in the right hindlimb, indicates a decrease in muscle force (torque) generated for the given motion, most commonly secondary to a decrease in functional muscular mass or activation [44]. Together, these biomechanical changes illustrate the lasting functional impairment of the right hindlimb following long term immobilization, without apparent normalization at six months post-immobilization (Day 360). Questions remain as to the capability for gait normalization after extended

immobilization and future research is required to characterize the long-term potential compensatory changes in quadrupedal gait after hindlimb immobilization. Further, studies aimed to quantitate the temporal effect of limb immobilization may aid researchers and clinicians in post-operative rehabilitative plans to minimize the potential for detrimental effects on animals and patients.

One limitation of the present study is the limited number of subjects included in data analysis. Thirteen goats out of a total population of thirty-two goats met the inclusion criteria for this study. These subjects were selected from an ongoing orthopedic research project exploring bone healing in goats, and they met inclusion criteria ensuring uniformity of gender, surgical fixation, postoperative care, and cast immobilization protocol. Pre-determination of sample size of the study population was not performed because we intended to enroll all qualified goats. On post hoc sample size analysis with type II error set at 0.2, the minimum sample size needed for statistical analysis was eleven goats. Therefore, total population statistical analysis met the appropriate power for interpretation, but further stratification based on demographic factors such as weight or age was not feasible given the current dataset.

CONCLUSIONS

This study documents the effects that locking plate stabilization of a tibial segmental defect and cast immobilization have on goat gait biomechanics. Postoperative data during the pre-immobilization period documented the functional stability of locking plate fixation of segmental bone defects. Due to the nature of the ongoing study, long-term effects of surgical fixation without cast immobilization could not be assessed, but the normalization of forelimb kinematics and lack of significant alterations to hindlimb symmetry and kinetics during the first month after surgery are encouraging. However, marked alterations in gait kinetics and kinematics were noted following cast stabilization, suggesting the potential for long-term and/or permanent detrimental effects of prolonged limb immobilization. In particular, the persistence of gait alteration for six months following coaptation and recovery highlights the profound effects that joint immobilization can have on force distribution and ambulation. Though both procedures affected gait, prolonged cast immobilization had significant and lasting effects which should be considered in the design of future orthopedic research using goat models.

REFERENCES

1. Dias, I.R.; Camassa, J.A.; Bordelo, J.A.; Babo, P.S.; Viegas, C.A.; Dourado, N.; Reis, R.L.; Gomes, M.E. Preclinical and Translational Studies in Small Ruminants (Sheep and Goat) as Models for Osteoporosis Research. *Curr. Osteoporos. Rep.* **2018**, *16*, 182–197. https://doi.org/10.1007/s11914-018-0431-2.
2. Christou, C.; Oliver, R.A.; Pelletier, M.H.; Walsh, W.R. Ovine model for critical-size tibial segmental defects. *Comp. Med.* **2014**, *64*, 377–385.
3. Atarod, M.; Frank, C.B.; Shrive, N.G. Kinematic and Kinetic Interactions During Normal and ACL-Deficient Gait: A Longitudinal In Vivo Study. *Ann. Biomed. Eng.* **2014**, *42*, 566–578. https://doi.org/10.1007/s10439-013-0914-3.
4. Diogo, C.C.; Camassa, J.A.; Fonseca, B.; Maltez da Costa, L.; Pereira, J.E.; Filipe, V.; Couto, P.A.; Raimondo, S.; Armada-da-Silva, P.A.; Maurício, A.C.; et al. A Comparison of Two-Dimensional and Three-Dimensional Techniques for Kinematic Analysis of the Sagittal Motion of Sheep Hindlimbs During Walking on a Treadmill. *Front. Vet. Sci.* **2021**, *8*, 545708. https://doi.org/10.3389/fvets.2021.545708.
5. Grzeskowiak, R.M.; Rifkin, R.E.; Croy, E.G.; Steiner, R.C.; Seddighi, R.; Mulon, P.-Y.; Adair, H.S.; Anderson, D.E. Temporal Changes in Reverse Torque of Locking-Head Screws Used in the Locking Plate in Segmental Tibial Defect in Goat Model. *Front. Surg.* **2021**, *8*, 637268–637268. https://doi.org/10.3389/fsurg.2021.637268.
6. McKinley, T.O.; Natoli, R.M.; Fischer, J.P.; Rytlewski, J.D.; Scofield, D.C.; Usmani, R.; Kuzma, A.; Griffin, K.S.; Jewell, E.; Childress, P.; et al. Internal Fixation Construct and Defect Size Affect Healing of a Translational Porcine Diaphyseal Tibial Segmental Bone Defect. *Mil. Med.* **2021**, *186*, e1115–e1123. https://doi.org/10.1093/milmed/usaa516.
7. Reichert, J.C.; Saifzadeh, S.; Wullschleger, M.E.; Epari, D.R.; Schütz, M.A.; Duda, G.N.; Schell, H.; Van Griensven, M.; Redl, H.; Hutmacher, D.W. The challenge of establishing preclinical models for segmental bone defect research. *Biomaterials* **2009**, *30*, 2149–2163. https://doi.org/10.1016/j.biomaterials.2008.12.050.
8. McGovern, J.A.; Griffin, M.; Hutmacher, D.W. Animal models for bone tissue engineering and modelling disease. *Dis. Model. Mech.* **2018**, *11*, dmm033084. https://doi.org/10.1242/dmm.033084.
9. Zeiter, S.; Koschitzki, K.; Alini, M.; Jakob, F.; Rudert, M.; Herrmann, M. Evaluation of Preclinical Models for the Testing of Bone Tissue-Engineered Constructs. *Tissue Eng. Part C Methods* **2020**, *26*, 107–117. https://doi.org/10.1089/ten.TEC.2019.0213.
10. Xu, G.-H.; Liu, B.; Zhang, Q.; Wang, J.; Chen, W.; Liu, Y.-J.; Peng, A.Q.; Zhang, Y.-Z. Biomechanical comparison of gourd-shaped LCP versus LCP for fixation of comminuted tibial shaft fracture. *J. Huazhong Univ. Sci. Technol. Med. Sci.* **2013**, *33*, 250–257. https://doi.org/10.1007/s11596-013-1106-y.
11. Stoffel, K.; Dieter, U.; Stachowiak, G.; Gächter, A.; Kuster, M.S. Biomechanical testing of the LCP—How can stability in locked internal fixators be controlled? *Injury* **2003**, *34* (Suppl 2), B11–B19. https://doi.org/10.1016/j.injury.2003.09.021.
12. Ahmad, R.A.; Aithal, H.P.; Amarpal; Kinjavdekar, P.; Gope, P.C.; Madhu, D.N. Biomechanical properties of a novel locking compression plate to stabilize oblique tibial osteotomies in buffaloes. *Vet. Surg.* **2021**, *50*, 444–454. https://doi.org/10.1111/vsu.13554.
13. Xue, Z.; Xu, H.; Ding, H.; Qin, H.; An, Z. Comparison of the effect on bone healing process of different implants used in minimally invasive plate osteosynthesis: Limited contact dynamic compression plate versus locking compression plate. *Sci. Rep.* **2016**, *6*, 37902. https://doi.org/10.1038/srep37902.
14. Henkel, J.; Medeiros Savi, F.; Berner, A.; Fountain, S.; Saifzadeh, S.; Steck, R.; Epari, D.R.; Woodruff, M.A.; Knackstedt, M.; Schuetz, M.A.; et al. Scaffold-guided bone regeneration in large volume tibial segmental defects. *Bone* **2021**, *153*, 116163. https://doi.org/10.1016/j.bone.2021.116163.

15. Reichert, J.C.; Cipitria, A.; Epari, D.R.; Saifzadeh, S.; Krishnakanth, P.; Berner, A.; Woodruff, M.A.; Schell, H.; Mehta, M.; Schuetz, M.A.; et al. A tissue engineering solution for segmental defect regeneration in load-bearing long bones. *Sci. Transl. Med.* **2012**, *4*, 141ra93. https://doi.org/10.1126/scitranslmed.3003720.
16. Marcondes, G.D.M.; Paretsis, N.F.; Souza, A.F.D.; Ruivo, M.R.B.A.; Rego, M.A.F.; Nóbrega, F.S.; Cortopassi, S.R.G.; De Zoppa, A.L.D.V. Locking compression plate fixation of critical-sized bone defects in sheep. Development of a model for veterinary bone tissue engineering. *Acta Cirúrgica Bras.* **2021**, *36*, e360601. https://doi.org/10.1590/acb360601.
17. Seebeck, P.; Thompson, M.S.; Parwani, A.; Taylor, W.R.; Schell, H.; Duda, G.N. Gait evaluation: A tool to monitor bone healing? *Clin. Biomech.* **2005**, *20*, 883–891. https://doi.org/10.1016/j.clinbiomech.2005.05.010.
18. Schell, H.; Thompson, M.S.; Bail, H.J.; Hoffmann, J.-E.; Schill, A.; Duda, G.N.; Lienau, J. Mechanical induction of critically delayed bone healing in sheep: Radiological and biomechanical results. *J. Biomech.* **2008**, *41*, 3066–3072. https://doi.org/10.1016/j.jbiomech.2008.06.038.
19. Stewart, H.L.; Werpy, N.M.; McIlwraith, C.W.; Kawcak, C.E. Physiologic effects of long-term immobilization of the equine distal limb. *Vet. Surg.* **2020**, *49*, 840–851. https://doi.org/10.1111/vsu.13441.
20. Oliveira Milani, J.G.P.; Matheus, J.P.C.; Gomide, L.B.; Volpon, J.B.; Shimano, A.C. Biomechanical Effects of Immobilization and Rehabilitation on the Skeletal Muscle of Trained and Sedentary Rats. *Ann. Biomed. Eng.* **2008**, *36*, 1641–1648. https://doi.org/10.1007/s10439-008-9542-8.
21. Kaneguchi, A.; Ozawa, J.; Minamimoto, K.; Yamaoka, K. Morphological and biomechanical adaptations of skeletal muscle in the recovery phase after immobilization in a rat. *Clin. Biomech.* **2020**, *75*, 104992. https://doi.org/10.1016/j.clinbiomech.2020.104992.
22. Clark, B.C.; Taylor, J.L.; Hoffman, R.L.; Dearth, D.J.; Thomas, J.S. Cast immobilization increases long-interval intracortical inhibition. *Muscle Nerve* **2010**, *42*, 363–372. https://doi.org/10.1002/mus.21694.
23. Kannus, R.; Jòzsa, L.; Renström, R.; Järvtoen, M.; Kvist, M.; Lento, M.; Oja, P.; Vuorl, I. The effects of training, immobilization and remobilization on musculoskeletal tissue. *Scand. J. Med. Sci. Sport.* **1992**, *2*, 100–118. https://doi.org/10.1111/j.1600-0838.1992.tb00330.x.
24. Aufwerber, S.; Heijne, A.; Edman, G.; Grävare Silbernagel, K.; Ackermann, P.W. Early mobilization does not reduce the risk of deep venous thrombosis after Achilles tendon rupture: A randomized controlled trial. *Knee Surg. Sport. Traumatol. Arthrosc.* **2020**, *28*, 312–319. https://doi.org/10.1007/s00167-019-05767-x.
25. Ishikawa, K.; Oga, S.; Goto, K.; Sakamoto, J.; Sasaki, R.; Honda, Y.; Kataoka, H.; Okita, M. Voluntary Forelimbs Exercise Reduces Immobilization-Induced Mechanical Hyperalgesia in the Rat Hind Paw. *Pain Res. Manag.* **2021**, *2021*, 1–8. https://doi.org/10.1155/2021/5592992.
26. Caplan, N.; Forbes, A.; Radha, S.; Stewart, S.; Ewen, A.; Gibson, A.S.C.; Kader, D. Effects of 1 Week of Unilateral Ankle Immobilization on Plantar-Flexor Strength, Balance, and Walking Speed: A Pilot Study in Asymptomatic Volunteers. *J. Sport Rehabil.* **2015**, *24*, 156–162. https://doi.org/10.1123/jsr.2013-0137.
27. Nahm, N.; Bey, M.J.; Liu, S.; Guthrie, S.T. Ankle Motion and Offloading in Short Leg Cast and Low and High Fracture Boots. *Foot Ankle Int.* **2019**, *40*, 1416–1423. https://doi.org/10.1177/1071100719868721.
28. Zhang, S.; Clowers, K.G.; Powell, D. Ground reaction force and 3D biomechanical characteristics of walking in short-leg walkers. *Gait Posture* **2006**, *24*, 487–492. https://doi.org/10.1016/j.gaitpost.2005.12.003.
29. Kadel, N.J.; Segal, A.; Orendurff, M.; Shofer, J.; Sangeorzan, B. The Efficacy of Two Methods of Ankle Immobilization in Reducing Gastrocnemius, Soleus, and Peroneal Muscle Activity during Stance Phase of Gait. *Foot Ankle Int.* **2004**, *25*, 406–409. https://doi.org/10.1177/107110070402500607.

30. Rifkin, R.E.; Grzeskowiak, R.M.; Mulon, P.-Y.; Adair, H.S.; Biris, A.S.; Dhar, M.; Anderson, D.E. Use of a pressure-sensing walkway system for biometric assessment of gait characteristics in goats. *PLoS ONE* **2019**, *14*, e0223771. https://doi.org/10.1371/journal.pone.0223771.
31. Reppert, E.J.; Kleinhenz, M.D.; Viscardi, A.; Montgomery, S.R.; Crane, A.R.; Coetzee, J.F. Development and evaluation of two different lameness models in meat goats, a pilot study. *Transl. Anim. Sci.* **2020**, *4*, txaa193. https://doi.org/10.1093/tas/txaa193.
32. Vieira, A.; Oliveira, M.D.; Nunes, T.; Stilwell, G. Making the case for developing alternative lameness scoring systems for dairy goats. *Appl. Anim. Behav. Sci.* **2015**, *171*, 94–100. https://doi.org/10.1016/j.applanim.2015.08.015.
33. Battini, M.; Renna, M.; Giammarino, M.; Battaglini, L.; Mattiello, S. Feasibility and Reliability of the AWIN Welfare Assessment Protocol for Dairy Goats in Semi-extensive Farming Conditions. *Front. Vet. Sci.* **2021**, *8*, 731927. https://doi.org/10.3389/fvets.2021.731927.
34. Coetzee, J.F.; Mosher, R.A.; Anderson, D.E.; Robert, B.; Kohake, L.E.; Gehring, R.; White, B.J.; Kukanich, B.; Wang, C. Impact of oral meloxicam administered alone or in combination with gabapentin on experimentally induced lameness in beef calves1. *J. Anim. Sci.* **2014**, *92*, 816–829. https://doi.org/10.2527/jas.2013-6999.
35. Netukova, S.; Duspivova, T.; Tesar, J.; Bejtic, M.; Baxa, M.; Ellederova, Z.; Szabo, Z.; Krupicka, R. Instrumented pig gait analysis: State-of-the-art. *J. Vet. Behav.* **2021**, *45*, 51–59. https://doi.org/10.1016/j.jveb.2021.06.006.
36. Egenvall, A.; Marr, C.M.; Byström, A. Study design synopsis: How to conduct, prepare, analyse and report equine biomechanical studies. *Equine Vet. J.* **2021**, *53*, 645–648. https://doi.org/10.1111/evj.13439.
37. Connor, P.; Ross, A. Biometric recognition by gait: A survey of modalities and features. *Comput. Vis. Image Underst.* **2018**, *167*, 1–27. https://doi.org/10.1016/j.cviu.2018.01.007.
38. Meijer, E.; Bertholle, C.P.; Oosterlinck, M.; Van Der Staay, F.; Back, W.; Van Nes, A. Pressure mat analysis of the longitudinal development of pig locomotion in growing pigs after weaning. *BMC Vet. Res.* **2014**, *10*, 37. https://doi.org/10.1186/1746-6148-10-37.
39. Meijer, E.; Oosterlinck, M.; Van Nes, A.; Back, W.; Van Der Staay, F.J. Pressure mat analysis of naturally occurring lameness in young pigs after weaning. *BMC Vet. Res.* **2014**, *10*, 193. https://doi.org/10.1186/s12917-014-0193-8.
40. Fanchon, L.; Grandjean, D. Accuracy of asymmetry indices of ground reaction forces for diagnosis of hind limb lameness in dogs. *Am. J. Vet. Res.* **2007**, *68*, 1089–1094. https://doi.org/10.2460/ajvr.68.10.1089.
41. Kano, W.T.; Rahal, S.C.; Agostinho, F.S.; Mesquita, L.R.; Santos, R.R.; Monteiro, F.O.B.; Castilho, M.S.; Melchert, A. Kinetic and temporospatial gait parameters in a heterogeneous group of dogs. *BMC Vet. Res.* **2016**, *12*, 2. https://doi.org/10.1186/s12917-015-0631-2.
42. National Research Council Committee for the Update of the Guide for the Care and Use of Laboratory Animals. The National Academies Collection: Reports Funded by National Institutes of Health. In *Guide for the Care and Use of Laboratory Animals*; National Academies Press (US): Washington, DC, USA; National Academy of Sciences: Washington, DC, USA, 2011.
43. Johnson, N.A.; Fairhurst, C.; Brealey, S.D.; Cook, E.; Stirling, E.; Costa, M.; Divall, P.; Hodgson, S.; Rangan, A.; Dias, J.J. One-year outcome of surgery compared with immobilization in a cast for adults with an undisplaced or minimally displaced scaphoid fracture: A meta-analysis of randomized controlled trials. *Bone Jt. J.* **2022**, *104-b*, 953–962. https://doi.org/10.1302/0301-620x.104b8.Bjj-2022-0085.R2.
44. Schilling, B.K.; Falvo, M.J.; Chiu, L.Z.F. Force-velocity, impulse-momentum relationships: Implications for efficacy of purposefully slow resistance training. *J. Sports Sci. Med.* **2008**, *7*, 299–304.

APPENDIX

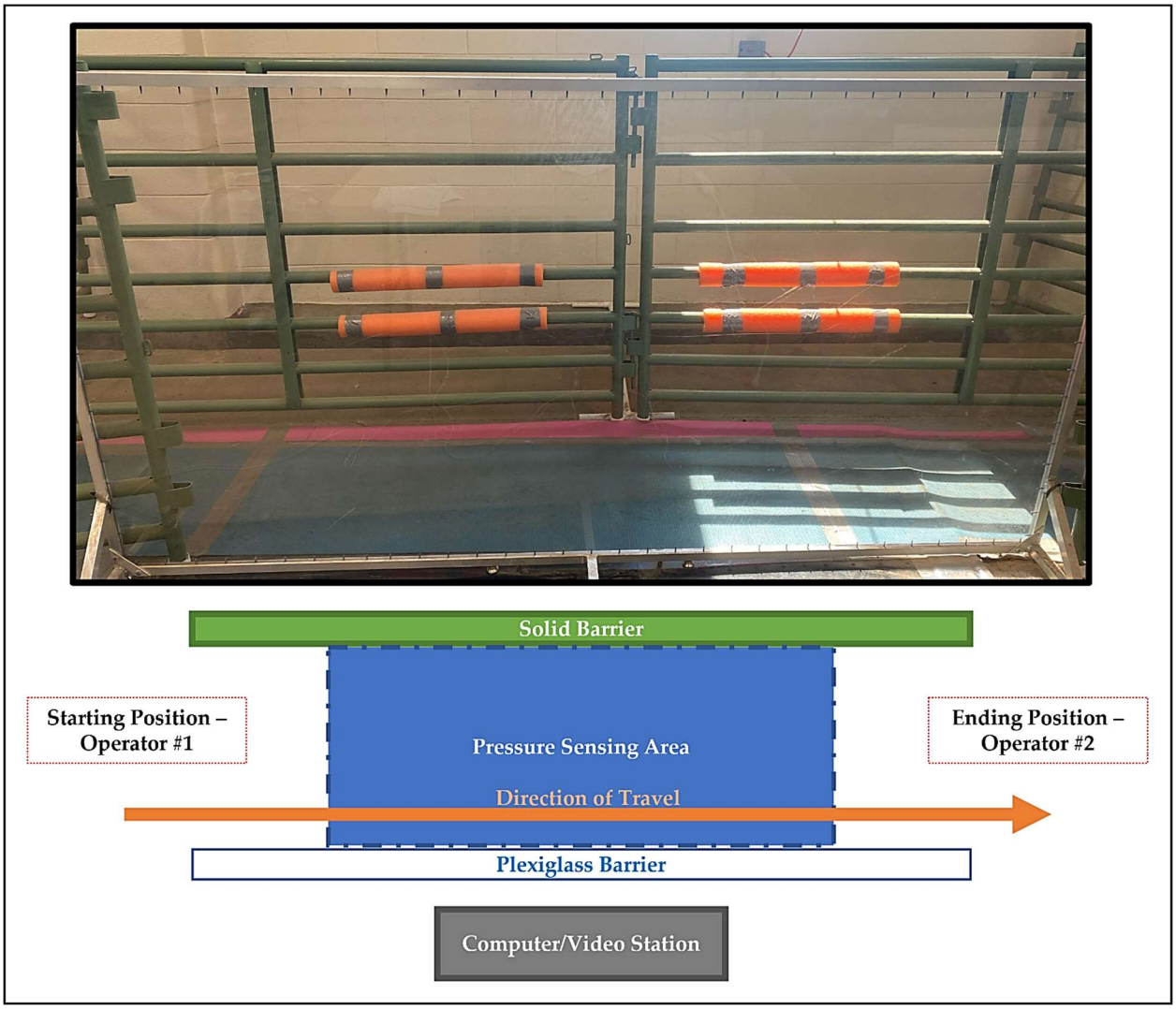

Figure 3.1: Photograph and Associated Diagram of Data Collection Area. Goats were allowed to walk at a self-selected pace in the indicated direction of travel from a starting handler to a second handler holding a halter with long lead. The lead was held without tension applied to the halter during the pass to allow for free movement at a normal pace. Enclosure surrounding ending position not pictured above.

Table 3.1: Forelimb and Hindlimb Kinematics Following Right Hindlimb Tibial Segmental Defect Locking Plate Stabilization and Cast Immobilization. All values are presented as mean ± standard deviation.

Timepoint	N	Stance Time (sec)		Swing Time (sec)		Stride Time (sec)		Stride Length (cm)		Stride Velocity (cm/sec)	
Limb		LF	RF	LF	RF	LF	RF	LF	RF	LF	RF
Preop	13	0.46±0.13	0.47±0.14	0.44±0.19	0.39±0.08	0.85±0.29	0.84±0.21	92.62±7.65	91.54±13.30	114.55±27.55	117.91±34.47
Day 1	12	0.55±0.16	0.53±0.21	0.35±0.07	0.37±0.08	0.84±0.22	0.88±0.30	74.17±15.15[a]	70.97±19.23[a]	96.96±38.51	94.30±34.29
Day 7	12	0.53±0.30	0.50±0.27	0.40±0.14	0.41±0.13	0.87±0.26	0.88±0.30	86.21±12.26	76.59±13.42	109.17±39.45	98.14±38.33
Day 30	10	0.49±0.39	0.48±0.36	0.34±0.09	0.35±0.08	0.84±0.57	0.81±0.45	86.79±13.17	84.02±13.29	136.28±55.33	129.42±56.47
Day 180	13	0.59±0.19	0.49±0.11	0.39±0.12	0.44±0.23	0.95±0.23	0.85±0.24	67.79±16.85[a,b,c]	69.28±10.57[a]	74.98±21.87[c]	89.92±25.17
Day 240	13	0.55±0.12	0.59±0.23	0.37±0.08	0.43±0.15	0.85±0.17	0.90±0.32	64.86±13.85[a,b,c]	63.21±14.79[a,c]	83.50±25.52[c]	80.81±33.17[c]
Day 300	13	0.53±0.09	0.50±0.11	0.37±0.06	0.41±0.09	0.86±0.20	0.88±0.18	71.23±12.28[a]	68.68±8.18[a,c]	87.51±19.74[c]	83.68±15.96[c]
Day 360	13	0.54±0.19	0.51±0.18	0.42±0.19	0.45±0.16	0.96±0.48	0.93±0.36	66.95±12.75[a,b,c]	65.68±10.66[a,c]	84.74±35.48[c]	81.72±29.46[c]
Timepoint	**N**	**Stance Time (sec)**		**Swing Time (sec)**		**Stride Time (sec)**		**Stride Length (cm)**		**Stride Velocity (cm/sec)**	
Limb		**LH**	**RH**	**LH**	**RH**	**LH**	**RH**	**LH**	**RH**	**LH**	**RH**
Preop	13	0.43±0.15	0.45±0.13	0.48±0.18	0.44±0.10	0.87±0.21	0.85±0.18	84.90±20.54	84.72±7.52	103.31±28.14	104.98±23.52
Day 1	12	0.55±0.16	0.34±0.14	0.46±0.21	0.58±0.23	0.88±0.30	0.95±0.31	70.71±19.23	70.60±22.58	87.38±45.34	84.39±40.59
Day 7	12	0.52±0.23	0.45±0.25	0.41±0.08	0.52±0.16	0.88±0.30	1.10±0.75	76.59±13.42	74.73±15.52	90.89±42.54	90.34±42.41
Day 30	10	0.47±0.24	0.41±0.26	0.40±0.12	0.54±0.20	0.81±0.45	0.98±0.44	84.02±13.29	74.56±13.72	121.86±42.49	90.29±41.60
Day 180	13	0.72±0.33[a]	0.36±0.10	0.34±0.06	0.62±0.31	0.93±0.15	1.01±0.37	69.28±10.57[a,c]	62.01±16.78[a]	71.35±18.23[c]	68.50±25.79
Day 240	13	0.70±0.18[a]	0.45±0.10	0.34±0.08	0.69±0.13	1.00±0.19	1.09±0.28	63.21±14.79[a,c]	56.65±13.07[a]	60.38±15.86[a]	54.71±17.73[a]
Day 300	13	0.61±0.11	0.37±0.09	0.34±0.07	0.59±0.16	0.87±0.14	0.99±0.21	68.68±8.18	64.36±9.74[a]	81.43±14.82[c]	72.13±35.74
Day 360	13	0.64±0.15	0.39±0.07	0.34±0.10	0.62±0.21	0.90±0.20	0.97±0.28	65.68±10.66[a,c]	58.97±13.52[a]	79.14±33.73[c]	69.10±27.80

[a] represents value significantly different from preoperative baseline in pairwise comparison; $p < 0.05$.
[b] represents value significantly different from Day 7 in pairwise comparison; $p < 0.05$.
[c] represents value significantly different from Day 30 in pairwise comparison; $p < 0.05$.

Table 3.2: Forelimb and Hindlimb Kinetics Following Right Hindlimb Tibial Segmental Defect Locking Plate Stabilization and Cast Immobilization. All values are presented as mean ± standard deviation.

Timepoint	N	Maximum Vertical Force (%BW)		Impulse (%BW*s)		Maximum Peak Pressure (kPa)	
Limb		LF	RF	LF	RF	LF	RF
Preop	13	49.49±9.43	52.48±11.50	15.42±6.41	15.88±6.16	212.62±61.57	236.15±54.94
Day 1	12	45.49±7.76	49.48±10.57	17.49±5.04	20.89±7.88	198.25±57.63	197.38±53.92
Day 7	12	46.93±13.76	47.18±13.83	15.11±11.37	13.50±5.84	216.44±59.55	194.00±56.39
Day 30	10	48.86±9.66	47.60±8.63	14.84±8.77	14.89±11.29	234.70±54.93	210.70±36.74
Day 180	13	56.02±10.45	47.54±11.23	20.58±5.55	15.42±5.39	209.54±43.87	172.38±52.81
Day 240	13	49.23±6.23	50.93±10.20	18.42±5.63	19.95±9.55	206.31±54.82	191.00±55.90
Day 300	13	51.89±5.43	48.62±11.07	18.87±4.52	15.40±3.52	213.17±48.92	205.50±47.35
Day 360	13	49.73±14.06	48.37±8.95	18.42±8.18	15.11±4.70	193.85±44.05	218.08±39.67

Timepoint	N	Maximum Vertical Force (%BW)		Impulse (%BW*s)		Maximum Peak Pressure (kPa)	
Limb		LH	RH	LH	RH	LH	RH
Preop	13	34.02±7.55	35.79±6.52	9.78±3.59	10.34±3.24	159.08±31.90	172.23±48.61
Day 1	12	29.96±4.71	25.99±5.93	11.50±3.59	7.11±3.04	164.00±33.65	150.25±43.85
Day 7	12	34.31±7.95	22.78±8.27	10.89±4.40	7.09±5.04	159.67±31.08	131.22±32.35
Day 30	10	36.54±7.75	23.03±7.59	10.81±4.20	6.34±2.88[a]	173.40±46.25	107.78±26.60[a]
Day 180	13	33.48±6.39	19.37±5.37[a]	16.07±8.54	5.41±2.08[a]	156.46±42.97	95.46±31.85[a,b]
Day 240	13	37.44±6.39	25.02±4.33[a]	17.35±6.54[a]	8.37±2.77	161.77±25.41	115.77±29.30[a]
Day 300	13	36.63±9.30	20.17±4.44[a]	14.28±4.82	5.80±2.11[a]	158.50±40.68	118.17±34.24[a]
Day 360	13	34.38±9.69	21.41±4.86[a]	14.18±5.64	5.86±1.64[a]	155.08±36.52	108.08±25.37[a]

[a] represents value significantly different from preoperative baseline in pairwise comparison; $p < 0.05$.
[b] represents value significantly different from Day 1 in pairwise comparison; $p < 0.05$.

Table 3.3: Forelimb and Hindlimb Asymmetry Indices Following Right Hindlimb Tibial Segmental Defect Locking Plate Stabilization and Cast Immobilization. All values are presented as mean ± standard deviation.

Forelimb Asymmetry Indices							
Timepoint	**N**	**Stance Time**	**Stride Length**	**Stride Velocity**	**Max Force**	**Impulse**	**MPP**
Preop	13	2.39±0.52	2.44±0.85	3.65±1.11	6.10±1.40	5.90±1.68	7.78±1.32
Day 1	12	3.76±1.06	2.84±0.88	3.21±1.23	6.59±1.47	6.90±1.78	8.60±2.41
Day 7	12	2.50±0.96	3.87±1.14	4.46±1.11	5.10±1.19	6.50±1.65	6.65±2.19
Day 30	10	3.53±0.84	1.57±0.68	3.98±1.95	6.06±1.33	7.10±2.19	6.87±1.00
Day 180	13	5.47±0.90	3.13±0.69	5.13±1.44	6.29±1.12	8.95±1.87	8.36±1.54
Day 240	13	3.39±0.64	1.89±0.61	5.04±1.63	5.20±1.06	7.39±1.04	5.31±1.22
Day 300	13	2.52±0.46	2.64±0.59	4.50±1.08	3.96±1.29	6.65±1.35	5.87±0.77
Day 360	13	3.07±0.88	1.81±0.40	3.03±0.71	5.67±1.37	7.90±1.41	4.77±1.00

Hindlimb Asymmetry Indices							
Timepoint	**N**	**Stance Time**	**Stride Length**	**Stride Velocity**	**Max Force**	**Impulse**	**MPP**
Preop	13	2.97±0.67	3.41±0.89	4.83±1.09	4.30±0.81	5.53±1.06	5.24±1.22
Day 1	12	12.35±2.41*	4.72±1.82	5.67±2.02	8.37±1.28	14.72±2.79	8.16±1.27
Day 7	12	5.91±1.33	4.38±1.30	7.85±1.80	10.40±3.20	13.16±3.19	7.06±2.33
Day 30	10	8.61±3.34	3.44±0.93	5.98±2.26	11.38±3.55	14.86±4.36	12.31±3.00
Day 180	13	15.77±1.71*	3.15±1.25	5.25±1.48	13.74±2.19*	24.23±2.10*	12.83±2.57
Day 240	13	10.61±1.20*	2.83±0.70	3.97±1.19	9.84±1.77	17.41±2.19*	8.51±1.53
Day 300	13	12.26±1.64*	2.68±0.58	6.71±1.16	14.17±2.13*	20.80±2.60*	9.71±1.66
Day 360	13	11.66±1.38*	3.80±0.97	7.20±1.77	10.91±1.98	19.35±2.21*	9.35±1.75

* represents value significantly different from preoperative baseline in pairwise comparison; $p < 0.05$.

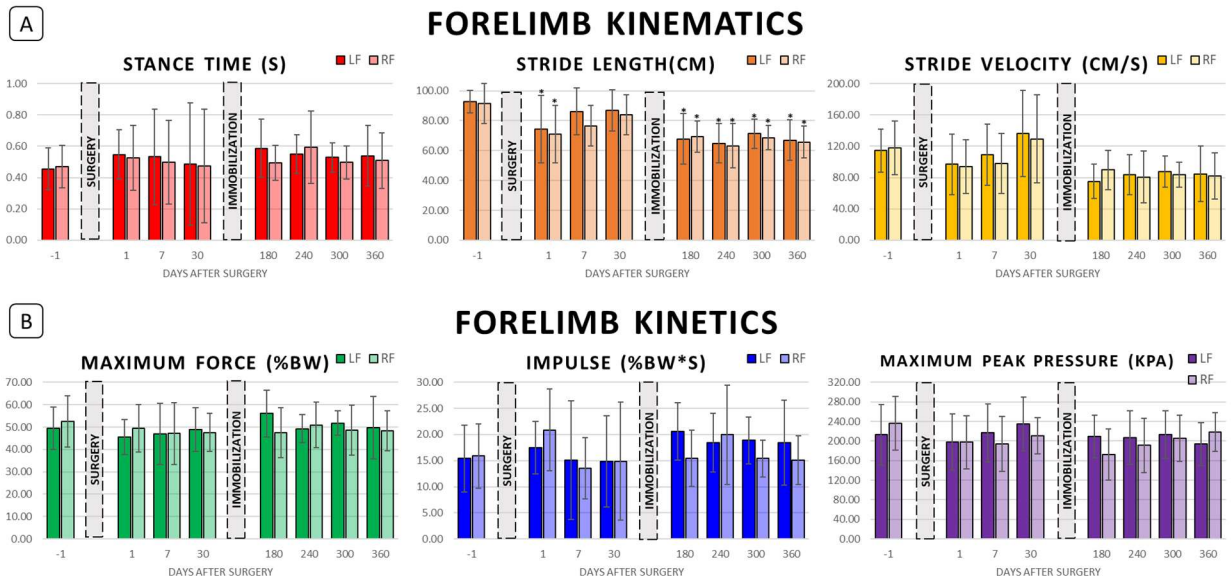

Figure 3.2: Forelimb Biomechanics Following Right Hindlimb Tibial Segmental Defect Locking Plate Stabilization and Cast Immobilization. (**A**) Forelimb kinematics preoperatively (Day -1) and postoperatively at Days 1, 7, 30, 180, 240, 300, and 360. (**B**) Forelimb kinetics at the same timepoints. "*" represents value significantly different from the respective preoperative baseline in pairwise comparison; $p < 0.05$.

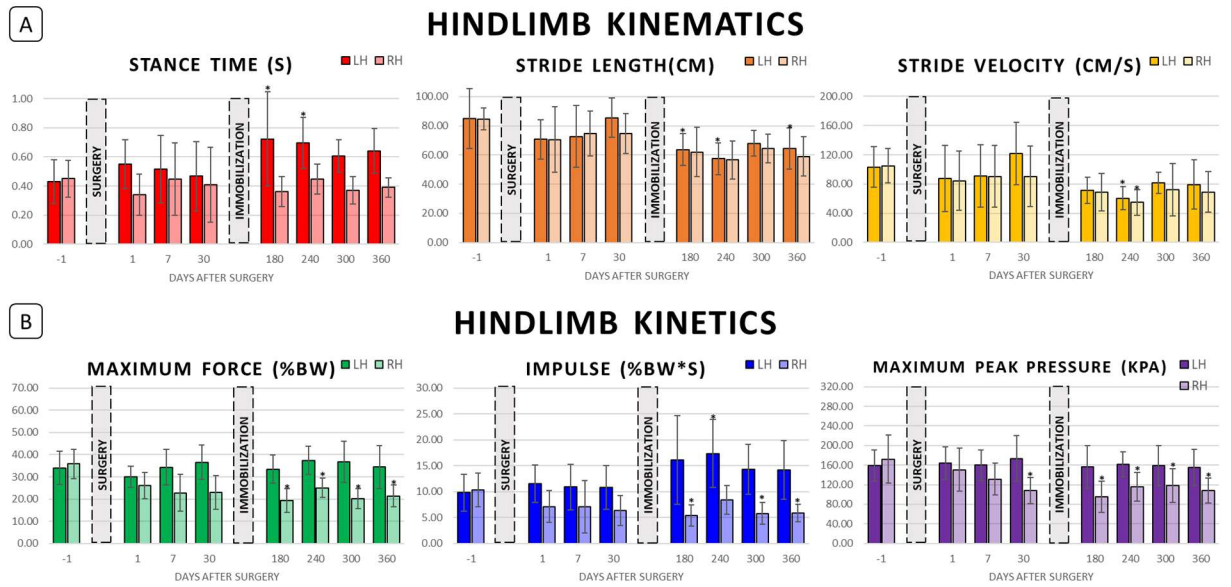

Figure 3.3: Hindlimb Biomechanics Following Right Hindlimb Tibial Segmental Defect Locking Plate Stabilization and Cast Immobilization. (**A**) Hindlimb kinematics preoperatively (Day -1) and postoperatively at Days 1, 7, 30, 180, 240, 300, and 360. (**B**) Hindlimb kinetics at the same timepoints. "*" represents value significantly different from the respective preoperative baseline in pairwise comparison; $p < 0.05$.

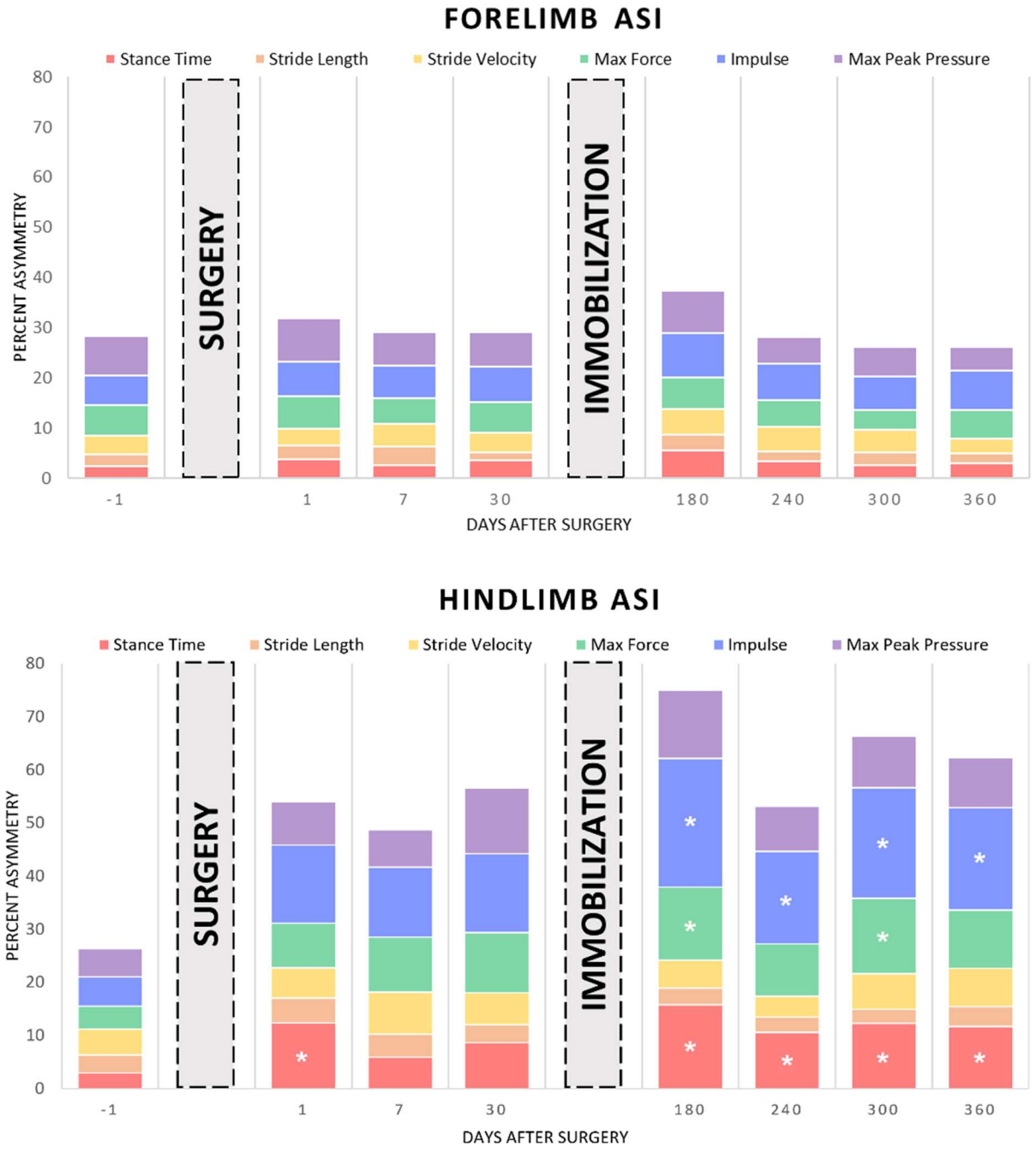

Figure 3.4: Asymmetry Indices. Asymmetry indices for the variables of stance time, stride length, stride velocity, maximum weight-normalized vertical force, impulse, and maximum peak pressure following right hindlimb tibial segmental defect locking plate stabilization and following right hindlimb cast immobilization. "*" represents value significantly different from the respective preoperative baseline in pairwise comparison; $p < 0.05$.

CHAPTER IV:

IN VITRO ANALYSIS AND IN VIVO ASSESSMENT OF FRACTURE COMPLICATIONS ASSOCIATED WITH USE OF LOCKING PLATE CONSTRUCTS FOR STABILIZATION OF CAPRINE TIBIAL SEGMENTAL DEFECTS

This chapter was previously published in *The Journal of Experimental Orthopaedics* by Kristin Marie Bowers and Pierre-Yves Mulon:

Kristin M. Bowers*[1], Ellis M. Wright[2], Lori D. Terrones[1], Xiaocun Sun[3], Rebecca Rifkin[1], Remi Grzeskowiak[1], Elizabeth Croy[1], Reza Seddighi[1], Stephanie Kleine[2], Chiara Hampton[1], Silke Hecht[2], Henry S. Adair III[1], David E. Anderson[1], Pierre-Yves Mulon[1]

Affiliations:
[1] Large Animal Clinical Sciences, University of Tennessee College of Veterinary Medicine, Knoxville, Tennessee, USA
[2] Small Animal Clinical Sciences, College of Veterinary Medicine, University of Tennessee, Knoxville
[3] Office of Information Technology, University of Tennessee, Knoxville

Corresponding Author:
Kristin Bowers, DVM, Large Animal Clinical Sciences, College of Veterinary Medicine, The University of Tennessee, 2407 River Dr., Knoxville, Tennessee, 37996, USA; email: kbower17@vols.utk.edu

This article was published by *The Journal of Experimental Orthopaedics*. 2023; 10(38). https://doi.org/10.1186/s40634-023-00598-9.

ABSTRACT

Locking plate fixation of caprine tibial segmental defects is widely utilized for translational modeling of human osteopathology, and it is a useful research model in tissue engineering and orthopedic biomaterials research due to its inherent stability while maintaining unobstructed visualization of the gap defect and associated healing. However, research regarding surgical techniques and long-term complications associated with this fixation method are lacking. The goal of this study was to assess the effects of surgeon-selected factors including locking plate length, plate positioning, and relative extent of tibial coverage on fixation failure, in the form of postoperative fracture. In vitro, the effect of plate length was evaluated using single cycle compressive load to failure mechanical testing of locking plate fixations of caprine tibial gap defects. In vivo, effects of plate length, positioning, and relative tibial coverage were evaluated using data from a population of goats enrolled in ongoing orthopedic research which utilized locking plate fixation of 2 cm tibial diaphyseal segmental defects to evaluate bone healing over 3, 6, 9, and 12 months. In vitro, no significant differences in maximum compressive load or total strain were noted between fixations using 14 cm locking plates and 18 cm locking plates. In vivo, both plate length and tibial coverage ratio were significantly associated with postoperative fixation failure. The incidence of any cortical fracture in goats stabilized with a 14 cm plate was 57%, as compared with 3% in goats stabilized with an 18 cm plate. Craniocaudal and mediolateral angular positioning variables were not significantly associated with fixation failure. Decreasing distance between the gap defect and the proximal screw of the distal bone segment was associated with increased incidence of fracture, suggesting an effect on proximodistal positioning on overall fixation stability. This study emphasizes the differences between in vitro modeling and in vivo application of surgical fixation methods, and, based on the in vivo results, maximization of plate-to-tibia coverage is recommended when using locking plate fixation of the goat tibial segmental defect as a model in orthopedic research.

INTRODUCTION

Bone healing is a complicated, non-linear process. Factors such as excessive bone loss, unfavorable healing environment, systemic disease, and biomechanical instability in long bone fracture fixation cases can lead to the formation of large defects with limited regenerative capability [1]. The risk of malunion or nonunion complications resulting in segmental defects pose innumerable surgical, socio-economic, and research challenges, and current standard treatment options are limited, sometimes necessitating limb amputation [1, 2]. In people, the tibial shaft is the most common site for segmental defects due to its size, relative lack of soft tissue coverage, and relatively frequent incidence of fracture [1, 3]. Thus, cutting-edge tissue engineering research has focused on the development of synthetic bone graft substitutes and complementary regenerative therapies for these cases of tibial bone loss, fostering a need for suitable translational models [1, 4].

The most relevant species utilized for translational long bone segmental defect modeling are dogs, sheep, goats, and pigs. These species demonstrate physiologic and pathophysiologic similarities to humans in terms of long bone composition and healing, but models utilizing dogs and pigs have declined due to public concerns and limitations in handling and behavior [2, 4]. Goats are a preferred model for translational orthopedic studies due to their trainability, cost-effectiveness, and translational characteristics including body weight, long bone dimensions, bone mineral composition, metabolic rate, and bone remodeling rate compared to humans [1, 4]. The caprine tibial segmental defect model has been well documented in the literature, but fixation and stabilization options vary among research groups [5-8]. Fracture fixation has varied based on clinical application, and reported methods for external and internal fixation include options such as intramedullary pins/nails, intramedullary interlocking nails, single bridging plates, or overlapping auto-compression plates [1, 9]. Orthopedic plate stabilization is a desirable option as it reflects the current standard of care for clinical management of fractures, does not interfere with the defect, and provides for ease of imaging assessment for evaluation of gap fillers including biomaterial scaffold and other implants [1]. However, plate systems used in this model utilize a range of options including dynamic compression plates (DCP), limited-contact dynamic compression plates (LC-DCP), point-contact fixators (PC-Fix), locking compression plates (LCP), and locking plates (LP) [10, 11].

Appropriate plate selection is vital to the use of plate stabilization of segmental defects as these models lack any load sharing by the bone under investigation. At early

stages of fixation, all loads exerted on the distal extremity are conducted along the plate, which is required to support the full range of biomechanical forces exerted in the tibia. As the bone defect heals and bony union is established, plate stresses decrease. However, if the plate reaches fatigue limit prior to bony union or if the fixation is biomechanically unsound, the construct will fail [4, 6, 10]. Bridge plating osteosynthesis relies on a small degree of interfragmentary motion to stimulate callus formation, thus discouraging excessively stiff fixation [10, 12]. Conventional dynamic compression plating requires adequate plate to bone contact during screw tightening to achieve desired stability between the plate and bone surface, and potential complications such as periosteal vascular compromise, stress risers, and loss of compression in compromised bone may lead to fracture complications [13-15]. In contrast, locking compression plating relies more on the screw-plate interface for construct stability, and locking plate fixation is particularly useful in cases of bone loss or poor bone integrity [6, 16]. Biomechanically, DCPs and LC-DCPs convert axial load to shear stress whereas LCPs convert axial load to compressive force, and the stability of a locking plate construct will reflect the sum of screw torques, not merely the friction of the bone-plate interface [17]. Biomechanical comparisons of dynamic and locking plating using both ex vivo bone and in vitro composite bone substitute models have established that LCP fixation (bridging) of a segmental defect yields significantly stiffer constructs in compression and bending [11, 18-22]. However, results have varied regarding the torsional stiffness of LCP constructs with relatively early failure of LCP constructs under torsional testing compared to similar constructs exposed to bending or compression forces [18, 22]. Notably, Gardner et al. documented a consistent mode of failure when human radial constructs stabilized with LCPs were torsion tested in a cyclic fatigue model. The authors noted that LCP constructs typically fractured in a longitudinal pattern originating at the gap and extending along multiple screw holes [22].

Due to its stability and suitability for tissue engineering and bone biomaterial research, locking compression plate fixation has gained widespread use in bone segmental defect models [1, 2]. However, questions regarding risk factors for locking plate implant failure and possible torsional instability persist, and relatively few studies have been published assessing complications associated with tibial locking plate gap stabilization, particularly in small ruminant species [6, 23, 24]. Finite element analysis (FEA) has allowed exploration of intrinsic factors of LCP fixation including plate length, positioning of the plate on the bone, screw number, and screw placement. In a human FEA model utilizing medial placement of an LCP at the tibial diaphysis, construct

rigidity increased directly with plate length, and the authors noted that clinically, the use of relatively longer plates could reduce the risk for fixation failure [25]. Biomechanical testing has corroborated this claim with multiple studies reporting a direct association between locking plate length and construct stiffness [26, 27]. The literature is more divided in regard to working length, the distance between the proximal and distal screws in closest proximity to the fracture gap, with studies reporting that an increase in LCP working length could be associated with increased, decreased, or no change in construct stiffness in axial compressive testing [17, 24, 26, 28]. In human patients, single locking plate internal fixation applied in bridging fashion is commonly applied to comminuted distal femoral fractures [23]. Several retrospective studies have examined risk factors associated with fixation failures in vivo [23, 29, 30]. Patient factors such as age, concurrent systemic disease, diabetes, a history of smoking, and obesity were consistently associated with postoperative complications including infection and reoperation, but additional plate-specific factors of plate length (total) and plate length proximal to the fracture line were significantly associated with implant failure [23]. In retrospective analysis of fracture nonunion following LCP fixation of human distal femoral fractures, plate characteristics including number of locking screws in the proximal fragment and plate material (stainless steel) were significantly associated with nonunion but the factors of plate length, working length, and total number of screws were not [29-32]. To our knowledge, these locking compression plate characteristics and the effect of plate position have not been assessed in vivo in a caprine segmental defect model. In addition, few studies report complications following the use of locking plate fracture fixation in animals and few focus on translational research species such as sheep and goats [5]. Therefore, the goal of this research was to assess a large cohort of goats enrolled in an unrelated orthopedic study in which a tibial segmental defect was stabilized with bridging locking plates and to analyze plate-bone positioning factors associated with implant failure in the form of postoperative fracture complication.

MATERIALS AND METHODS

In Vitro Experiments

Specimen Preparation

Seventeen left hindlimbs were collected from adult goats that had died or were euthanized for reasons other than orthopedic disease. Specimens were frozen at -20°C and thawed at room temperature (22°C) 24 hours prior to testing. Prior to surgical manipulation, limbs were randomly assigned to either long (18 cm) or short (14 cm) plate length groups. All surgeries were performed by the same investigator under the supervision of a veterinary surgeon with extensive orthopedic experience. The tibia was approached via a roughly 20 cm incision along the medial surface of the limb, extending from immediately proximal to the medial malleolus to immediately distal to the medial condyle of the tibia. Overlying soft tissue and periosteum were elevated from the bone to allow plate placement over the craniomedial mid-diaphysis. Custom-designed 316 stainless steel low contact round double threaded 8-hole, 4.5-mm thick locking plates with a solid central portion (Veterinary Orthopedic Implants, St. Augustine, FL, USA) were used for both the in vitro and vivo experimentation. Prior to limb dissection and creation of the defect, the locking plates were secured to the tibias using eight 4.0 mm self-tapping locking screws. Perpendicular alignment was ensured during screw hole drilling using a 3.2 mm diameter locking-head drill sleeve. Screws were hand tightened until tight engagement between the screw and plate threads was achieved at a 4.0 nm torque. Once the plate was secured to the bone the remaining soft tissue around the tibia was excised to harvest the plated tibia. Tibial length and mid-diaphyseal width and depth measurements were obtained using electronic calipers or standard tape measure and were recorded for future analysis. A 1 cm segmental ostectomy was created at the mid-diaphysis of the tibia using a diamond-blade band saw. Care was taken to avoid saw damage to the plate during ostectomy. Proximal and distal epiphyses of each specimen were embedded in poly-methyl-methacrylate (Technovit, Jorgensen Laboratories, Loveland, CO) in a 5 cm diameter, 2.5 cm high cylindrical mold for axial compression testing (Figure 4.1, see Appendix for all figures and tables).

Mechanical Testing

The tibia/plate constructs were assessed using a materials testing system (Instron 5965, Instron, Norwood, MA, USA) with a custom jig to ensure stable hold of the constructs during testing. Specimens were tested in single cycle axial monotonic

compression until failure at a rate of 20 mm/min. End of test criteria were plate failure defined as plastic deformation (bending) of the plate such that the two bone segments touched, bone failure defined as apparent fracture, or arrival at maximal load for the mechanical testing system, pre-set at 4.9 kN. Data was recorded using commercially available software (Bluehill3, Instron, Norwood, MA, USA) and processed using a custom Matlab script (The MathWorks Inc., Natick, MA, USA).

In Vivo Experiments

Goats

All study procedures were approved by the University of Tennessee Animal Care and Use Committee (protocol numbers 2741 and 2383) and adhered to the National Institute of Health's Guide for the Care and Use of Laboratory Animals [33]. Boer-cross, adult goats (n=161 females; mean weight 50.6 ± 7.58 kg, weight range 29 – 73 kg) were used in this study. Preoperatively, goats were housed in small group pens in groups of four to six (≥17 ft^2 per goat); postoperatively, goats were housed individually in adjacent pens (≥20 ft^2 per goat) for a minimum of seven days, followed by group housing based on goat behavior, clinician discretion, and housing availability. Flooring included a layer of wood shavings laid on top of rubber mats over concrete flooring in a conditioned housing facility for the duration of the study. The goats were fed a balanced ration of grass hay, supplemental grain mix, and alfalfa as needed based on body condition and weight change. Free choice fresh water was provided via automatic waterers in group housing and in water buckets in individual pens. Goats were weighed at study entry, weekly for the first thirty days postoperatively, and monthly for the remainder of the study. The goats enrolled in this study were part of a series of orthopedic research projects assessing bone healing following segmental tibial ostectomy. Criteria for inclusion of goats in this study included those having a segmental tibial ostectomy (2 cm defect), bridging fixation using the single, custom designed locking plate, and a minimum of two postoperative orthogonal radiographs available for review and measurement at various time intervals. Exclusion criteria included diagnosis of postoperative osteomyelitis or identification of plate bending on postoperative radiographs during the goats' enrollment in the ongoing orthopedic research.

Surgery

A mid-diaphyseal 2.0 cm segmental ostectomy was performed on the right hind tibia of each goat. The tibia was stabilized using a custom-designed low contact, round locking screw hole, double threaded 8-hole, 4.5-mm thick locking buttress plate with a solid central portion between the screw holes (Veterinary Orthopedic Implants, St. Augustine, FL, USA). Three options for plate length (14 cm, 16 cm, and 18 cm; Figure 4.2) were available for use and plate selection was made at the time of surgery based on surgeon assessment of the tibia. The plate was centered over the ostectomy and secured with eight 4.0-mm diameter self-tapping locking screws (Veterinary Orthopedic Implants, St. Augustine, FL, USA), four in the proximal tibial segment and four in the distal tibial segment. Surgical procedures were conducted as previously described [34]. Postoperatively, goats were maintained in full limb bandages with medial and lateral plastic splints (Premier1Supplies, Washington, IA, USA) that spanned the limb from foot to stifle. Bandage changes occurred every two days for the first two weeks, and then were discontinued between 2 and 4 weeks postoperative based on clinical condition and at the discretion of the supervising veterinarian.

Radiographic examination of the tibia, consisting of a minimum of two orthogonal views centered at mid-tibia, were performed immediately postoperatively, one day following surgery, and then at monthly or bi-monthly intervals as directed by the ongoing orthopedic research protocol. Computed tomographic examination of the operated limb was performed at the time of plate removal, either postmortem or under general anesthesia as dictated by the experimental design. Goats were humanely euthanized at predetermined timepoints of 3, 6, 9, or 12 months postoperatively.

Goats were categorized into two outcome categories, fracture morbidity and no fracture morbidity, based on medical record review and radiographic confirmation of any complete or incomplete tibial fracture. Cases with minor fragmentation of the trans-cortex at the region of bi-cortical screw engagement were not classified as fractures for this analysis.

Plate Position Analysis

Proximodistal Positioning and Tibial Coverage

Proximodistal position, tibial length, and relative tibial coverage were assessed using postoperative craniocaudal and lateromedial radiographic views (Figure 4.3).

Plate lengths were either 14 cm, 16 cm, or 18 cm, and these known distances were used to calibrate the images for further measurements. Screws were numbered proximally to distally with "1" as the most proximal screw and "8" as the most distal screw. Recorded variables included measured tibial length, distance from proximal tibia to proximal extent of locking plate (PrT-Pl), distance from distal tibia to distal extent of locking plate (Pl-DT), distance from the fourth screw to defect (S4-D), and distance from defect to fifth screw (D-S5). The tibial medial condyle served as a repeatable landmark for the proximal extent of the tibia and the medial malleolus was used as the distal extent. With the exception of S4-D and D-S5, all measurements were performed in duplicate utilizing the craniocaudal and lateromedial views, and respective averages were utilized for calculations and statistical analysis. S4-D and D-S5 measurements were performed utilizing the craniocaudal view only, and raw data was statistically analyzed. Relative tibial coverage ratios (TCR) were calculated using the following equation:

$$Tibial\ Coverage\ Ratio = \frac{\text{Plate Length}}{\text{Measured Tibial Length}}$$

Craniocaudal Positioning

Craniocaudal (anterior-posterior, AP) positioning was assessed using computed tomographic examinations at the time of plate removal with the screw tracks serving as positional markers (Figure 4.3). Craniocaudal positions of the plate at the proximal and distal tibia were assessed using the most proximal (S1) and most distal screw tracks (S8), and position was expressed as a ratio using the following equation:

$$Position = \frac{\text{CrS}}{\text{TD}}$$

where CrS represents the distance from the cranial tibia to cranial extent of screw track and TD represents tibial depth at screw midpoint.

Craniocaudal position of the plate at its midpoint (Mid-AP) was calculated as the linear mean of the proximal screw craniocaudal position (Pr-AP) and the distal screw craniocaudal position (D-AP), and the change in relative plate position between the proximal and distal tibia (PrD-Diff) was expressed as the difference between Pr-AP and D-AP. The angle of plate position relative to tibial transverse axis (AP-Angle) was calculated using the following equation:

$$AP - Angle\ = \cos^{-1}\left(\frac{CrS_P\ -\ CrS_D}{Z}\right)$$

where CrS_P represents the distance from cranial tibia to cranial extent of screw track at the most proximal screw and CrS_D represents the same measurement at the most distal screw track. Z designates the known distance between the first and last screw holes on either the 14 cm, 16 cm, or 18 cm plates and served as a conditional constant based on plate length group.

Mediolateral Angular Positioning

Mediolateral angular positioning, in terms of biocentric deviation from the mediolateral plane, was assessed using computed tomographic examinations at the time of plate removal with the screw tracks serving as positional markers (Figure 4.3). All plates were applied in a craniomedial to caudolateral fashion at the time of surgery. To estimate the magnitude of deviation from the tibial frontal axis, the change in relative plate position between the medial (cis) cortex and lateral (trans) cortex (ML-Diff) was calculated using the following equation:

$$ML - Diff = \frac{CrS_L}{TD_L} - \frac{CrS_M}{TD_L} \quad (4)$$

where CrS_L represents the distance from the cranial tibia to cranial extent of screw track immediately adjacent to the lateral (trans) cortex and CrS_M represents the distance from the cranial tibia to cranial extent of screw track immediately adjacent to the medial (cis) cortex. TD_L and TD_M represents tibial depth at the selected lateral and medial points.

Statistical Analysis

Mechanical testing variables, in vitro bone measurements, and in vivo sample characteristics such as body weight distribution were examined using multivariate analysis of variance (MANOVA) and univariate analysis of variance (ANOVA) with treatment as the independent variable. Diagnostic analyses were conducted on residuals for normality model assumption using Shapiro–Wilk test. Post hoc multiple comparisons were performed with Tukey's adjustment. Data were presented as mean $\pm$ SD.

The effects of plate positioning and length on fracture status were evaluated using logistic regression. To detect multicollinearity issues, the variables of goat intake body weight, tibial length, selected plate length, plate positioning, and tibial coverage were assessed for correlation using Pearson's product moment correlation coefficients and variables expressing significant correlation were limited in final analysis. Then, the

effects of plate position, length, and relative tibial coverage on fracture status were screened using multivariate logistic regression analysis controlling for known plate length with the fracture status as the binary response variable. The effects of craniocaudal and mediolateral position on fracture status were analyzed using multivariate logistic regression analysis with incidence of fracture as the binary response variable. Qualitative data are presented as percentages and count numbers. Statistical significance was identified at the level of 0.05. Analyses were conducted in SAS 9.4 TS1M6 for Windows 64x (SAS institute Inc., Cary, NC, USA) and IBM SPSS Statistics v. 28 (IBM Corp. Armonk, NY, USA).

RESULTS

In Vitro Mechanical Testing

A total of seventeen tibias were utilized in this experiment. Each tibia was randomly assigned to either long (18 cm, n=9) or short (14 cm, n=8) plate length groups. Tibial characteristics are presented in Table 4.1. Tibial length and diaphyseal depth did not differ significantly between groups ($p = 0.753$ and $p = 0.282$ respectively), but the long plate group had statistically significantly larger mean diaphyseal width than the short plate group (2.0 cm and 1.8 cm respectively, $p = 0.005$). As per in vitro study design, tibial coverage ratios differed between groups with significantly more tibial diaphysis spanned by the plate in the long plate group ($p < 0.001$).

Fourteen of seventeen tibia-plate constructs failed during axial compression testing limited to 4.9 kN (Table 4.2). Of these, four failed by bone fracture (2 short plate and 2 long plate constructs), six failed by plate bending to the point of impingement of the opposite cortex (4 short plate and 2 long plate constructs), and four failed by initial bending followed by acute bony fracture (2 short plate and 2 long plate constructs). Three constructs, all of which were long plate constructs, reached the test endpoint without apparent failure; these constructs were included in statistical analysis with the measured load and strain at time of test endpoint utilized as maximum load and total strain.

Mean maximum loads for the short and long plate groups were 4314 ± 700 N and 4396 ± 874 N, respectively, and total strains were 7.46 ± 2.48 mm and 7.56 ± 2.99, respectively (Figure 4.4). No significant differences in compressive maximum load or total strain were observed between plate length conditions ($p = 0.793$ and $p = 0.668$, respectively).

Clinical Morbidity

Of 161 goats, 133 met the inclusion criteria for this study. Thirty goats received the 14 cm plate, 38 received the 16 cm plate, and 65 received the 18 cm plate. On initial correlation analysis, surgeon-selected plate length was significantly associated with both the body weight of the goat and the measured radiographic tibial length (p= 0.043 and $p < 0.001$, respectively). However, goat body weight and measured tibial length were not significantly correlated ($p = 0.322$), and body weights of goats with and without fracture were not significantly different ($p = 0.236$). Due to these correlations that cause multicollinearity issues in logistic analysis, only the variable of plate length was included in further analysis for association with postoperative fracture complications. Of the 133 goats, 22 (16.5%) experienced a fracture complication during their assigned postoperative period ranging from 3 to 12 months. Fracture incidence as a function of plate length was 56.7% (17/30) for 14 cm plates, 7.9% (3/38) for 16 cm plates, and 3.1% (2/65) for 18 cm plates. The most common fracture configuration noted was a longitudinal oblique fracture of the proximal tibial segment with the fracture line typically following the screw holes proximally (Figure 4.5).

Plate length was significantly associated with postoperative fracture complication (Table 4.3) with greatest fracture incidence noted in the 14 cm group ($p < 0.0001$). Exploring further, calculated tibial coverage ratios were significantly less in goats that suffered a postoperative fracture compared to those without (0.682 ± 0.039 and 0.748 ± 0.039 respectively, $p < 0.001$). Analysis of measured proximodistal, craniocaudal, and mediolateral positioning variables is presented in Table 4.4. Of these variables, only the proximodistal distance from the gap defect to the fifth screw, the closest screw to the gap within the distal segment, was significantly associated with fracture. Goats that experienced a fracture complication had a mean distance of 21.4 ± 8.34 mm between the defect and fifth screw whereas goats without fracture had a mean distance of 28.5 ± 7.67 mm ($p = 0.008$). No craniocaudal positioning variables or mediolateral deviation from the bicentric plane were significantly associated with the development of postoperative fracture complications.

DISCUSSION

This study highlights the importance of caution when translating in vitro modeling to in vivo application of orthopedic techniques. Mechanical testing of two

locking plate constructs of varying length and tibial coverage showed no difference in mechanical strength or construct stability when exposed to single cycle to failure compressive force in vitro, but upon in vivo application of the construct, significant associations of plate length and tibial coverage with construct failure, in the form of postoperative fracture, were noted. The locking plate and locking compression plate combine mechanical stability of a type-1 external fixator with the benefits of internal fixation such as lower infection risk and lack of external interference [9]. Mechanical testing of LCP stabilized gap defects in vitro have documented superior strength against bending and compressive forces in vitro when compared to conventional dynamic compression plates, but questions have been raised regarding the fixation's torsional strength [11, 12, 17-19, 21]. In a biomechanical study of tibiofemoral contact forces in sheep, Taylor et al. documented significant axial force conveyed to the tibia from the tibiofemoral joint, but unlike humans, sheep experience a greater magnitude of craniocaudal and mediolateral sheer force originating at the stifle [35]. The authors hypothesized that these forces were caused by the obliquity of muscular forces acting on the joint due to a comparatively wide range of motion, and these forces translate to significant off-planar sheer and torsional stresses exerted on the ovine tibia [35]. Similar biomechanical analysis of caprine tibiofemoral forces and tibial stresses has not been conducted, but similarities in body mass, gait, and relative musculoskeletal size/segment lengths allow for crossover comparison. In this context, we suspect that the differences in LP construct stability between in vitro modeling and in vivo implementation may be attributed to the secondary sheer and torsional stresses exerted on the tibia during gait, as opposed to mere compressive overloading. Further biomechanical research is necessary to explore this theory.

As noted above, no significant differences in compressive maximal load or total strain were observed during compressive mechanical testing of two LP constructs of markedly different plate lengths. This differs from several in vitro models that noted a direct relationship between LP construct rigidity and plate length [25-27]. In a mechanical study utilizing simulated human supracondylar femoral fractures, locking plate length was significantly associated with construct stiffness, and longer plates generated significantly stiffer constructs regardless of number of screws and working length [26]. Cao et al. utilized finite element analysis modeling of human tibial fractures to test numerous surgeon-controlled fixation elements, including plate length, positioning, and material; they noted that construct rigidity increased with plate length under medial plating conditions and suggested that appropriate plate length selection is vital to reducing the risk of fixation failure [25]. The current study also evaluated

varying working lengths of fixation, due to the custom nature of the locking plates utilized. Similar to previous mechanical studies, no significant effect of working length on construct stability was noted during compressive testing to failure [26, 27]. However, one study noted differences in yield load, specifically, between constructs of short and long working lengths, and shorter working lengths were significantly associated with greater maximum load but not overall construct stiffness during cyclic compressive testing followed immediately by compressive load to failure [24].

One limitation of the current study is the utilization of only one mode of in vitro mechanical testing, compressive load to failure. Due to restrictions in sample size and specimen availability during this experiment, further modes of loading such as bending or torsion and further test conditions such as cyclic loading were not conducted; therefore, interpretation of in vitro mechanical data is limited to ultimate compressive strength and stability. Further mechanical studies evaluating caprine tibial gap defect LP fixation are recommended to evaluate the effects of plate length and working length under additional loading conditions. In addition, following random allocation of caprine tibias into either the long or short plate fixation groups, a significant difference in tibial diaphyseal width was noted. However, no corroborating differences in tibial length or diaphyseal depth were appreciated, and the difference, while significant, represents only two millimeters. Therefore, while this group difference could, in theory, affect the results of mechanical testing, we suggest that its clinical relevance is limited and does not represent a major limitation of the mechanical tests.

The current study retrospectively assessed certain surgeon-selected factors such as plate length and plate positioning during locking plate stabilization of a 2 cm caprine tibial segmental defect. To our knowledge, this is the first publication to explore these factors in small ruminants (sheep and goats) and few publications regarding long-term outcome of long bone locking plate fixation exist in the veterinary literature [5]. In human medicine, locking compression plate fixation is commonly applied to supracondylar femoral fractures, and retrospective analysis of patient and surgeon-related factors related to fixation failure has associated shorter plate lengths with increased incidence of implant failure and fracture [23]. In one retrospective analysis of locking plate fixation of human femoral fractures (n = 335 fractures), Ricci et al. concluded that constructs with a plate length corresponding to 9 holes or greater were significantly less likely fail than shorter constructs, as associated with the possibility of stress riser formation with the application of plates with lesser femoral coverage [23]. In the current study, both plate length, alone, and calculated tibial coverage ratios were significantly associated with risk of postoperative fracture. In contrast, plate

positioning, as described by radiologically measured proximodistal, craniocaudal, and mediolateral variables, was not significantly associated with fracture complications with one exception, the distance between the gap margin and the fifth screw (first screw in distal tibia). In fracture cases, the distance between the gap margin and fifth screw was significantly shorter (by roughly 7 mm) than that in cases without fracture. Utilizing a two-dimensional finite element analysis model of bridging locking plate fixation of a simple transverse diaphyseal human femoral fracture, Giordano et al. demonstrated that the highest concentration of stress occurred around the screws closest to the fracture margin and suggested that a threshold of distance between the fracture line and closest screws is necessary to allow for safe deflection of stress and overall construct stability [28]. This provides a possible explanation for the significant association between shorter distance from the defect to fifth screw and postoperative fracture complication observed in the current study.

Plate working length is defined as the distance between the two screws closest to the fracture or gap margin [30]. In the current study, custom locking plates of three lengths were utilized, and working length was fixed for each of the plate length categories; thus, experimental working lengths directly reflect the plate lengths selected, representing absolute correlation, and only plate length variables were included in the final logistic regression analysis. Due to the retrospective nature of the study, we are unable to differentiate between the effects of overall plate length and the effects of fixation working length on fracture outcomes, and this represents a major limitation of the study. Previous in vitro and in vivo analyses of the effects of working length on locking plate fixation have yielded mixed results [24, 26, 28, 30]. Using in vitro FEA modeling, Giordano et al. describe a direct correlation between increasing working length and construct stability through effective deflection of stress, but in mechanical testing of various working lengths for LCP fixation of canine femoral gap defects, Chao et al. described significantly higher strength (yield load) in short compared to long working length constructs [24, 28]. In retrospective analyses of in vivo factors associated with distal femoral LCP fixation failure in humans, working length was not significantly associated with implant failure or with nonunion [23, 30]. In addition, in a retrospective analysis of locking plate fixation stiffness as a function of working length, neither fixation working length nor the ratio of working length to plate length were correlated with overall fixation stiffness or with complications such as delayed union or nonunion [32]. In the current study, working length was directly reflective of the selected plate length, and both short plate length and lower tibial coverage ratios were significantly associated with fixation failure. Follow-up experimentation employing

either consistent plate length and variations of working length or vice versa are necessary to differentiate the effects of plate length and fixation working length in locking plate fixation of caprine tibial gap defects.

Due to the retrospective nature of this study, certain limitations including differences in group sample sizes with relative overrepresentation of 18 cm plate length are inherent. As noted above, plate length selection was carried out by the attending surgeon at the time of gap fixation, based on evaluation of the surgical site. Thus, reported correlations of goat weight and tibial measured length with selected plate length are logical, and we suggest that these conditions reasonably simulate a clinical setting. However, conclusions regarding potential confounding effects of body weight, tibial length or size, and plate length selection cannot be made from this study. In the current study, the additional variable of tibial coverage ratio was included to link the factors of surgeon-selected plate length and goat-specific tibial size, and lesser degrees of tibial coverage, regardless of absolute tibial length, was significantly associated with postoperative fracture. In this model, goats immediately bear weight on the operated limb and though their activity is limited to stall rest, behaviors such as pacing and standing on their hindlimbs were unrestricted. Thus, quantification of stresses to the construct is goat-specific and reliant on individual behavior. Further research into the association of veterinary patient demographic factors such as age, weight, and bone dimensions, surgeon-selected factors, goat behaviors and activity levels, and orthopedic complications is warranted.

CONCLUSIONS

Although in vitro modeling of variable plate length in relation to tibial length suggested that similar failure modes and rates could be anticipated, in vivo application revealed that both plate length and tibial coverage ratio were significantly associated with the incidence of postoperative fracture complications under the condition of segmental defects in which the bone does not contribute to load sharing. Interestingly, decreasing distance between the gap defect and the first screw distal to the gap was associated with increased incidence of fracture. Based on the results of this study, optimization of plate-to-tibia coverage through maximization of plate length may lessen the risk of postoperative fracture morbidity following locking plate fixation of diaphyseal gap defects.

REFERENCES

1. Reichert, J.C., et al., *The challenge of establishing preclinical models for segmental bone defect research.* Biomaterials, 2009. **30**(12): p. 2149-2163.
2. McKinley, T.O., et al., *Internal Fixation Construct and Defect Size Affect Healing of a Translational Porcine Diaphyseal Tibial Segmental Bone Defect.* Military Medicine, 2021. **186**(11-12): p. e1115-e1123.
3. Christou, C., et al., *Ovine model for critical-size tibial segmental defects.* Comp Med, 2014. **64**(5): p. 377-85.
4. McGovern, J.A., M. Griffin, and D.W. Hutmacher, *Animal models for bone tissue engineering and modelling disease.* Disease Models & Mechanisms, 2018. **11**(4): p. dmm033084.
5. Marcondes, G.D.M., et al., *Locking compression plate fixation of critical-sized bone defects in sheep. Development of a model for veterinary bone tissue engineering.* Acta Cirúrgica Brasileira, 2021. **36**(6).
6. Grzeskowiak, R.M., et al., *Temporal Changes in Reverse Torque of Locking-Head Screws Used in the Locking Plate in Segmental Tibial Defect in Goat Model.* Frontiers in surgery, 2021. **8**: p. 637268-637268.
7. Liu, X., et al., *Repairing goat tibia segmental bone defect using scaffold cultured with mesenchymal stem cells.* J Biomed Mater Res B Appl Biomater, 2010. **94**(1): p. 44-52.
8. Luangphakdy, V., et al., *The Effect of Surgical Technique and Spacer Texture on Bone Regeneration: A Caprine Study Using the Masquelet Technique.* Clin Orthop Relat Res, 2017. **475**(10): p. 2575-2585.
9. Stoffel, K., et al., *Biomechanical testing of the LCP--how can stability in locked internal fixators be controlled?* Injury, 2003. **34 Suppl 2**: p. B11-9.
10. Xu, G.-H., et al., *Biomechanical comparison of gourd-shaped LCP versus LCP for fixation of comminuted tibial shaft fracture.* Journal of Huazhong University of Science and Technology [Medical Sciences], 2013. **33**(2): p. 250-257.
11. Blake, C.A., et al., *Single cycle to failure in bending of three standard and five locking plates and plate constructs.* Vet Comp Orthop Traumatol, 2011. **24**(6): p. 408-17.
12. Hu, J., et al., *Spatial Bridge Locking Fixator versus Traditional Locking Plates in Treating AO/OTA 32-A3.2 Fracture: Finite Element Analysis and Biomechanical Evaluation.* Orthopaedic Surgery, 2022. **14**(8): p. 1638-1648.
13. Fulkerson, E., et al., *Fixation of diaphyseal fractures with a segmental defect: a biomechanical comparison of locked and conventional plating techniques.* J Trauma, 2006. **60**(4): p. 830-5.
14. Xue, Z., et al., *Comparison of the effect on bone healing process of different implants used in minimally invasive plate osteosynthesis: limited contact dynamic compression plate versus locking compression plate.* Scientific Reports, 2016. **6**(1): p. 37902.
15. Miranda, M.A., *Locking plate technology and its role in osteoporotic fractures.* Injury, 2007. **38 Suppl 3**: p. S35-9.
16. Uhl, J.M., et al., *Ex vivobiomechanical comparison of a 3.5 mm locking compression plate applied cranially and a 2.7 mm locking compression plate applied medially in a gap model of the distal aspect of the canine radius.* Veterinary Surgery, 2013: p. n/a-n/a.
17. Miller, D.L. and T. Goswami, *A review of locking compression plate biomechanics and their advantages as internal fixators in fracture healing.* Clin Biomech (Bristol, Avon), 2007. **22**(10): p. 1049-62.
18. Aguila, A.Z., et al., *In vitro biomechanical comparison of limited contat dynamic compression plate and locking compression plate.* Vet Comp Orthop Traumatol, 2005. **18**(4): p. 220-6.
19. Liu, W., et al., *Stiffness of the locking compression plate as an external fixator for treating distal tibial fractures: a biomechanics study.* BMC Musculoskeletal Disorders, 2017. **18**(1): p. 26.
20. Hoerdemann, M., et al., *In-vitro comparison of LC-DCP- and LCP-constructs in the femur of newborn calves – a pilot study.* BMC Veterinary Research, 2012. **8**(1): p. 139.

21. Ahern, B.J., et al., *In vitro biomechanical comparison of a 4.5 mm narrow locking compression plate construct versus a 4.5 mm limited contact dynamic compression plate construct for arthrodesis of the equine proximal interphalangeal joint.* Vet Surg, 2013. **42**(3): p. 335-9.
22. Gardner, M.J., et al., *The mechanical behavior of locking compression plates compared with dynamic compression plates in a cadaver radius model.* J Orthop Trauma, 2005. **19**(9): p. 597-603.
23. Ricci, W.M., et al., *Risk factors for failure of locked plate fixation of distal femur fractures: an analysis of 335 cases.* J Orthop Trauma, 2014. **28**(2): p. 83-9.
24. Chao, P., et al., *Effect of plate working length on plate stiffness and cyclic fatigue life in a cadaveric femoral fracture gap model stabilized with a 12-hole 2.4 mm locking compression plate.* BMC veterinary research, 2013. **9**: p. 125-125.
25. Cao, Y., et al., *The impact of plate length, fibula integrity and plate placement on tibial shaft fixation stability: a finite element study.* Journal of Orthopaedic Surgery and Research, 2019. **14**(1).
26. Weaver, M.J., et al., *The effect of surgeon-controlled variables on construct stiffness in lateral locked plating of distal femoral fractures.* BMC Musculoskelet Disord, 2021. **22**(1): p. 512.
27. Riedel, M.D., et al., *Biomechanical comparison of distal femoral fracture fixation: Analysis of non-locked, locked, and far-cortical locked constructs.* J Orthop Res, 2020. **38**(12): p. 2573-2579.
28. Giordano, V., et al., *Mind the gap between the fracture line and the length of the working area: a 2-D finite element analysis using an extramedullary fixation model.* Revista Brasileira de Ortopedia (English Edition), 2018. **53**(1): p. 88-93.
29. Rodriguez, E.K., et al., *Predictive factors of distal femoral fracture nonunion after lateral locked plating: a retrospective multicenter case-control study of 283 fractures.* Injury, 2014. **45**(3): p. 554-9.
30. Harvin, W.H., et al., *Working length and proximal screw constructs in plate osteosynthesis of distal femur fractures.* Injury, 2017. **48**(11): p. 2597-2601.
31. Rodriguez, E.K., et al., *Mechanical Construct Characteristics Predisposing to Non-union After Locked Lateral Plating of Distal Femur Fractures.* J Orthop Trauma, 2016. **30**(8): p. 403-8.
32. Parks, C., et al., *In-vivo stiffness assessment of distal femur fracture locked plating constructs.* Clin Biomech (Bristol, Avon), 2018. **56**: p. 46-51.
33. National Research Council Committee for the Update of the Guide for the, C. and A. Use of Laboratory, *Guide for the Care and Use of Laboratory Animals*, in *The National Academies Collection: Reports funded by National Institutes of Health*. 2011, National Academies Press Washington D.C.
34. Bowers, K.M., et al., *Assessment of Gait Following Locking Plate Fixation of a Tibial Segmental Defect and Cast Immobilization in Goats.* Biomechanics, 2022. **2**(4): p. 575-590.
35. Taylor, W.R., et al., *Tibio-femoral joint contact forces in sheep.* J Biomech, 2006. **39**(5): p. 791-8.

APPENDIX

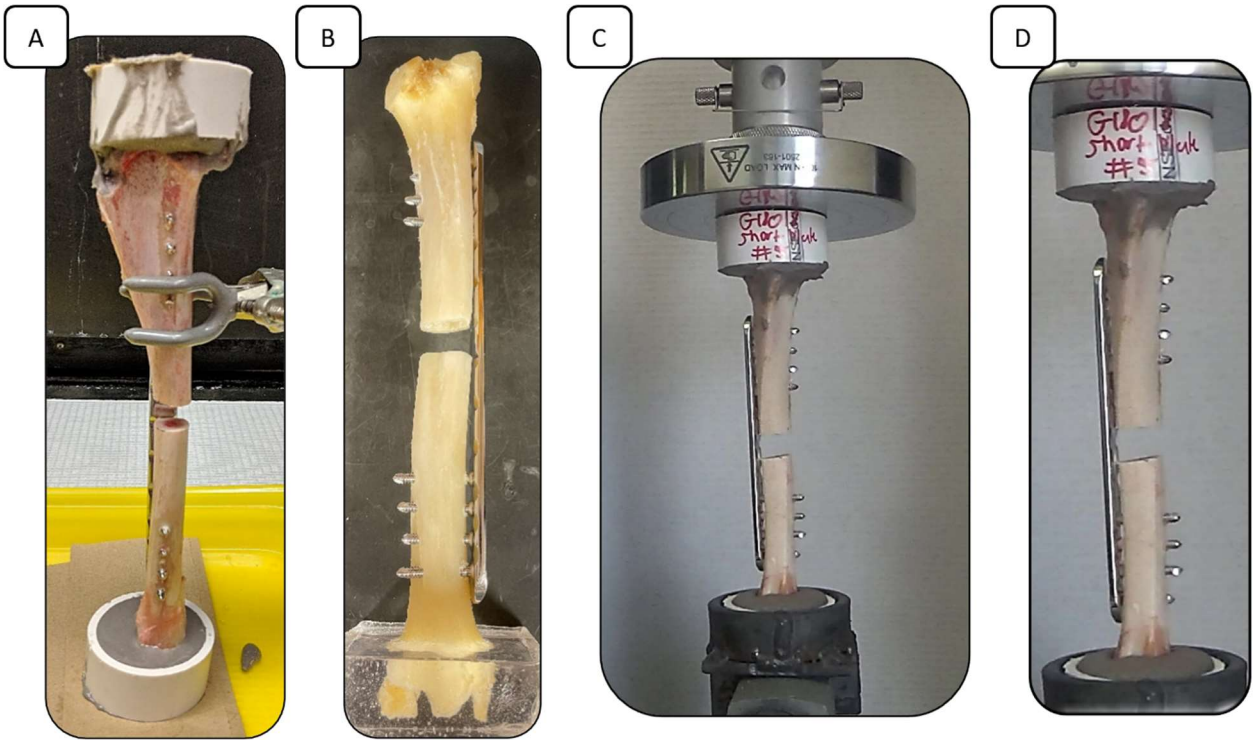

Figure 4.1: Mechanical Testing Setup. (**A**) Lateral view of tibia specimen mounted in poly-methyl-methacrylate prior to mechanical testing. (**B**) Caudal view of tibia specimen utilized for model illustration. (**C**) and (**D**) Cranial and lateral views of tibia specimens mounted in mechanical testing system prior to compression testing. In all specimens, the 1 cm segmental ostectomy is stabilized using an 18 cm (A and B) or 14 cm (C and D) 316 stainless steel low contact round double threaded 8-hole, 4.5-mm thick locking plate applied in a bridging fashion with four bicortical locking screws proximal to the defect and four distal.

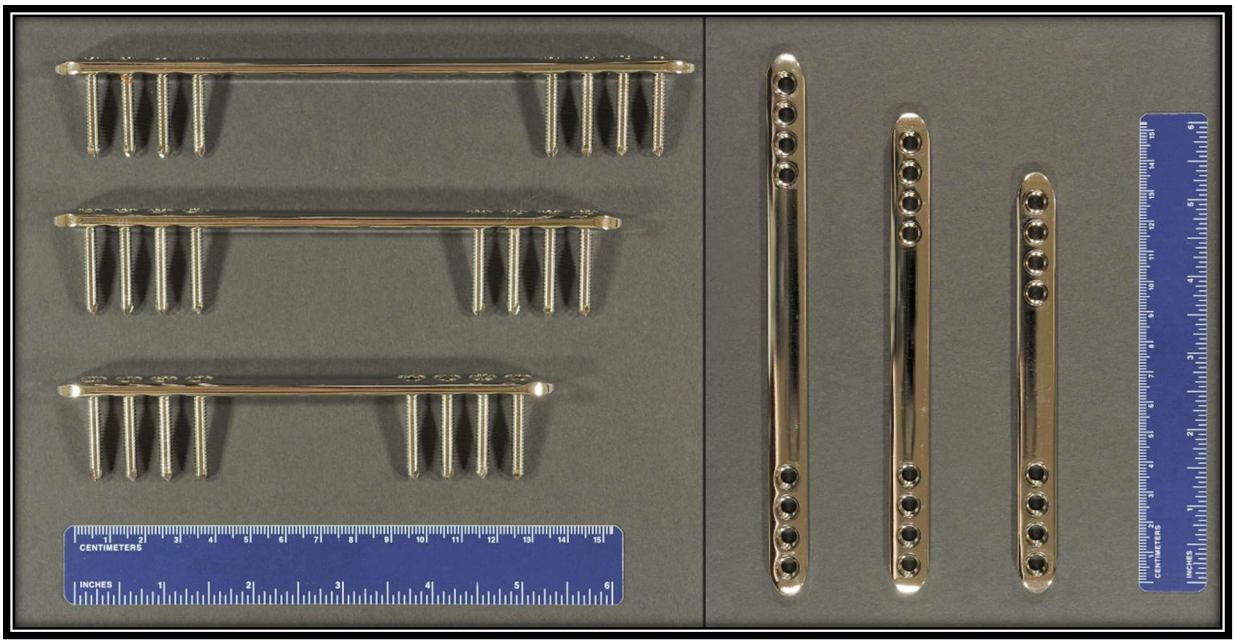

Figure 4.2: Locking Plates Utilized In Vitro and In Vivo. Custom-designed low contact, round screw hole, double threaded 8-hole, 4.5-mm thick locking plates. Three plate lengths were utilized: 14 cm, 16 cm, and 18 cm. In surgery, the plate was centered over the ostectomy and secured with eight 4.0-mm diameter locking-head self-tapping screws, four in the proximal tibial segment and four in the distal tibial segment. Fixation working length directly reflected the plate length selected.

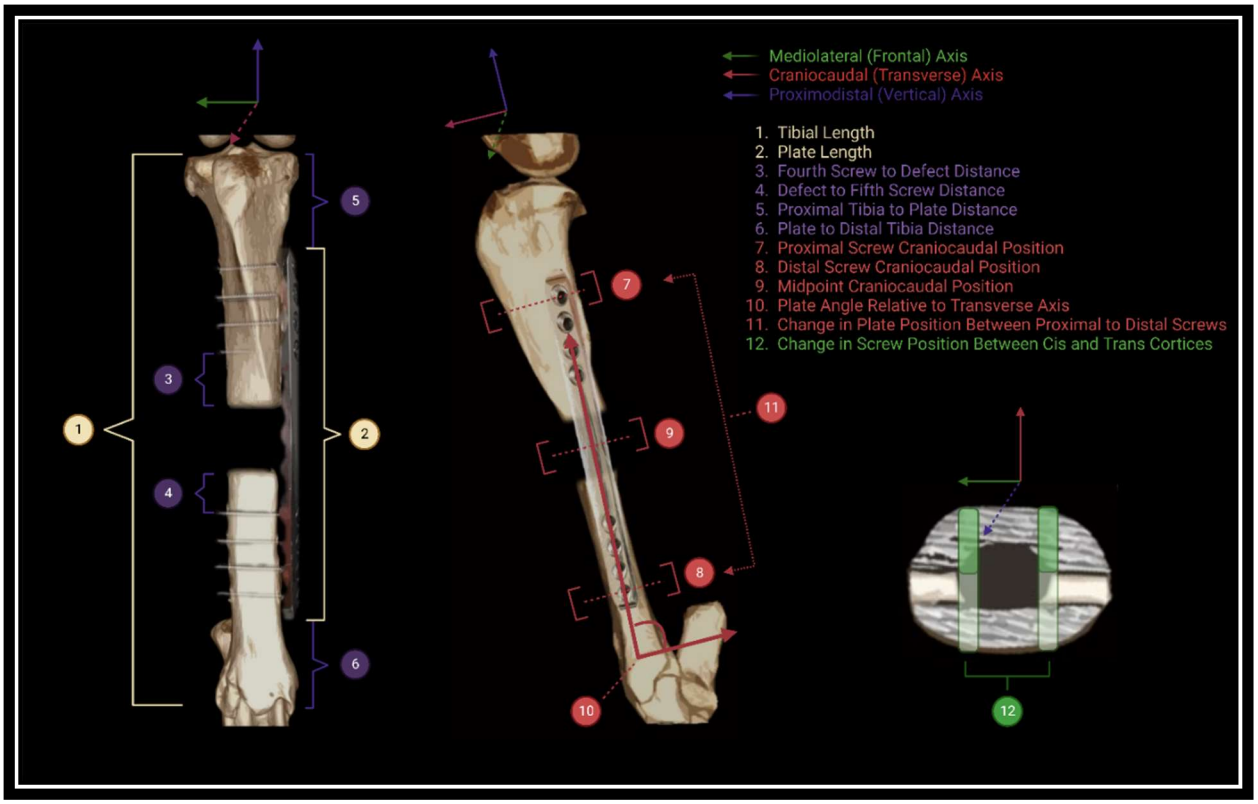

Figure 4.3: Diagram of Tibial Axes and Measurements Included in Plate Characteristics and Positioning Variables. Distances were measured in millimeters from calibrated radiographic or computed tomographic data. Positions were calculated as ratios of calibrated distances, and angles were calculated from calibrated distances and known constants. Image created using Biorender.com.

Table 4.1: Results of In Vitro Plate Length Analysis. Despite significant differences in tibia coverage ratio, no significant differences in maximum load or total strain were detected during axial compression to failure.

Classification	Variable Name	Unit	Plate Length		*P* Value
			14 cm *(Mean ± St. Dev.)*	**18 cm** *(Mean ± St. Dev.)*	
Tibial Characteristics	Tibial Length	cm	24.0 ± 1.3	24.0 ± 1.6	0.753
	Tibial Diaphyseal Width (Mediolateral)	cm	1.8 ± 0.14	2.0 ± 0.12	**0.005**
	Tibial Diaphyseal Depth (Craniocaudal)	cm	1.6 ± 0.11	1.6 ± 0.14	0.282
Plate Characteristics	Tibial Coverage Ratio	N/A (ratio)	0.591 ± 0.032	0.754 ± 0.052	**<0.001**
Biomechanical Testing	Maximum Load	Newtons	4314 ± 700	4396 ± 874	0.793
	Total Strain	mm	7.46 ± 2.48	7.56 ± 2.99	0.668

Table 4.2: Outcomes and Modes of Failure for Plate-Bone Construct Mechanical Testing. Fourteen of seventeen constructs failed by either bone fracture, plate bending to the point of bone impingement at the opposite cortex, or initial plate bending followed by fracture. Three long plate constructs reached the 4.9 kN test endpoint without failure.

Outcome	Mode of Failure	Number of Constructs	
		14 cm n = 8	**18 cm** n = 9
Failure	Fracture	2	2
	Plate Bending	4	2
	Plate Bending, then Fracture	2	2
Non-Failure *4.9 kN test endpoint*	N/A	0	3

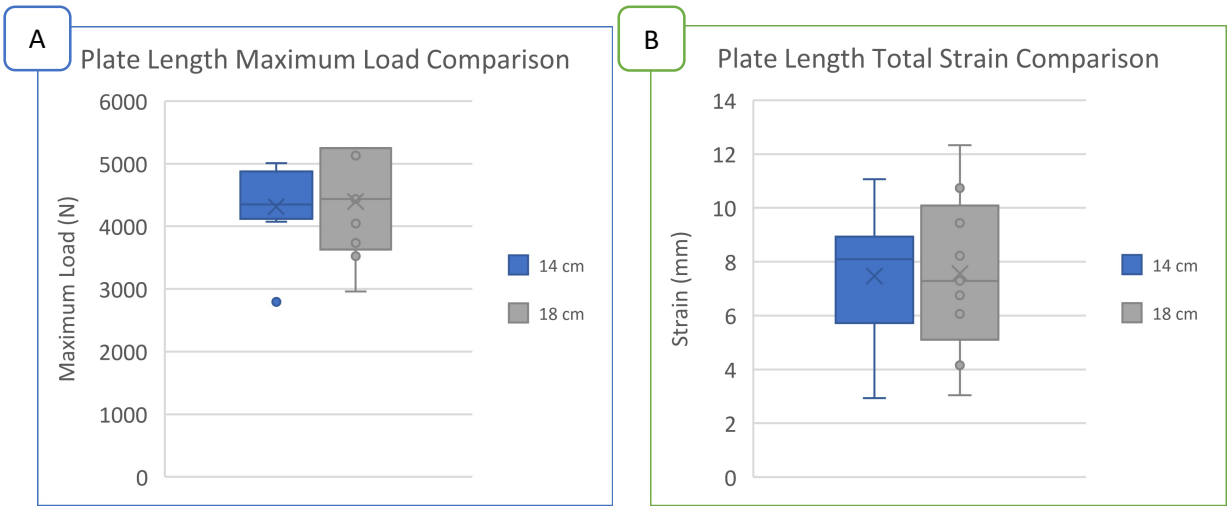

Figure 4.4: In Vitro Results. Box-and-whisker plots of (**A**) maximum load (N) and (**B**) total strain (mm) during compression to failure as a function of plate length. No significant differences were detected between 14 cm and 18 cm plates in vitro.

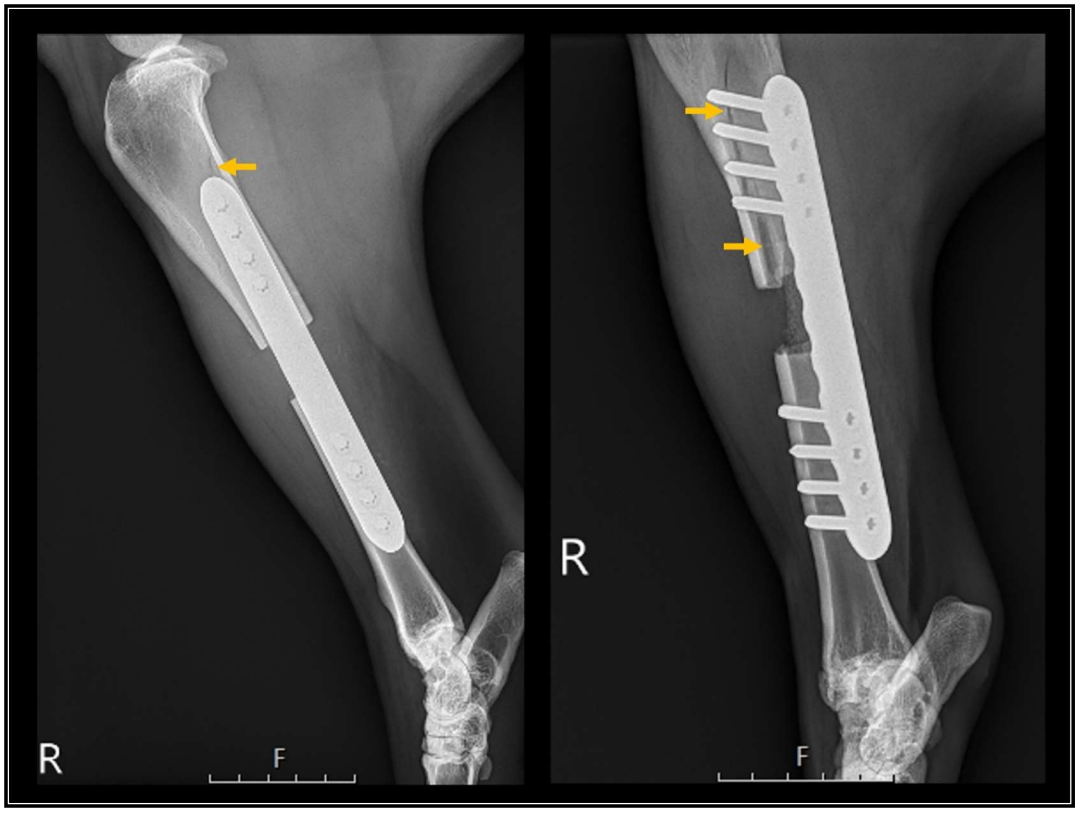

Figure 4.5: Tibial Fracture. Lateromedial and caudolateral-craniomedial oblique radiographic projections of fractured caprine tibia (yellow arrows). These images illustrate the most common fracture configuration, an incomplete, longitudinal oblique fracture of the proximal tibial segment with the fracture line following the screw holes.

Table 4.3: Plate Length Descriptives and Analysis. Selected plate lengths for all goats included in retrospective radiographic review are depicted. Plate length was significantly associated with fracture complication ($p < 0.001$) with increased fracture incidence in the 14 cm plate group.

Plate Selection		**Outcome**		**P-Value**
Plate Length (cm)	N	No Fracture	Fracture	
14	30	13	17	
16	38	35	3	
18	65	63	2	
Total	**133**	**111**	**22**	**<0.0001**

Table 4.4: **Plate Characteristics and Positioning Descriptives and Analysis.** Plate characteristics and positioning variables identified on radiographic and computed tomographic examination and their association with fracture complication outcome is depict

Classification	Variable Name	Variable Description	Unit	Outcome		P-Value
				No Fracture *(Mean ± St. Dev.)*	Fracture *(Mean ± St. Dev.)*	
Plate Characteristics	TCR	Tibial coverage ratio	N/A (ratio)	0.748 ± 0.047	0.682 ± 0.039	**<0.001**
Proximodistal Positioning	PrT-Pl	Distance from proximal tibia to proximal extent of plate	mm	26.30 ± 9.89	35.51 ± 7.74	0.201
	Pl-DT	Distance from plate to distal tibia	mm	30.89 ± 5.69	32.66 ± 7.86	0.535
	S4-D	Distance from fourth screw to defect	mm	28.64 ± 8.91	18.69 ± 5.69	0.219
	D-S5	Distance from defect to fifth screw	mm	28.53 ± 7.67	21.39 ± 8.34	**0.008**
Craniocaudal Positioning	Pr-AP	CrCd plate position at proximal tibia	N/A (ratio)	0.667 ± 0.085	0.659 ± 0.047	0.228
	D-AP	CrCd plate position at distal tibia	N/A (ratio)	0.436 ± 0.079	0.399 ± 0.067	0.32
	Mid-AP	CrCd plate position at mid-tibia	N/A (ratio)	0.552 ± 0.056	0.529 ± 0.041	N/A
	AP-Angle	Angle of plate position relative to tibial transverse axis	Degrees	84.63 ± 1.44	84.15 ± 1.37	0.221
	PrD-Diff	Change in relative plate position between proximal and distal tibia	N/A	0.231 ± 0.120	0.260 ± 0.082	N/A
Mediolateral Positioning	ML-Diff	Change in relative plate position between medial (cis) and lateral (trans) cortices	N/A	0.052 ± 0.048	0.052 ± 0.048	0.825

CHAPTER V:

CHANGES IN TIBIAL CORTICAL DIMENSIONS AND DENSITY ASSOCIATED WITH LONG-TERM LOCKING PLATE FIXATION

This chapter is in submission to *The Journal of Experimental Orthopaedics*:

Kristin M. Bowers*[1], Lori D. Terrones[1], Xiaocun Sun[3], Rebecca Rifkin[1], Elizabeth Croy[1], Henry S. Adair III[1], Pierre-Yves Mulon[1], Silke Hecht[2], David E. Anderson[1]

Affiliations:
[1] Large Animal Clinical Sciences, University of Tennessee College of Veterinary Medicine, Knoxville, Tennessee, USA
[2] Small Animal Clinical Sciences, College of Veterinary Medicine, University of Tennessee, Knoxville, Tennessee, USA
[3] Office of Information Technology, University of Tennessee, Knoxville, Tennessee, USA

Corresponding Author:
Kristin Bowers, DVM, Large Animal Clinical Sciences, College of Veterinary Medicine, The University of Tennessee, 2407 River Dr., Knoxville, Tennessee, 37996, USA; email: kbower17@vols.utk.edu

ABSTRACT

Cortical porosis, secondary to either vascular injury or stress-shielding, is a comorbidity of fracture fixation using compression bone plating. Locking plate constructs have unique mechanics of load transmission and lack of reliance on contact pressures for fixation stability, so secondary cortical porosis adjacent to the plate has not been widely investigated. Therefore, this study aimed to assess the effects of long-term locking plate fixation on cortical dimensions and density in a caprine tibial segmental ostectomy model. Data was acquired from a population of goats enrolled in ongoing orthopedic research which utilized locking plate fixation of 2 cm tibial diaphyseal segmental defects to evaluate bone healing over periods of 3, 6, 9, and 12 months. Quantitative data included tibial cortical width measurements and three-dimensionally reconstructed slab density measurements, both assessed using computed tomographic examinations performed at the time of plate removal. Additional surgical and demographic variables were analyzed for effect on cortical widths and density, and all cis-cortex measurements were compared to both the trans-cortex and to the contralateral limbs. The tibial cis-cortex was significantly wider and more irregular than the trans-cortex at the same level. This width asymmetry differed in both magnitude and direction from the contralateral limb. The bone underlying the plate was significantly less dense than the trans-cortex, and this cortical density difference was significantly greater than that of the contralateral limb. These cortical changes were independent of both duration of fixation and degree of ostectomy bone healing. This study provides evidence that cortical bone loss consistent with cortical porosity is a comorbidity of locking plate fixation in a caprine tibial ostectomy model. Further research is necessary to identify risk factors for locking-plate-associated bone loss and to inform clinical decisions in cases necessitating long-term locking plate fixation.

INTRODUCTION

Internal fixation through plate osteosynthesis remains a mainstay for effective treatment of fractures, but fixation methods, plate composition and design, and surgical techniques have evolved over time [1]. Even in its earliest stages, orthopedic plate designs reflected the challenges at hand, each aiming to improve outcome and reduce complications. Landmark achievements include the development of metallic alloys for orthopedic plates, the establishment of the Arbeitgemeinschaft fur Osteosynthesefragen (AO) principles of effective fracture treatment, the invention of compression plates to encourage primary bone healing of fractures, the refinement of plate hole designs to allow for tension or dynamic compression plating, and the establishment of minimally invasive plate osteosynthesis [1-3]. Fixed angle devices, such as point-contact fixators and locking plates, were developed to respond to the challenges observed during conventional compression plating including marked soft tissue and periosteal damage during fixation, stress shielding of the underlying bone, and complications such as cortical porosis and/or refracture following plate removal [2, 4-7].

Conventional compression plating aims to maximize fracture stability, minimize fragmentary motion, and minimize strain across the fracture gap to encourage primary bone healing, defined as the reestablishment of cortical bone without callus formation [8-10]. During early fixation, all load exerted on the bone is transferred from extremity to extremity through the plate and in compression plating, axial load is converted to shear stress [11-13]. Compression plates counteract these shear forces through frictional force generated by both plate-to-bone contact and summed screw torques, and once the external load exceeds frictional force, the strength of fixation directly reflects the axial stiffness of the screws furthest from the fracture site [2, 9]. Compression plating comorbidities and complications reflect these fixation biomechanics. Each screw is loaded individually at the screw-bone interface and repetitive loads can lead to screw toggle, failure, or pullout complications [2, 14]. These interfaces can be further compromised by cortical bone loss, either during the fracture itself or as a result of the fracture fixation (periosteal injury, soft tissue damage, or cortical stress-shielding) [7, 9].

Cortical porosis is a comorbidity of compression plating [7]. Initially described as a cancellous transformation of cortical bone under the plate, cortical porosis represents a structural change to bone in contact with the plate characterized by bone resorption, medullary widening, and cortical thinning [15]. This comorbidity has been associated with increased refracture rates following plate removal and poses a challenge to clinicians who must balance radiographic fracture healing with increasing cortical

porosity risk in their plate removal decisions [5, 16]. The definitive etiology of cortical porosis following compression plate fixation remains unclear [7]. Proposed etiologies include stress-shielding of the bone leading to disuse resorption or disruption of cortical perfusion either by surgical trauma or compression between the plate and periosteum [1, 5]. However, plate alterations aimed at reducing plate contact (e.g., limited contact dynamic compression plate) and/or stress differential between plate and bone (e.g., plate material compositions) have not succeeded in eliminating porosis and reducing refracture rates [7, 16-18].

In contrast to compression plates, locking plates do not depend on individual screw torques nor on plate-to-bone frictional forces for fixation stability [12, 19]. Locking plates act as single beam constructs in which there is no motion between the components of the beam (plate and screws), and axial external load is converted to compressive force, not shear forces [12, 20, 21]. The strength of locking plate fixation reflects the sum of all screw-bone interfaces, avoiding comorbidities of screw toggle and/or breakage and proving ideal for fracture cases with weak or lacking cortical bone (osteoporosis, comminution, etc.) [14, 20, 21]. Locking plates also are periosteal sparing, as the stability of locking plate fixation does not rely on frictional force generated by compressive contact between the plate and underlying bone [5, 10]. Generalized locking plate contact forces and surface areas have been described, but the true extent of locking plate contact is case-specific, depending on the fracture configuration, bone contours, cortical integrity, and overlying soft tissue [4, 5, 22, 23]. In theory, the differing contact profiles and fixation biomechanics between locking and compression plate fixation should reduce the incidence of cis-cortical porosis following locking plate fixation. However, Moens describes several clinical case series and studies that found no difference in cortical necrosis or porosity between locking and compressive plates [5]. Also, progressive bone atrophy (characterized by cortical thinning and porosis) following locking plate fixation of diaphyseal forearm fractures has been reported [24-26]. Moens challenged the claim that locking plates do not induce cortical porosis, citing a lack of in depth and rigorous comparisons between traditional compression and locking plates [5].

The current study aimed to assess the effects of long-term locking plate fixation in a caprine tibial segmental ostectomy model, focusing on cortical changes such as thinning, porosity, or loss of density under the plate as compared to both the trans cortex and to the cortical characteristics of the opposite limb. We hypothesized that long-term locking plate fixation would be associated with a loss of cortical integrity in the form of cortical thinning and decreasing cortical density of the bone underlying the

plate. We hypothesized that these effects would be associated with time but would be independent of bone healing, fixation characteristics, and goat body weight.

MATERIALS AND METHODS

Goats

All study procedures were approved by the University of Tennessee Animal Care and Use Committee (protocol numbers 2741 and 2383). Boer-cross, adult goats (n=160 females; mean weight 50.6 ± 7.58 kg, weight range 29 – 73 kg) were used in this study. Preoperatively, goats were housed in small group pens in groups of two to six (≥17 ft^2 per goat); postoperatively, goats were housed individually in adjacent pens (≥20 ft^2 per goat) for a minimum of seven days, followed by group housing based on goat behavior, clinical indication, and housing availability. Flooring included a layer of wood shavings laid on top of rubber mats over concrete flooring in a conditioned housing facility for the duration of the study. The goats were fed a balanced ration of grass hay, supplemental grain mix, and alfalfa as needed based on body condition. Free choice fresh water was provided via automatic waterers in group housing and in water buckets in individual pens. The goats used in this study were part of a series of orthopedic research projects assessing bone fillers in a tibial segmental defect model. Treatment groups included negative control (empty defect), positive control (autologous cortical bone graft), and intramedullary bone fillers with and without recombinant human bone morphogenic protein 2 (rhBMP-2). Goats from two projects in this series were included in this study, and cases were identified as either from Study A (2018) or Study B (2021); surgical technique, postoperative management, and postoperative monitoring did not differ between Studies A and B, but treatment group allocation and duration of the postoperative period differed by design. Criteria for inclusion of goats in this study included those having a segmental tibial ostectomy (2 cm defect, right hindlimb), bridging fixation using a single, custom designed locking plate, and computed tomographic examination of the operated limb immediately following plate removal. Exclusion criteria included goats diagnosed with surgical site infection, osteomyelitis, loose screws, broken screws, or cortical fractures during the study.

Surgery

A mid-diaphyseal 2.0 cm segmental ostectomy was performed on the right hind tibia of each goat. The tibia was stabilized using a custom-designed low contact, round locking screw hole, double threaded 8-hole, 4.5-mm thick locking buttress plate with a solid portion between the 4th and 5th screw holes (Veterinary Orthopedic Implants, St. Augustine, FL, USA). Plate lengths varied based on tibia length, and plate selection (14 cm, 16 cm, or 18 cm) was made at the time of surgery following assessment of the tibia and surgical site. The plate was centered over the ostectomy and secured with eight 4.0-mm diameter self-tapping locking screws (Veterinary Orthopedic Implants, St. Augustine, FL, USA), four in the proximal tibial segment and four in the distal tibial segment. Each screw was tightened manually by the lead surgeon to ensure adequate engagement between screw and plate. Surgical procedures were performed as previously described [27]. Postoperatively, goats were fully weight-bearing and were maintained in full-limb bandages with medial and lateral plastic splints (Premier1Supplies, Washington, IA, USA) that spanned the limb from foot to femorotibial joint (knee). Bandages were discontinued between 2 and 4 weeks postoperative based on clinical condition as assessed by the supervising veterinarian. Goats were maintained in either group or individual housing as described above but no additional activity, behavior, or mobility restrictions were in place in the postoperative period. Goats were humanely euthanized at predetermined timepoints of 3, 6, 9, or 12 months postoperatively.

Radiographic examinations of the tibia, consisting of a minimum of two orthogonal views centered at mid-tibia, were performed immediately postoperatively and one day following surgery. Bone healing was assessed radiographically throughout the postoperative period at monthly or bi-monthly intervals as directed by the ongoing orthopedic research protocol. Computed tomographic examination of either the operated limb alone or both hindlimbs was performed at the time of plate removal, either postmortem or under general anesthesia as dictated by the experimental design. Computed tomography (CT) was performed using a 40-slice helical CT scanner (Philips® Brilliance-40™, Philips International B.V., Amsterdam, Netherlands). Prior to imaging, the CT scanner was calibrated according to manufacturer specifications. Transverse images were acquired as a multislice helical dataset and were reconstructed into 0.67-mm to 1-mm slice thickness using a bone algorithm. Images were uploaded into a picture archival and communications system (Sectra® PACS™ IDS7, Sectra AB, Linkoeping, Sweden) for further evaluation.

Bone Healing Assessment

Per the ongoing orthopedic research protocols, each postoperative radiographic study and computed tomographic examination was reviewed by a board-certified veterinary radiologist (SH). Bone healing was assessed using an ostectomy gap filling score, referred to as "Bone Healing Score," outlined in Table 5.1 and based on both the Radiographic Union Score for Tibial fractures (RUST) treated with intramedullary fixation and the modified RUST scoring system for plate fixation [28-30]. Scores ranged from 1 to 5 with a bone healing score of 5 representing complete filling of the ostectomy gap with bridging callus on all cortices. For both cortical thickness assessment and cortical density assessment using computed tomographic (CT) data, the bone healing score assigned to the respective CT examination was utilized for correlation analysis described below.

Cortical Thickness Assessment

Cortical thickness and cortical density were measured using computed tomographic data of the operated and, if available, contralateral limbs obtained at the time of plate removal. Manipulation of image files, cortical thickness measurements, and cortical slab density measurements were performed using a picture archive and communication system (PACS) and digital radiographic imaging system (Sectra PACS, Sectra AB, Linköping, Sweden). Cis (medial cortex underlying the plate) and trans (lateral cortex opposing the plate) tibial cortical widths were measured using digital calipers on transverse CT frames (slice thickness 0.67-1 mm). For all operated limbs, standardized measurement loci were implemented using the visible screw tracts from locking plate fixation. Briefly, each fixation was performed using eight locking screws with bicortical engagement, four proximal to the ostectomy gap and four distal to the gap. The screws were referred to by number with screw 1 (S1) as the most distal screw and screw 8 (S8) as the most proximal screw (see Figure 5.1). The midpoint frames between each adjacent pair of screws on the same bone segment were identified and utilized for measurements, yielding three measurement loci in the proximal tibial segment and three in the distal. For all contralateral limbs, three standardized measurement loci were determined using tibial length, measured in CT frames. Briefly, measurements were conducted at the appropriate frames representing ¼, ½, and ¾ tibial length to correspond to repeatable proximal metaphysis, mid-diaphysis, and distal metaphysis loci. On the contralateral limb, the medial cortical measurements

were compared to operated cis-cortical measurements, and the lateral cortical measurements were compared to operated trans-cortical measurements.

At each measurement location, cis- and trans-cortical widths at the craniocaudal midpoint of the bone were recorded. Additionally, a qualitative binary assessment of cis-cortical irregularity was conducted by the reviewer with cortical irregularity defined as any disruption to the uniform tibial cortical structure such as bone porosity or periosteal new bone formation. Differences in cortical width were determined mathematically as trans width minus cis width.

Cortical Density Assessment

Cortical density measurements were conducted at each operated and contralateral limb measurement location described above. To enhance density measurement accuracy and reduce frame-to-frame variability, density measurements were conducted as previously described on three-dimensional cylindrical cortical slab regions of interest (ROI) generated using Sectra PACS's multiplanar reconstruction software (Sectra AB, Linköping, Sweden) [30, 31]. Slabs were generated using maximum intensity projections (MIP), slab thickness was set at 3 mm with 1 mm step, and ROI cylinders were generated with 2.5 mm diameter and 5 mm^2 area. At each operated and contralateral limb measurement point, cis (medial) and trans (lateral) cortical slab densities at the craniocaudal midpoint of the bone were determined using manual placement of ROI cylinders within the appropriate cortex. Differences in cortical density were determined mathematically as trans density minus cis density.

Statistical Analysis

For both the operated and contralateral limbs, cis- and trans-cortical tibial cortical widths and densities were compared at each measurement locus using paired Student's t tests. Additional demographic and surgical factors were screened for any effects on operated or contralateral tibial cortical width or density differences. These factors included body weight at study admission, orthopedic research project group (Study A or Study B), allocated treatment group, selected locking plate length, time in months that the locking plate was in place, cortical irregularity status, and bone healing score at the time of plate removal and CT exam. Descriptive statistics (including mean, median, standard deviation, frequency, percentile, and range) were generated as appropriate for the given dataset. The effects of cortical irregularity status, project group, and treatment group on width and density differences were analyzed using an analysis of variance (ANOVA), and the effects of numeric factors including body

weight, plate length, bone healing score, and time were assessed using Pearson correlation analysis. For all demographic and surgical factors, effects were assessed first at the whole tibia level and then at each measurement locus individually. For ANOVA analyses, rank data transformation was applied when diagnostic analysis on residuals exhibited violation of normality and equal variance assumptions using Shapiro–Wilk test and Levene's test. Post hoc multiple comparisons were performed with Tukey's adjustment.

Operated and contralateral limb width and density differences were compared using paired Student's t tests. Briefly, calculated width and density differences on the operated limb were matched with contralateral differences at the same location on the bone. The two proximal operated limb measurement loci were compared to the proximal metaphysis contralateral locus, the two loci immediately adjacent to the ostectomy site were compared to the contralateral mid-diaphysis locus, and the two distal operated limb measurement loci were compared to the contralateral distal metaphysis locus. Statistical significance was identified at $p<0.05$. Analyses were conducted in SAS 9.4 TS1M7 (SAS institute Inc., Cary, NC) and IBM SPSS Statistics v. 28 (IBM Corp. Armonk, NY, USA).

RESULTS

Goats

Out of a total population of 160 goats, 84 (mean body weight 50.11 ± 7.13 kg; range 35-66.6 kg) met the inclusion criteria for this study. Study groups, treatment groups, locking plate lengths, duration (in months) of plate fixation, and bone healing scores are presented in Table 5.2. Due to differences in experimental design between Study A (70 goats) and Study B (14 goats), significant differences in treatment group allocations and durations of fixation were observed ($p<0.001$). Additionally, significant differences in allocated plate lengths and body weights at intake were noted between study groups ($p<0.001$). Goats in Study A were slightly lighter than those in Study B (49.1 ± 6.6 kg and 55.4 ± 7.6 kg, respectively), and selected plate lengths were longer in Study A as compared to Study B (Table 5.3).

Tibial Cortical Width

Operated limb cortical widths and width differences are presented for each measurement location in Table 5.4. At all points on the operated tibia, the cis cortex was significantly wider than the trans cortex (p<0.001 for all comparisons). Mean contralateral limb cortical width differences, expressed as trans-cortex minus cis-cortex, are presented for each measurement locus in Table 5.5. At all locations on the contralateral tibia, the lateral cortex was significantly wider than the medial cortex (p<0.001 for all comparisons). As described in Table 5.5 and illustrated in Figure 5.2, mean cortical width differences were significantly different in magnitude and direction between operated and contralateral limbs (p<0.001 for all comparisons), with the greatest disparity in cortical dimensions at the operated and contralateral proximal metaphyses (-0.836 ± 0.935 mm and 0.433 ± 0.412 mm, respectively). Qualitative cortical irregularity scores were significantly different between the operated cis-cortex and contralateral limb medial cortex (53.1% irregularity and 0.9% irregularity, respectively, p<0.001).

On the contralateral tibia, the factors of treatment group, body weight, duration of locking plate fixation on the operated limb, locking plate length, and bone healing score of the operated limb were assessed for correlation with contralateral tibial width differences. No significant correlations were detected for treatment group, body weight, locking plate length, and time, but bone healing score on the operated limb was significantly correlated with contralateral limb mid-diaphyseal width difference (p = 0.042). As bone healing improved, the width difference at mid-diaphysis on the contralateral tibia decreased.

On the operated limb, the factors of orthopedic study group, body weight, locking plate length, treatment group, duration of locking plate fixation, and bone healing score were assessed for correlation with tibial width differences (Table 5.2). No significant correlations were detected for treatment group, time, and bone healing score. Study group, body weight, and locking plate length were each significantly correlated with operated tibial cortical width difference (p<0.001 for each). The effects of study group were inconsistent when broken down by measurement foci. At the proximal metaphysis, goats from Study A had greater width differences than Study B, but at the mid-diaphyseal and distal metaphyseal loci, Study B had greater width differences. At the distal mid-diaphysis locus (S43) and distal metaphyseal locus (S32), increasing body weight was directly correlated in increasing width difference, but no significant effect of body weight was detected at the remaining measurement loci. Plate length was

significantly correlated with width difference; as plate length increased, the operated tibial cortical width difference decreased.

Based on these results, further analysis of interactions between the demographic and surgical variables was performed. Bone healing score had no significant interactions with the other variables. Duration of locking plate fixation (time) was significantly associated with study group only ($p<0.001$). The variables of study group, treatment group, body weight, and plate length were significantly codependent ($p<0.001$ for all comparisons).

Tibial Cortical Density

Operated limb cortical densities and density differences are presented in Hounsfield Units (HU) for each measurement location in Table 5.6. At all locations on the operated tibia, the cis cortex was significantly less dense than the trans cortex ($p<0.001$ for all comparisons). Mean contralateral limb cortical density differences, expressed as lateral cortical density minus medial cortical density, are presented in Table 5.7. Similar to the operated tibia, the medial cortex was significantly less dense than the lateral cortex at all measurement points ($p<0.001$ for all comparisons). As described in Table 5.7 and illustrated in Figure 5.3, mean cortical density differences were significantly greater in the operated limbs compared to contralateral ($p<0.001$ for all comparisons), with the greatest disparity in cortical densities at the mid-diaphyseal region.

On the contralateral tibia, no significant correlations with cortical density differences were found for the factors of treatment group, locking plate length, and body weight. At the contralateral proximal metaphysis only, both bone healing score of the operated tibia and time that the locking plate was in place were significantly correlated with contralateral cortical density difference ($p = 0.003$ and $p = 0.030$, respectively). Greater bone healing scores, representing more complete bridging of the ostectomy, were associated with greater differences in density between the contralateral medial and lateral proximal metaphyseal cortices, but increasing duration of plate fixation was association with decreased density differences on the contralateral limb.

On the operated limb, the factors of bone healing score, locking plate length, study group, and time exhibited no significant correlation with cortical density differences (Table 5.2). Body weight at intake and assigned treatment groups were significantly correlated with whole-bone cortical density differences ($p = 0.048$ and $p = 0.031$, respectively). When broken down by measurement foci, increasing body weight

at intake was significantly correlated with decreasing density differences at the mid-diaphysis proximal to the fracture gap (S65), but no additional significant interactions were noted. At two locations in the proximal metaphysis, significant differences in cortical densities were noted between the positive and negative control groups; no additional effects of treatment group reached significance.

DISCUSSION

Locking plate fixation combines the mechanical stability of an external fixator with the antimicrobial safety of an internal fixator [6]. Locking plate mechanics allow for stable fixation in cases of weak or limited cortical bone, and while they do not provide interfragmentary compression, locking plate fixations have similar strength, stiffness, and generalized success in terms of fracture healing and functional recovery when compared to matched compression plate fixations [21, 23, 32-35]. Locking plate complications generally reflect those of all internal fixations, and the most common reasons for reoperation are infection, most commonly associated with patient factors such as obesity, diabetes, smoking, or other underlying disease, and implant failure, most commonly associated with loss of screw purchase in compromised bone [21, 36, 37]. However, an increased rate of nonunion associated with locking plate fixation, particularly in distal femoral fractures (nonunion rates range from 14% to 41% of cases), has been identified, and upon further investigation, cortical atrophy and loss of cortical integrity under the locking plates was observed [26, 38-40]. Also, cortical porosis and bone loss have been observed in cases of locking plate fixation of proximal humeral fractures, resulting in both nonunion and refracture complications [24, 26]. In a single-subject prospective trial, Hirashima et al. evaluated atrophic bone changes associated with locking plate fixation of paired radial and ulnar fractures without subsequent plate removal over 5 years of follow-up [25]. They reported a rapid loss of volumetric bone density in the radius and ulna under the plate (roughly 8% and 15%, respectively) during the first year of follow-up, relatively unchanged bone density between years 1 and 3, and rapid, marked declines in bone density from year 3 onward (roughly 34% volumetric bone loss under the plate in both the radius and ulna at year 5 of follow-up) [25]. Throughout this period, the volumetric bone mineral density outside of the margins of the plate did not significantly change [25]. Therefore, the goal of this study was to screen for cortical thinning, porosity, or loss of density following locking plate fixation of a caprine tibial defect.

Changes in cortical dimensions were assessed through measurements of operated and contralateral tibial cortical widths. Significant differences in cortical widths were noted at all measurement points on the contralateral tibia with the lateral cortex wider than the medial. These differences are expected due to normal tibial functional anatomy, tension surface, stress distribution, and muscular attachments, and similar relative cortical widths have been documented in focused caprine breed-associated anatomical studies [41-43]. However, the cortical geometry of the operated limb differed from that of the contralateral tibia both in magnitude and direction of cortical width differences (Figure 5.2). Contrary to our hypothesis, the cis-cortex underlying the locking plates was significantly wider than the trans-cortex at all measurement points. Upon qualitative review, this wider bone was significantly more irregular and porous than the contralateral comparisons. Biomechanical analysis of tibial mechanics and strain distribution following plate removal was outside the scope of this study. Thus, we can only speculate from previous mechanical studies that the operated tibias would undergo markedly different patterns of tension, strain, and load distribution based on geometry alone, and the observed cortical irregularities may act as stress risers during load transfer as seen in previous osteoporosis models [44-49]. Cortical widening in this study was rapid, and the duration of locking plate fixation had no significant effect on the geometric changes. In addition, operated limb cortical width differences were independent of bone healing score, suggesting that the fixation itself and not the degree of load sharing of the healed ostectomy was responsible for medial (cis) cortical widening.

Changes in cortical density and cortical porosity were assessed through multiplanar CT reconstruction and three-dimensional cortical slab density measurements. Similar to cortical widths, expected differences in cortical density between the contralateral tibia's medial and lateral cortices reflect normal anatomic adaptations to the bone's functions in load bearing and locomotion [30, 43]. In both the operated and contralateral limb, the cis-cortex was less dense than the trans-cortex, but the difference between three-dimensionally reconstructed cortices was significantly greater on the operated limb (Figure 5.3). This translates to increased bone porosity and overall bone loss under the plate that corroborates what has been described following long-term locking plate fixation of human forearm and upper arm fractures [24-26]. Similar to cortical width differences, operated limb cortical density differences were not affected by either duration of fixation or bone healing score, suggesting rapid, fixation-associated changes that were independent of the defect's degree of healing and load sharing status. We suggest that the significant correlations between operated cortical

density differences and the variables of body weight at intake and treatment group are reflective of convenience sampling limitations discussed below. However, the interesting correlations between both cortical width and density differences and body weight is worthy of further investigation. In this study, as body weight increased, cortical width disparities between cis and trans at the mid-diaphysis increased while cortical density disparities at the proximal metaphysis decreased. Due to the codependence of body weight, study group, treatment group, and plate length in this study, further conclusions regarding the effect of body weight and, by extension, external axial load on locking-plate-associated cortical bone loss cannot be made, but this is a compelling topic for future research.

Another interesting finding worthy of further exploration is the significant correlation between bone healing score on the operated limb and cortical width and density differences on the contralateral limb. As operated limb healing scores improved, reflective of increasing load sharing of the defect, contralateral limb width differences decreased and density differences increased. Alterations in quadrupedal load distribution and biomechanical gait following induction of lameness have been well-described [50-52]. As the contralateral cortical measurements in this study were only intended to provide a contralateral comparison for observations in the operated limb, further exploration into lameness biomechanics and contralateral limb loads were outside the scope of this project. However, we hypothesize that these changes in contralateral tibial geometry and composition may reflect adaptive bone responses to alterations in loading environment as previously described [27, 52, 53].

The data from this study was obtained as a convenience sample from a series of orthopedic research projects using the caprine tibial ostectomy model. Thus, study population limitations including unequal distribution of study and treatment groups, lack of control for body weights and plate lengths, and overall codependence of study group, treatment group, body weights, and plate lengths are inherent. On individual factor analysis, orthopedic study group, body weight at intake, and locking plate length were significantly correlated with operated limb cortical width differences. However, due to the significant interaction effects among these variables and inconsistency of effect on cortical width differences when broken down by measurement location, conclusions regarding the influence of one variable over another and recommendations for future surgical planning cannot be made. To account for these inherent limitations, strict inclusion criteria was enacted to maximize uniformity in fixation mechanics, bone metabolism, and wound environment. This resulted in a relatively high exclusion rate (47.5%) and limitation of overall sample size, and we acknowledge these limitations to

data interpretation. However, on post hoc sample size analysis with type II error set at 0.2, all demographic and surgical variable stratifications retained adequate power for whole tibial analysis and inclusion in our results.

In addition to the study population limitations discussed above, additional limitations in methodology and standardization must be acknowledged. This study compared measurements between the operated and contralateral limbs, but direct matching of measurement methods was not feasible due to the presence of screw tracts and gap ostectomies in the operated tibias. For that reason and to ensure standardized and repeatable measurements in both two- and three-dimensional reconstructions, the mathematical midpoints between screw tracts were used on the operated limb whereas relative tibial length was used on the contralateral tibias. Variations in plate lengths, plate positions, and tibial anatomy introduced minor and unavoidable variability in operated tibia measurements, and we acknowledge this as a limitation to the study. Finally, all contralateral CT examinations were performed as a part of Study A, so no correlation analysis of study group effect was able to be performed on contralateral tibial measurements. Contralateral CT examination was not included in Study B's methodology, and the limitations to contralateral dataset size and matching are acknowledged.

CONCLUSIONS

This study describes significant alterations in cortical dimensions and density following long-term locking plate fixation of caprine tibial segmental defects. Cortical porosis is an accepted comorbidity of compression plating, but due to locking plates' unique mechanics and contact profile, it has not been widely investigated in association with locking plate fixation. In this study, the tibial cortex underlying the plate was significantly wider and more irregular than the opposite cortex at the same level, and this width asymmetry differed in both magnitude and direction from the contralateral limb. The bone underlying the plate was significantly less dense than the opposite cortex, and the magnitude of difference between operated cis and trans was significantly greater than that of the contralateral limb. This study provides evidence that cortical bone loss consistent with cortical porosity is a comorbidity of locking plate fixation and may contribute to nonunion or refracture complications in cases of extended duration of fixation. Further research is necessary to identify risk factors for locking-plate-associated bone loss and to inform clinical decisions in cases necessitating long-term locking plate fixation.

REFERENCES

1. Uhthoff, H.K., P. Poitras, and D.S. Backman, *Internal plate fixation of fractures: short history and recent developments.* Journal of Orthopaedic Science, 2006. **11**(2): p. 118-126.
2. Augat, P. and C. von Rüden, *Evolution of fracture treatment with bone plates.* Injury, 2018. **49**: p. S2-S7.
3. Schmierer, P. and A. Pozzi, *Minimally Invasive Plate Osteosynthesis*, in *Locking Plates in Veterinary Orthopedics*. 2018. p. 41-50.
4. Fulkerson, E., et al., *Fixation of diaphyseal fractures with a segmental defect: a biomechanical comparison of locked and conventional plating techniques.* J Trauma, 2006. **60**(4): p. 830-5.
5. Moens, N.M.M., *The Biology of Locking Plate Applications*, in *Locking Plates in Veterinary Orthopedics*. 2018. p. 13-24.
6. Stoffel, K., et al., *Biomechanical testing of the LCP--how can stability in locked internal fixators be controlled?* Injury, 2003. **34 Suppl 2**: p. B11-9.
7. Klaue, K., I. Fengels, and S.M. Perren, *Long-term effects of plate osteosynthesis: comparison of four different plates.* Injury, 2000. **31**: p. 51-86.
8. Einhorn, T.A. and L.C. Gerstenfeld, *Fracture healing: mechanisms and interventions.* Nature Reviews Rheumatology, 2015. **11**(1): p. 45-54.
9. Egol, K.A., et al., *Biomechanics of locked plates and screws.* J Orthop Trauma, 2004. **18**(8): p. 488-93.
10. Larson, A.N. and M. Rizzo, *Locking plate technology and its applications in upper extremity fracture care.* Hand Clin, 2007. **23**(2): p. 269-78, vii.
11. Xu, G.-H., et al., *Biomechanical comparison of gourd-shaped LCP versus LCP for fixation of comminuted tibial shaft fracture.* Journal of Huazhong University of Science and Technology [Medical Sciences], 2013. **33**(2): p. 250-257.
12. Miller, D.L. and T. Goswami, *A review of locking compression plate biomechanics and their advantages as internal fixators in fracture healing.* Clin Biomech (Bristol, Avon), 2007. **22**(10): p. 1049-62.
13. Greiwe, R.M. and M.T. Archdeacon, *Locking plate technology: current concepts.* J Knee Surg, 2007. **20**(1): p. 50-5.
14. Grzeskowiak, R.M., et al., *Temporal Changes in Reverse Torque of Locking-Head Screws Used in the Locking Plate in Segmental Tibial Defect in Goat Model.* Frontiers in surgery, 2021. **8**: p. 637268-637268.
15. Paavolainen, P., et al., *Effect of Rigid Plate Fixation on Structure and Mineral Content of Cortical Bone.* Clinical Orthopaedics and Related Research®, 1978(136).
16. Uhthoff, H.K., D. Boisvert, and M. Finnegan, *Cortical porosis under plates. Reaction to unloading or to necrosis?* JBJS, 1994. **76**(10).
17. Kregor, P.J., et al., *Cortical bone perfusion in plated fracutured sheep tibiae.* Journal of Orthopaedic Research, 1995. **13**(5): p. 715-724.
18. Baggott, D.G., A.E. Goodship, and L.E. Lanyon, *A quantitative assessment of compression plate fixation in vivo: An experimental study using the sheep radius.* Journal of Biomechanics, 1981. **14**(10): p. 701-711.
19. Uhl, J.M., et al., *Ex vivobiomechanical comparison of a 3.5 mm locking compression plate applied cranially and a 2.7 mm locking compression plate applied medially in a gap model of the distal aspect of the canine radius.* Veterinary Surgery, 2013: p. n/a-n/a.
20. Miranda, M.A., *Locking plate technology and its role in osteoporotic fractures.* Injury, 2007. **38 Suppl 3**: p. S35-9.
21. Ricci, W.M., *Use of Locking Plates in Orthopaedic Trauma Surgery.* JBJS Reviews, 2015. **3**(3).

22. Xiong, Y., et al., *Comparison of interface contact profiles of a new minimum contact locking compression plate and the limited contact dynamic compression plate.* International Orthopaedics, 2010. **34**(5): p. 715-718.
23. Cao, Y., et al., *The impact of plate length, fibula integrity and plate placement on tibial shaft fixation stability: a finite element study.* Journal of Orthopaedic Surgery and Research, 2019. **14**(1).
24. Padolino, A., et al., *Comparison of CFR-PEEK and conventional titanium locking plates for proximal humeral fractures: a retrospective controlled study of patient outcomes.* MUSCULOSKELETAL SURGERY, 2018. **102**(1): p. 49-56.
25. Hirashima, T., et al., *Long-term Evaluation Using Finite Element Analysis of Bone Atrophy Changes after Locking Plate Fixation of Forearm Diaphyseal Fracture.* Journal of Hand Surgery Global Online, 2021. **3**(5): p. 240-244.
26. Matsuura, Y., et al., *Evaluation of Bone Atrophy After Treatment of Forearm Fracture Using Nonlinear Finite Element Analysis: A Comparative Study of Locking Plates and Conventional Plates.* J Hand Surg Am, 2017. **42**(8): p. 659.e1-659.e9.
27. Bowers, K.M., et al., *Assessment of Gait Following Locking Plate Fixation of a Tibial Segmental Defect and Cast Immobilization in Goats.* Biomechanics, 2022. **2**(4): p. 575-590.
28. Whelan, D.B., et al., *Development of the radiographic union score for tibial fractures for the assessment of tibial fracture healing after intramedullary fixation.* J Trauma, 2010. **68**(3): p. 629-32.
29. Litrenta, J., et al., *Determination of Radiographic Healing: An Assessment of Consistency Using RUST and Modified RUST in Metadiaphyseal Fractures.* J Orthop Trauma, 2015. **29**(11): p. 516-20.
30. Field, J. and G. Ruthenbeck, *Qualitative and Quantitative Radiological Measures of Fracture Healing.* Veterinary and Comparative Orthopaedics and Traumatology, 2018. **31**(01): p. 001-009.
31. Grigoryan, M., et al., *Quantitative and qualitative assessment of closed fracture healing using computed tomography and conventional radiography.* Acad Radiol, 2003. **10**(11): p. 1267-73.
32. Piątkowski, K., et al., *Comparison of different locking plate fixation methods in distal tibia fractures.* Int Orthop, 2015. **39**(11): p. 2245-51.
33. Baba, T., et al., *Comparison of therapeutic outcomes of periprosthetic femoral fracture between treatments employing locking and conventional plates.* European Journal of Orthopaedic Surgery & Traumatology, 2013. **23**(4): p. 437-441.
34. Stoffel, K., K.U. Lorenz, and M.S. Kuster, *Biomechanical considerations in plate osteosynthesis: the effect of plate-to-bone compression with and without angular screw stability.* J Orthop Trauma, 2007. **21**(6): p. 362-8.
35. Xue, Z., et al., *Comparison of the effect on bone healing process of different implants used in minimally invasive plate osteosynthesis: limited contact dynamic compression plate versus locking compression plate.* Scientific Reports, 2016. **6**(1): p. 37902.
36. Ricci, W.M., et al., *Risk factors for failure of locked plate fixation of distal femur fractures: an analysis of 335 cases.* J Orthop Trauma, 2014. **28**(2): p. 83-9.
37. Neslihan, A., et al., *Complications encountered in proximal humerus fractures treated with locking plate fixation.* Acta orthopaedica et traumatologica turcica, 2010. **44**(2): p. 89-96.
38. Rodriguez, E.K., et al., *Predictive factors of distal femoral fracture nonunion after lateral locked plating: a retrospective multicenter case-control study of 283 fractures.* Injury, 2014. **45**(3): p. 554-9.
39. Harvin, W.H., et al., *Working length and proximal screw constructs in plate osteosynthesis of distal femur fractures.* Injury, 2017. **48**(11): p. 2597-2601.
40. Rodriguez, E.K., et al., *Mechanical Construct Characteristics Predisposing to Non-union After Locked Lateral Plating of Distal Femur Fractures.* J Orthop Trauma, 2016. **30**(8): p. 403-8.
41. Makungu, M., *Gross osteology and radiology of the pelvic limb of the adult small East African goat.* Anatomia, histologia, embryologia, 2019. **48**(3): p. 234-243.

42. Salami, S., et al., *Comparative osteometric study of long bones in Yankasa sheep and Red Sokoto goat.* Nigerian Veterinary Journal, 2010. **31**(4).
43. Hiney, K.M., et al., *High-intensity exercise of short duration alters bovine bone density and shape.* J Anim Sci, 2004. **82**(6): p. 1612-20.
44. Skedros, J.G., et al., *Evidence of structural and material adaptation to specific strain features in cortical bone.* Anat Rec, 1996. **246**(1): p. 47-63.
45. Skedros, J.G., et al., *The influence of collagen fiber orientation and other histocompositional characteristics on the mechanical properties of equine cortical bone.* J Exp Biol, 2006. **209**(Pt 15): p. 3025-42.
46. Endo, D., et al., *Reduced cortical bone thickness increases stress and strain in the female femoral diaphysis analyzed by a CT-based finite element method: Implications for the anatomical background of fatigue fracture of the femur.* Bone Reports, 2020. **13**: p. 100733.
47. Prasad, J., et al., *Characterizing gait induced normal strains in a murine tibia cortical bone defect model.* Journal of Biomechanics, 2010. **43**(14): p. 2765-2770.
48. Iesaka, K., F.J. Kummer, and P.E. Di Cesare, *Stress risers between two ipsilateral intramedullary stems: a finite-element and biomechanical analysis.* J Arthroplasty, 2005. **20**(3): p. 386-91.
49. Zhou, S., S. Jung, and J. Hwang, *Mechanical analysis of femoral stress-riser fractures.* Clinical Biomechanics, 2019. **63**: p. 10-15.
50. Stavrakakis, S., et al., *Pre-clinical and clinical walking kinematics in female breeding pigs with lameness: A nested case-control cohort study.* The Veterinary Journal, 2015. **205**(1): p. 38-43.
51. Serra Bragança, F.M., M. Rhodin, and P.R. van Weeren, *On the brink of daily clinical application of objective gait analysis: What evidence do we have so far from studies using an induced lameness model?* The Veterinary Journal, 2018. **234**: p. 11-23.
52. Fischer, S., et al., *Compensatory load redistribution in walking and trotting dogs with hind limb lameness.* The Veterinary Journal, 2013. **197**(3): p. 746-752.
53. McBride, S.H. and M.J. Silva, *Adaptive and Injury Response of Bone to Mechanical Loading.* Bonekey Osteovision, 2012. **1**.

APPENDIX

Table 5.1: Bone Healing Score. Values and criteria based on ostectomy gap filling.

Ostectomy Gap Filling	Score
New bone filling <25% of ostectomy gap	1
New bone filling 25-50% of ostectomy gap	2
New bone filling 51-75% of ostectomy gap	3
New bone filling >75% of ostectomy gap but not completely healed	4
Ostectomy gap filled completely and/or bridging callus present on all cortices	5

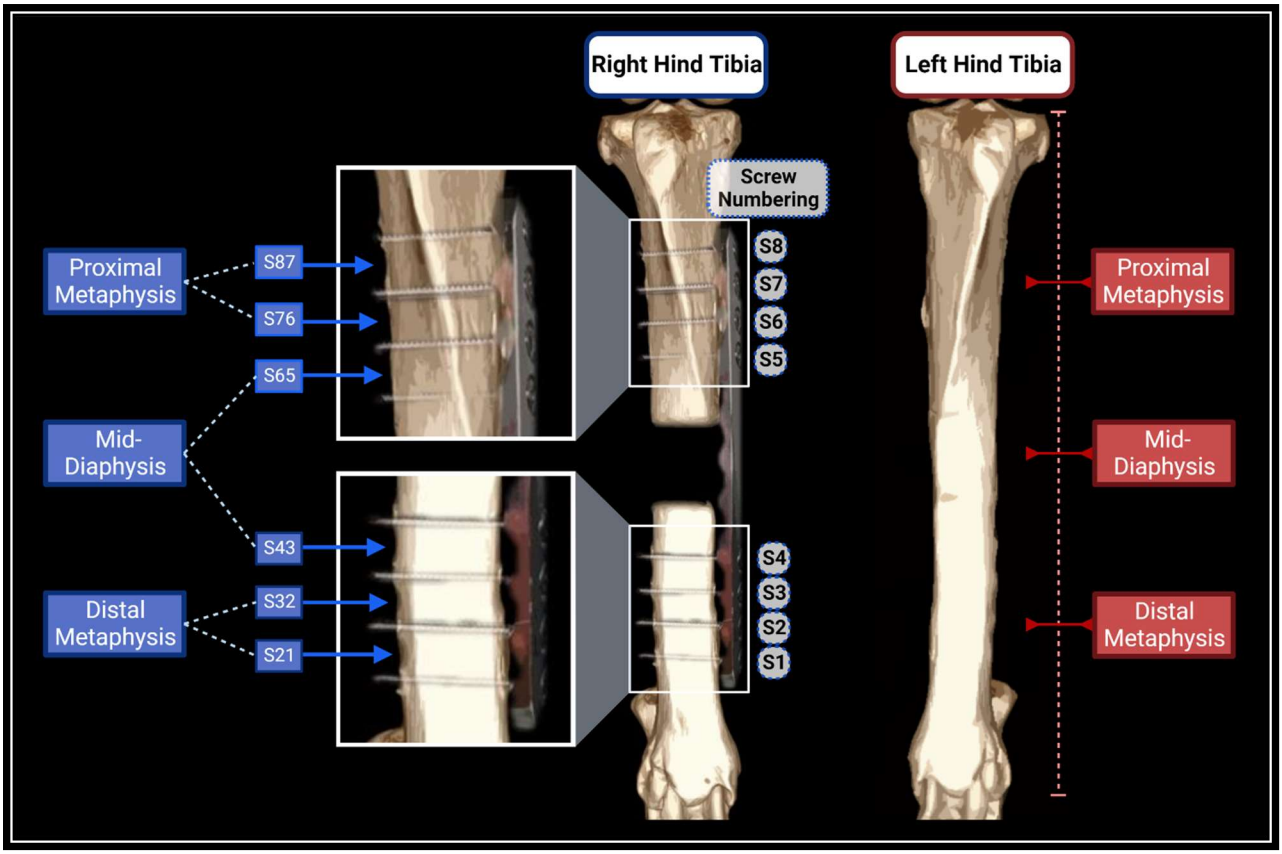

Figure 5.1: Illustration of Measurement Locations for Operated and Contralateral Tibias. Contralateral limb measurement locations were determined using tibial length with each measurement point, indicated by a solid red line and label, representing a 25% increment in tibial length. Operated limb measurements were taken at the midpoint between each adjacent screw and grouped by anatomic localization (indicated by blue lines and labels). Screws were numbered for reference and each midpoint measurement location was identified using the two adjacent screws' numbers. Figure created using BioRender.

Table 5.2: Demographic and Surgical Factors' Descriptives and Correlation Analysis Results. Statistical significance is denoted by bolded text.

Factors of Interest			Operated Limb Cortical Width Difference Correlation	Operated Limb Cortical Density Difference Correlation
			P-Value	*P-Value*
Orthopedic Study			**<0.001**	0.234
	Number of Goats	*Percent of Total*		
Study A	70	83.3		
Study B	14	16.7		
Body Weight at Intake			**<0.001**	**0.048**
	Mean ± St. Dev.	*Range*		
Body Weight (kg)	50.11 ± 7.13	35, 66.6		
Locking Plate Length			**<0.001**	0.762
	Number of Goats	*Percent of Total*		
14 cm	13	15.5		
16 cm	21	25.0		
18 cm	50	59.5		
Treatment Group			0.457	**0.031**
	Number of Goats	*Percent of Total*		
Autologous Graft	5	6.0		
rhBMP-2 Bone Filler	30	35.7		
Bone Filler Alone	22	26.2		
Empty Defect	27	32.1		
Time Locking Plate in Place			0.310	0.591
	Number of Goats	*Percent of Total*		
3 months	14	16.7		
6 months	20	23.8		
9 months	24	28.6		
12 months	26	30.9		
Bone Healing Score			0.651	0.400
	Number of Goats	*Percent of Total*		
1	13	15.5		
2	3	3.6		
3	13	15.5		
4	19	22.6		
5	36	42.9		

Table 5.3: Plate Length Distribution Between Study Groups. Selected plate lengths were significantly different between Study A and Study B (p<0.001).

Study Group Plate Lengths				
	14 cm Plates	**16 cm Plates**	**18 cm Plates**	**Total**
	Number of Goats	*Number of Goats*	*Number of Goats*	*Number of Goats*
Study A	0	20	50	**70**
Study B	13	1	0	**14**

Table 5.4: Operated Limb Mean Tibial Cortical Widths and Width Differences. Values organized by location. Statistical significance was identified at p<0.05 and significant differences between cis and trans cortical widths are denoted by bolded text.

Operated Limb Cortical Widths					
Tibial Regions	**Measurement Points**	**Cis-Cortex Width (mm)**	**Trans-Cortex Width (mm)**	**Width Difference (mm)**	***P*-Value**
		Mean ± St. Dev.	*Mean ± St. Dev.*	*Mean ± St. Dev.*	
Proximal Metaphysis	S87	4.842 ± 0.999	3.922 ± 0.727	-0.920 ± 1.019	**<0.001**
	S76	4.871 ± 0.914	4.119 ± 0.659	-0.752 ± 0.846	**<0.001**
Mid-Diaphysis Proximal to Defect	S65	4.818 ± 0.955	4.390 ± 0.633	-0.428 ± 1.049	**<0.001**
Mid-Diaphysis Distal to Defect	S43	5.057 ± 0.658	4.986 ± 0.807	-0.071 ± 0.862	**<0.001**
Distal Metaphysis	S32	4.962 ± 0.702	4.596 ± 0.668	-0.365 ± 0.685	**<0.001**
	S21	5.144 ± 0.856	4.445 ± 0.589	-0.699 ± 0.860	**<0.001**

Table 5.5: Comparison of Cortical Width Differences Between Operated and Contralateral Tibias. Values organized by location. Statistical significance was identified at p<0.05 and significant associations are denoted by bolded text.

Cortical Width Difference			
	Operated Limbs	**Contralateral Limbs**	***P*-Value**
	Mean (mm) ± St. Dev.	*Mean (mm) ± St. Dev.*	
Proximal Metaphysis	-0.836 ± 0.935	0.433 ± 0.412	**<0.001**
Mid-Diaphysis	-0.249 ± 0.970	0.317 ± 0.361	**<0.001**
Distal Metaphysis	-0.532 ± 0.791	0.126 ± 0.236	**<0.001**

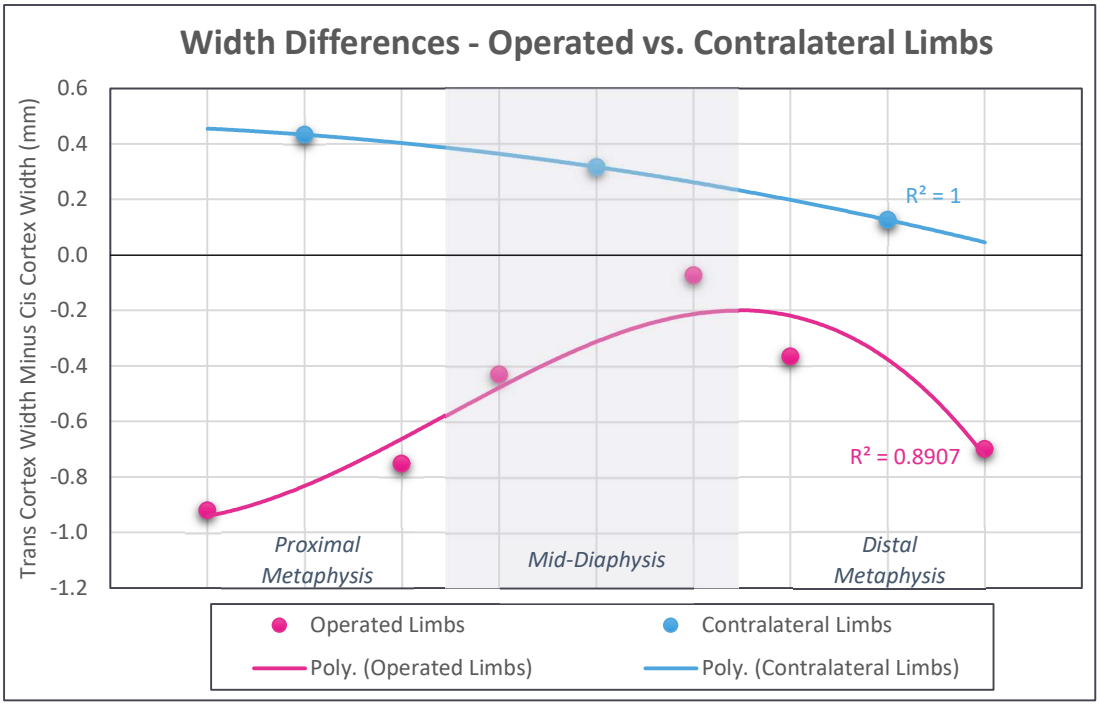

Figure 5.2: Operated and Contralateral Cortical Width Differences. Values organized by location on the bone. Polynomial lines of best fit were generated to aid in visualization, and R^2 values are included adjacent to the appropriate line.

Table 5.6: Operated Limb Mean Tibial Cortical Densities and Density Differences. Values organized by location. Statistically significant differences between cis and trans cortical densities are denoted by bolded text.

Operated Limb Cortical Densities

Tibial Regions	Measurement Points	Cis-Cortex Density (HU)	Trans-Cortex Density (HU)	Density Difference (HU)	P-Value
		Mean ± St. Dev.	*Mean ± St. Dev.*	*Mean ± St. Dev.*	
Proximal Metaphysis	S87	1437.7 ± 226.3	1604.0 ± 232.4	166.2 ± 166.3	**<0.001**
	S76	1471.8 ± 216.5	1689.3 ± 172.2	217.5 ± 125.4	**<0.001**
Mid-Diaphysis Proximal to Defect	S65	1441.4 ± 278.3	1746.8 ± 134.7	305.4 ± 251.4	**<0.001**
Mid-Diaphysis Distal to Defect	S43	1643.9 ± 154.5	1846.0 ± 127.4	202.1 ± 111.9	**<0.001**
Distal Metaphysis	S32	1641.5 ± 143.9	1812.6 ± 124.9	171.0 ± 83.8	**<0.001**
	S21	1638.2 ± 138.6	1789.3 ± 132.8	151.2 ± 92.7	**<0.001**

Table 5.7: Comparison of Cortical Density Differences Between Operated and Contralateral Tibias. Values organized by location. Statistical significance was identified at $p<0.05$ and significant associations are denoted by bolded text.

Cortical Density Difference			
	Operated Limbs	**Contralateral Limbs**	***P*-Value**
	Mean (HU) ± St. Dev.	*Mean (HU) ± St. Dev.*	
Proximal Metaphysis	192.0 ± 148.5	88.5 ± 48.2	**<0.001**
Mid-Diaphysis	253.8 ± 200.2	62.2 ± 123.9	**<0.001**
Distal Metaphysis	161.1 ± 88.4	49.5 ± 25.9	**<0.001**

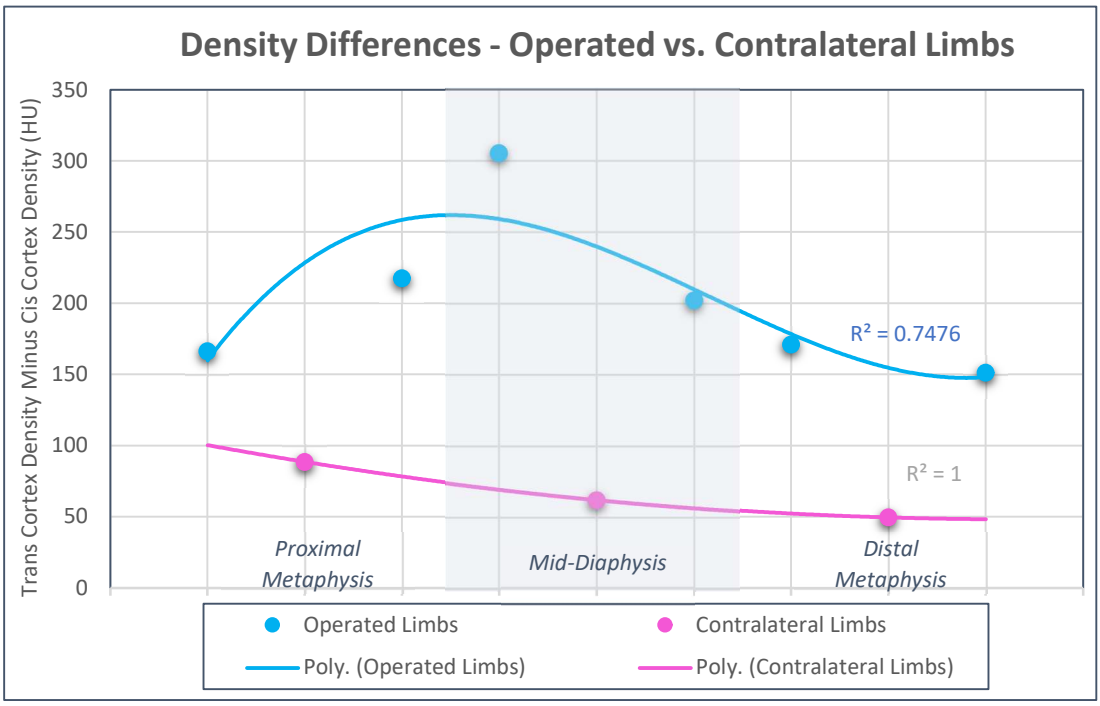

Figure 5.3: Operated and Contralateral Cortical Density Differences. Values organized by tibial regions. Polynomial lines of best fit were generated to aid in visualization and comparisons, and R^2 values are included adjacent to the appropriate line.

VITA

Kristin Marie Bowers was born and raised in Arlington, VA. She attended Clemson University in South Carolina, receiving her Bachelor of Science with a concentration in Pre-Veterinary Sciences in 2014. Then, she switched coasts, heading to Davis, CA to attend the University of California, Davis, School of Veterinary Medicine. She received her Doctorate of Veterinary Medicine in 2018 and immediately dove into a series of large animal medical and surgical internships at North Carolina State University and University of Wisconsin. In mid-2020, she joined the laboratory of Dr. David Anderson as a graduate student, focusing first on literature review, didactic curriculum, and project planning during the height of COVID. Once in vivo research began again, her research focused on tissue engineered therapeutics including stem cell therapy for acute tendon injury and bone biomaterials for critically sized defects. During her graduate coursework, Kristin discovered a love of biomechanics and developed several programs to refine biomechanical data collection in her species of choice, goats. She is incredibly grateful to her mentors, family, and friends for their support and encouragement as she continues her career in veterinary and translational research.